# The Production of Bronze Geistingen Axes

Master Thesis Materials Science and Engineering

Janneke Nienhuis

Supervisor:

prof. dr. ir. J. Sietsma

December 2009

Technische Universiteit Delft

# Table of Contents

# Abstract

Samples from two bronze Geistingen axes, one from Nijmegen and one from Tongeren, are examined and analysed in order to answer the question 'How are they produced?'.

It is concluded that both axes do not have the same composition: the Nijmegen axe is identified as a binary copper-tin bronze, while the Tongeren axe is regarded as a ternary copper-antimony-nickel alloy. Both axes possess a porous dendritic microstructure with an interdendritic phase, which is typical for a cast material. In between these phases, $Cu_2S$- and lead-antimony particles are present. The axe from Nijmegen also contains silver particles in addition to the previously mentioned ones. It is assumed that these particles all originate from the raw material, namely the ores used, and that they are formed in the melt.
The melt of both axes has been at least at a temperature of 1150 °C, based on the presence of $Cu_2S$-particles. Probably, both objects are water-cooled after pouring the liquid in the mould, according to the secondary dendrite arm spacing. This spacing indicates that the two axes are formed with different cooling rates. No subsequent working of the axes has taken place on the sampling locations.

In conclusion, the two Geistingen axes are produced by co-smelting the same types of ore in different ratios. The bronze is consequently cast into a bi-valve mould. This is then water-cooled to let the object solidify. No subsequent hot- or cold-working has taken place.

# Acknowledgements

Usually, I skip the section 'acknowledgements' when I encounter one. I am therefore very happy that you took some time to read mine. But with whom to start? I think the safest option is the 'random order', but one person needs some extra attention here. Jilt Sietsma proved to be the best supervisor I could wish for: he trusts my independency, but he is always somewhere in the background if I need help. And of course the cooking of nice food, but perhaps I'm now giving him too much credit. Without Ronny Meijers and Louis Swinkels from Museum Het Valkhof in Nijmegen and Else Hartoch and Guido Creemers from the Gallo-Romeins Museum in Tongeren, no samples were ever sawn out of prehistoric axes (or even by me). David Fontijn and Maikel Kuijpers provided me with the required archaeological knowledge and enthusiasm. Roumen Petrov performed very useful EBSD-measurements that unfortunately couldn't be implemented in this thesis. Kees Kwakernaak has done a lot of useful work with electrons on too small samples in too little time. Useful work with x-rays is done by Hans Huisman and Bertil van Os from the Rijksdienst voor het Cultureel Erfgoed. Heleen Schnitger proved to be a real chatterbox who drinks a lot of tea with me, and she became a dear friend during my thesis. Ernst van der Stok must be fed up by now, listening for hours to my blablabla. The same is true for my family.
Another big bunch of very helpful people in no particular order: Hans Drop, Mirella Frassine, Erik Peekstok, Jeroen Zuiderwijk, Olga Wens, Hans Brouwer, Arjan Mol, Richard Huizenga, David Farias Moreno, Bart Norbart, Amarante Böttger, Murugaiyan Amirthalingam, Peter van Liempt, Rob Delhez, Anneke van Veen, Joris Dik and Nico Geerlofs.

Thank you all (and the people I forgot to mention here) a lot for supporting me in any way!

# 1 Introduction

Late Bronze Age Geistingen axes are peculiar axes. They are socketed, but show no traces of being hafted. Their cutting edges are sharp, but show no use traces. They look like axes, but their thin walls prevent the tools from being used as such. They seem to be part of a serial production, but all have a different chemical composition. And last, but not least: all are deposited in the ground, seemingly without ever being used as tool or weapon.
In the Bronze Age, other functions were attributed to axes as well. They could serve as a specialised form of currency or have a ritual function. But the function of Geistingen axes is still a mystery for archaeologists and more research needs to be done to get a better understanding.
Materials science is capable of generating a part of this knowledge by using techniques developed for modern metals. The composition and possible corrosion products of the object, on macro- as well as on microscale, can be measured with different techniques. The phases present and how they are situated in the microstructure can be observed. This will ultimately lead to models with physical parameters of the formation of the microstructure and corrosion. Interpretation of this knowledge from an archaeological point of view can yield information about the production process of Geistingen axes and possibly about their function.

Therefore the research question that will be answered in this research will be:
**"How are Geistingen axes made?"**

Two already damaged Geistingen axes are available for material research. They are kindly provided by Museum Het Valkhof in Nijmegen and the Gallo-Romeins Museum in Tongeren. In total, seven bronze samples are taken from the damaged parts, near the socket mouth. These samples are examined with an optical microscope and an electron microscope to characterise their oxidation state and their microstructure. The composition is measured using X-Ray Fluorescence and Electron Probe MicroAnalysis. The phases that are present in both bronze axes is determined using X-Ray Diffraction. The information resulting from these analyses will be combined to answer the research question.

# 2 Theory

Archaeology meets materials science in this chapter. The first sections cover the theory about bronze* and its significance and appearance from an archaeological point of view. Then, the metallurgy* of bronze will be treated, as well as the technologies to form and examine bronze. The definition of words marked with an asterisk can be found in the glossary on page 65.

## 2.1 The Bronze Age

During the Bronze Age*, man has learned that certain kinds of 'stone' could be heated to yield a substance that can be modelled and retains its shape after cooling. This substance is now known as the metal 'bronze'. The discovery of bronze was an important one, leading to prehistoric metallurgy and arguably more complex societies (Kuijpers2009). This chapter treats the appearance of bronze in the world and subsequently the southern Netherlands. The phenomenon of deposition* will be discussed, concluding with the subject of this thesis: Geistingen axes.

### *2.1.1 Definition*

Since more than one definition is used to characterise 'the' Bronze Age, the following definition is used in this report: "The Bronze Age is defined by the predominant use of intentional alloys of copper in metallurgical production." In north-western Europe this means that the Bronze Age is the period between roughly 2200 and 800 BC (Pare2000, Fontijn2007), see Fig. 1. The Neolithic Age is considered as the last part of the Stone Age. It is followed by a transitional period, the Chalcolithic Age, where copper appeared alongside stone. The Bronze Age is defined as above and is followed by the Iron Age, where iron became the most used material.

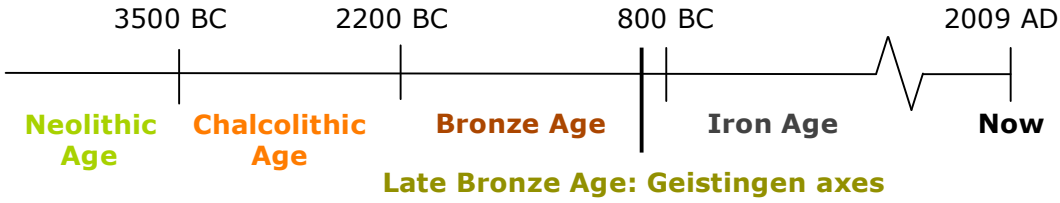


*Fig. 1: Timeline denoting different periods in the prehistory of north-western Europe.*

### *2.1.2 Bronze in the World*

Copper is part of the earth's crust: there are certain regions where ores* containing copper are concentrated; these areas are called 'deposits'*. Copper deposits are found all over the world, from South-America to Europe and Africa (Tatsch1975) and are known since prehistoric times. Tin deposits are rare in the Old World* and copper ores, as well as arsenic-containing ores, are unevenly distributed in Europe and the Near East (see Fig. 2) (Ottaway2008). Copper objects are known from about 7700 BC in South-Asia and 4000 BC in Europe (Muhly1973, Butler2005, Ottaway2008). About 2000 years later, the Bronze Age in the Old World gradually developed by the introduction of copper-arsenic alloys.

This probably was the result of the geological co-occurrence of arsenic and copper and because there is a relatively large and widespread amount of these ores (Lechtman1991). Tin bronzes gradually replaced arsenic bronzes, a phenomenon for which several explanations have been given (see section 2.2.5). As time progresses, more different alloys like lead bronze and antimonal copper come into use. From about 800 BC, the frequency of the use of copper alloys is gradually decreasing, when iron becomes the most prominent metal for objects in north-western Europe (Fontijn2007).


*Fig. 2: Distribution of copper and tin ores in north-western Europe (Ottaway2008).*

This research focuses on bronze axes in the north-western part of Europe, where a large amount of metalwork must have circulated during the 1400 years of the Bronze Age. The estimated amount of copper extracted from mines in Europe is at least 40.000 tons since the Early Bronze Age until the Late Bronze Age (O'Brien1996). The majority of this metal was recycled, reworked or remelted in a form that was appealing to the people involved (Fontijn2007, Kuijpers2008). While concentrating on bronze in Europe, the marked difference between melting* and smelting* metal becomes important:

'*Melting is changing a metal from the solid to liquid state; smelting is the process by which a metal ore is converted to metal through the agency of heat and chemical energy*.' (*Coghlan1975*)

Melting is the process that is used to shape an object; smelting is the process to make the (pure) metal. Both actions took place in the Old World (Europe and the Near East) and care must be taken in describing 'production practices' of bronze axes.

## *2.1.3 Bronze in the southern Netherlands*

### 2.1.3.1 Production

The total amount of bronze artefacts found in the Netherlands numbers around 2400 (Butler2005). Since no suitable ores for copper production are mined in the Netherlands, it can be assumed that hardly any primary production (smelting of ores) took place here.

Paradoxically, tin bronze alloying was first introduced and developed in precisely those parts of the Old World that did not have significant sources of tin ores, among which the Netherlands (see Fig. 2). However, secondary production, the (re-)melting of imported scrap or ingots, was probably carried out more often in the lower countries. For example, excavated fragments from clay moulds* used for casting* and small bronze droplets indeed suggest metalworking practices in the Netherlands (Butler1973, Kuijpers2008). (Northover1982, Bradley1988, Fontijn2002, Ottaway2008)
It is likely that these regions obtained their tin and copper from eastern or British sources through exchange (Northover1982, Pare2000). This implies a trade of knowledge and material over long distances. It is also argued that the southern Netherlands was linked to a wider, regular system of long-distance exchange (Muhly1973, Fontijn2002, Kristiansen2005, Ottaway2008).
Another possibility for the appearance of bronze in the Netherlands is that itinerant smiths or traders produced it here by melting ingots or scrap metal in order to cast a new bronze object (Childe1930). Butler sees these itinerant smiths as the tutors of the first indigenous metalworkers in the Netherlands (Kuijpers2008).
However, archaeological evidence is difficult to assign conclusively to melting and casting of bronze since all the artefacts that would be visible to the archaeologist may be related to other forms of metalworking as well. For example, hammers and grinding stones can be used to make new objects, but are also used in the sharpening and repair of already existing bronze tools. (Kuijpers2008)

#### 2.1.3.2 Deposition in General

Bronze (and its deposition) gradually played a more pronounced role in the manipulation of social relationships in Bronze Age communities. During the Bronze Age, the individual became important. One started to gain status by the possession and deposition of bronze objects, emphasising the increasing role of the individual (Broeke2005:667, Fontijn2002). Objects were deposited in conditions varying from pristine to heavily-used, thereby contradicting any notions that they were simply discarded when thoroughly worn (Ottaway2008:213). During the entire Bronze Age, bronze artefacts were thus intentionally and selectively deposited: specific objects were put into the ground only on specific locations in the landscape while other places were clearly avoided (Fontijn2002). When multiple (valuable) objects are deliberately deposited in the ground, one speaks of a 'hoard'*. The frequency with which deposition took place increased from the Early Bronze Age to the Late Bronze Age. An estimate for the Late Bronze Age of one deposition per generation per community shows that deposition was not practiced very often. (Fontijn2002, Huth2003, Fontijn2007)
The current and widely accepted interpretation regards bronze deposition as a ritual act related to the prestigious value of metalwork. Deliberate deposition would have been regarded as some sort of offering, a gift to the gods (Fontijn2002:5).
Another theory is that hoards are in fact examples of buried traders' stock, conform the itinerant smith suggested by Childe (Childe1930). However, since the objects were deposited in a wet context (also at that time), it would make retrieving the material very hard. Hence, it is more likely that this is a permanent (ritual) deposition rather than a buried traders' stock. This led to the explanation that bronzes circulated in a sacrificial economy, in which part of the supply was deposited ('pars pro toto' sacrifice). (Fontijn2002)

On the one hand, there is large-scale deposition of mostly non-local, complete, ready-to-use weapons only in watery places, where graves are avoided. On the other hand, deposition (with a much lower frequency) of incomplete, damaged bronze artefacts in dry places like settlements and burials is seen.

This phenomenon of selective deposition implicates that different objects have different meanings. It seemed to be the intention that the cycle of use and passing on to successors ended by throwing the object in a swamp or river. Two variants of these 'cultural biographies' are recognised. The first comprises weapons and jewellery, objects that acted as constituents of a specific social role and status in the life cycle of an individual. Their deposition in a wet location can be related to the deconstruction of personal identity. In the second variant, objects (mostly axes) seem to be linked more with the group identities than with personal identities. (Fontijn2002, Huth2003, Fontijn2007) More information about this specific phenomenon will be given in the next section.

### 2.1.3.3 Deposition of Axes

Axes are the most occurring objects in depositions. The reason for this lies in their dual function. They were not only used as a tool, but axes also represented the generally accepted form in which interregional metal circulation took place.
In Early and Middle Bronze Age depositions, axes that had an intense use-life are the main objects. In the Late Bronze Age, this changed. The axe's dual role led to the production of specialised forms, which only look like axes but actually are non-functional (Geistingen axes, see sections 2.1.3.4 and 2.2.7). *En masse* deposition of these axes in hoards emerged. These hoards contained distinctly local axe types that were serially produced. Additionally, some were deposited in a marshy context, a practice that previously seems to have been restricted to axes that had intensively been used. Either more people than before were involved in axe deposition, or the significance of individual items diminished (Fontijn2007:364). This change in depositional practices could reflect a crisis in the traditional system of supply and exchange. It is advocated by some scholars that there was indeed a recession in the movement of bronze (from the British Isles to the European mainland), together with a decline in operational activity in most copper mines in Britain (Northover1982, Pare2000, Huth2003). Also, there was a problem with the supply of tin since the end of the Middle Bronze Age (Northover1982). Finally, the emergence of iron axes may also have played a role in the decrease of depositional practices. (Fontijn2002, Huth2003, Fontijn2007, Ottaway2008)

### 2.1.3.4 Geistingen Axes

Axes of the Geistingen type are long, thin, socketed axes*. They are regionally made items that look like axes, but are practically unusable as such. Their low weight (approximately half that of many functional socketed axes) and thin walls exclude the use of Geistingen axes as functioning tools or weapons. These axes are named after a hoard of 26 or 28[1] examples, all of the same type, found in 1935 in Geistingen (Belgium). Their approximate date of origin is about 925-800 BC. There are also counterparts found in Germany and the Netherlands. All are characterised by a mostly oval socket mouth, a long, narrow body outline, a small, low-placed thin D-loop and, especially, very thin walls (1-2 mm in thickness), see Fig. 3. (Butler2001/2002) The chemical composition of six typologically uniform Geistingen axes seems to be anything but homogeneous. It differs from object to object (see section 2.2.7). This suggests that the smiths had to work with metal of various compositions (Postma2005, Lechtman1996).
Flaws in the supply of metal sources and bronze exchange might have led to this situation that is characteristic for the Early Iron Age. It is stated on basis of typology that these axes were serially produced, maybe even the product of a single workshop over a short period of time.

1 Since the axes were dispersed among family and friends of the finder, the amount of objects is not clear.

All Type Geistingen axes were subsequently deposited in as-cast* condition with sharpening of the cutting edge and a fine external finish. Most of them probably have not been hafted at all. (Butler2001/2002).

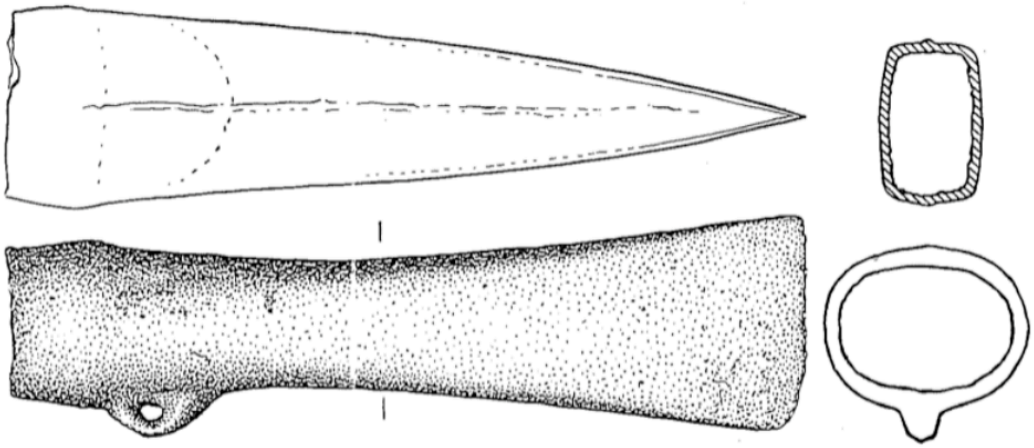

*Fig. 3: Example of an axe of the Geistingen type. Length: 14.3 cm, width 4.1 cm. (cat. no. 551, Butler2001/2002)*

There are several hypotheses concerning their function. Kibbert states that Geistingen axes were a form of 'axe money', or they were votive* objects (Butler2001/2002). Fontijn and Fokkens state that the role of the axe as an exchangeable, convertible ingot was for the first time manifested in a specialised ingot form in the Late Bronze Age, leading to the production of axes of the so-called Geistingen type (Fontijn2007:364). Butler mentions that the repeated occurrence (about 11 find-spots besides the Geistingen hoard) and limited geographical distribution of the type would seem more appropriate for a votive than a currency function. The large Geistingen hoard must represent some kind of distribution centre. (Butler2001/2002:304)
These axes probably never had a kind of biography that was in any way comparable to those of regular axes. Before the Late Bronze Age, it was the object's life-path by which it acquired its culturally recognised meaning. In the Late Bronze Age, the individuality and use life of objects became less and less important. This idea is supported by the deposition of Geistingen axes: it signals the decline of the fundamental idea that the object's life really mattered and led to a break in tradition. (Fontijn2002, Huth2003, Fontijn2007).

## 2.2 Bronze as a Material

Before bronze, there was copper. Native* copper (pure copper found in the earth's crust) was probably the first copper to be found by man, around the 4$^{th}$ millennium BC in Europe. It was widely distributed in nature in the Old World and easily recognised through its purplish colour. Hammering small pieces of copper could shape it, but larger pieces proved difficult to work cold because it turned brittle*. Forging* or melting and casting became suitable processes by which the copper could be turned into implements. It is not unlikely that man kept on looking for new and better materials for their tools in the meantime. It was probably during these searches that ores containing copper were found. Man discovered that the metal could be extracted from the ores by the smelting process. Some of these ores contained other elements in addition to copper, like arsenic. When smelted, (unintentional) alloys of copper with arsenic can be produced: the first (arsenic) bronze was made.

The process was refined when it became clear that the mechanical properties of bronze were in many aspects superior to that of pure copper. This intentional alloying developed and later, tin-bronze was made and became the predominant bronze in the Late Bronze Age. The use of bronze decreased rapidly at the start of the Iron Age, around 800 BC in the Old World, when iron substituted copper and its alloys for the use of tools. (Thompson1958, Coghlan1975, Lechtman1996, Pare2000, Fontijn2007)

### *2.2.1 General*

The properties required of a metal in ancient times were high ductility* for ease of working (malleability* and forgeability*), hardness* (often synonymous with strength) and the right viscosity of the liquid for casting (Lechtman1996, Junk2003). In addition, most bronzes are highly corrosion resistant in diverse environments, including the ambient atmosphere (Callister2003).

The temperatures needed for the conversion of ore to metallic copper can be attained with an open, charcoal fire, which can reach a maximum temperature of at least 700 °C. However, a problem with the use of an open fire can be the type of atmosphere. For most copper ores, the atmosphere is not sufficiently reducing to produce the metallic form. Pottery kilns* are capable of sustaining a highly reductive atmosphere together with a temperature of about 1100 °C. Since both campfires and kilns were already known in prehistory, people in the Bronze Age had the tools to smelt (and melt) metals and special types of hearths* for alloying and metal production were developed. Bellows were used to provide constant and sufficient airflow to increase the temperature. (Coghlan1975, Thompson1985, Ottaway2008)

It is difficult to relate a metal object to a specific ore. The first reason is the complexity of the smelting process (which will not be explained in detail here), the second is the variation in composition of the ore. This problem makes it also difficult to establish whether a certain element is added to provide better end characteristics, or if it is an unintentional by-product of the materials used.
Also, reworking and remelting of bronzes indicates that metal analysis cannot directly link objects with their ore sources. However, these analyses can still provide information about for example refining techniques and metalworking and alloying practices. (Thompson1958, Tylecote1977, Northover1982, Lechtman1991)

### *2.2.2 The Phase Diagram*

The properties of a metal are partly determined by its microstructure*. This structure varies with composition and temperature of the metal. For a binary alloy*, this can be shown in a binary equilibrium phase diagram* like Fig. 4. The next sections will explain the use of these diagrams. (Callister2003, Porter2001)

#### 2.2.2.1 Determination of Phase Compositions and Amounts

A binary equilibrium diagram represents the relationships between temperature and the compositions and the quantities of the phases at equilibrium. Phase equilibrium* is reflected by constancy with time in the phase* characteristics of a system, usually at constant pressure. An example of a typical eutectic* binary diagram and the development of the microstructure upon cooling is shown in Fig. 4. More explanation about resulting microstructures can be found in sections 2.2.2.2 and 2.3.2.3.
The establishment of the phases in equilibrium is relatively simple: the location of the temperature-composition point in the diagram provides this information.

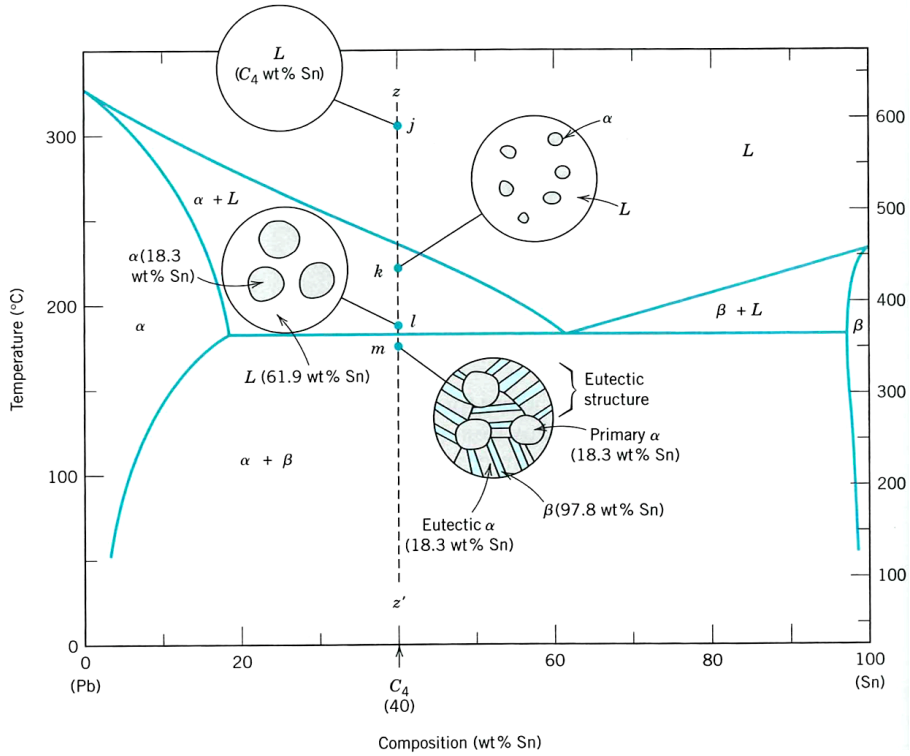


*Fig. 4: Schematic representation of equilibrium microstructures for a lead-tin alloy with an average composition $C_4$ as it is cooled from the liquid-phase region (Callister2003).*

In a single-phase region the concentration of the two components is straightforward. Take for example point *j* in Fig. 4, which is situated in the liquid-phase region and has the average composition of 40 wt% tin and 60 wt% lead. The situation becomes more complicated in the determination of the phase compositions if the point is located in a two-phase region. There, one can imagine a series of horizontal lines, one at every temperature. A set of these so-called 'tie lines' can be see in Fig. 5. The composition at the intersection of the tie line with the phase boundary will give both phase compositions.

The relative amount (for example as a fraction) of the phases present in a two-phase region can also be computed using tie lines: a ratio of tie line segment lengths is taken according to the position of the point on the line. At point *c* in Fig. 5, (43–35)/(43–32) = 0.73 is the fraction of liquid phase, and the fraction of $\alpha$-phase in the two-phase region is (35–32)/(43–32) = 0.27.

### 2.2.2.2 Microstructure Development during Equilibrium Cooling

In this section, the situation in which the cooling proceeds very slowly is treated, wherein phase equilibrium is constantly maintained. However, the rate of approach to equilibrium is often very low. Therefore, most processes occur under non-equilibrium conditions. The development of the microstructure in that case will be partly described in section 2.3.2.3. Other phases than shown in the equilibrium phase diagrams can appear in the material. Different types of diagrams, like continuous cooling transformation diagrams, should then be used to explain their occurrence.

The enlarged portion of the copper-nickel phase diagram in Fig. 5 shows what happens if a 35 wt% Ni-65 wt% Cu is cooled from 1300 °C. This corresponds to moving down the vertical dashed line.

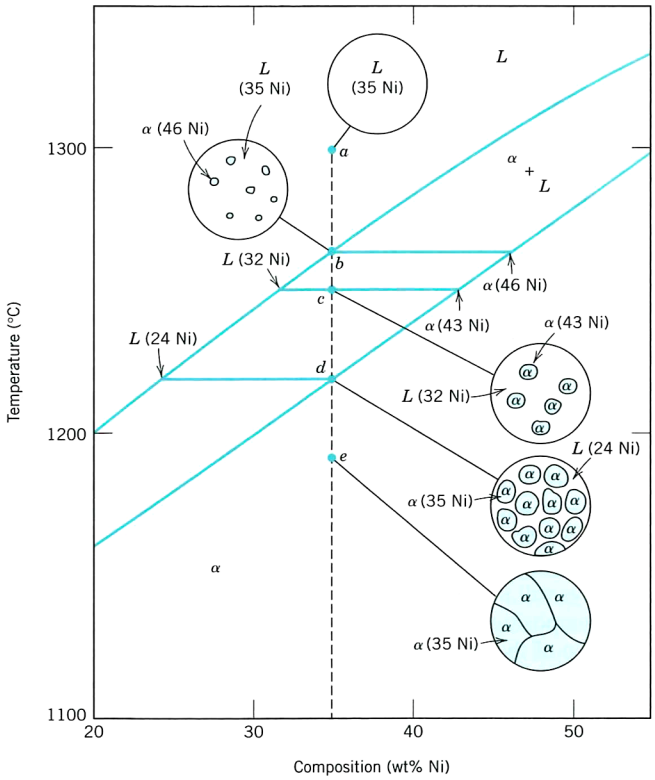


*Fig. 5: Schematic representation of the development of microstructure during equilibrium solidification of a 35 wt% Ni-65 wt% Cu alloy (Callister2003).*

At point *a*, the metal is completely liquid and no microstructural or compositional changes will be realised until point *b* is reached. The first solid α begins to form, as shown in the circle, with a composition determined by the associated tie-line (i.e. 46 wt% Ni-54 wt% Cu). When the cooling continues, the compositions of the liquid and α will further change and their relative amounts as well. The compositions will follow the liquidus and solidus lines, respectively, and the fraction of α will increase with decreasing temperature.
Even though there is a redistribution of copper and nickel between the phases, the average composition will always remain the same. From point *d* to *e*, the solidification of the alloy is complete and the final product is a polycrystalline* α-phase solid solution* that has a uniform 35 wt% Ni-65 wt% Cu composition. Subsequent cooling will not alter the microstructure or composition.

### 2.2.2.3 Ternary and Pseudo-binary Diagrams

The binary diagram can help explaining the microstructural processes in metals, but in practice, metals contain more than two components. In that case, ternary and/or pseudo-binary diagrams should be used. In a ternary equilibrium phase diagram, the ideas developed for binary systems can still be applied, although the situation is more complicated (Fig. 6).

There are two instructive representations of a system comprising three components: a cross-section through the ternary diagram at constant temperature (isothermal section, Fig. 7), and one at constant concentration of one of the components (pseudo-binary diagram).
The composition of a ternary alloy can be indicated on an equilateral triangle whose corners represent 100% A, B or C as shown in Fig. 7, left.

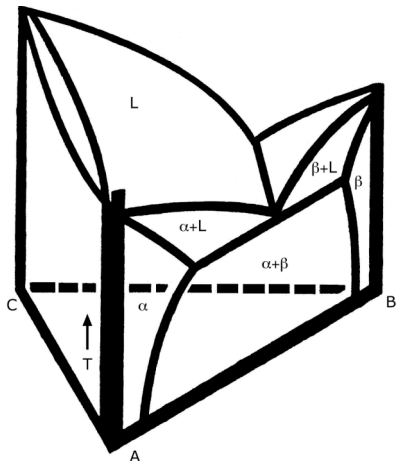


*Fig. 6: Simplified representation of a ternary equilibrium phase diagram (Massalski1990).*

All points on lines parallel to for example line AC represent constant compositions of B, so all points on line RS contain 30% B. If the alloy contains 10% C, 30% B and 60% A, the intersection of these lines parallel to the sides of the triangle forms its position at X in the diagram. To find out which phases are present at point X at a certain temperature, one looks at the horizontal isothermal section through a ternary phase diagram (Fig. 6) at the right temperature, Fig. 7, right and locates point X in the same way as described before.

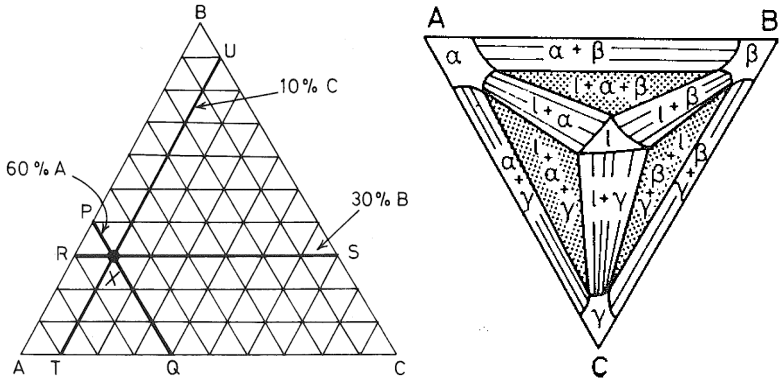


*Fig. 7: Schematic representations of how to read an isothermal section through a ternary diagram (left) and how the phases are distributed (right) (Porter2001).*

When it is assumed that the alloy has a constant percentage of one of the components, it is possible to draw a pseudo-binary equilibrium diagram. A vertical section through the ternary diagram (Fig. 6) on a line like AC will yield a pseudo-binary phase diagram looking like an equilibrium binary phase diagram as in Fig. 4. However, three-phase regions can appear in pseudo-binary phase diagrams and the equilibrium compositions and phase fractions cannot be derived from these diagrams.

### *2.2.3 Pure Copper*

The purity of native lumps of copper is high. In most cases, the total amount of impurities is smaller than 0.2 wt%. There are many ores from which copper can be extracted and they are divided into two major classes: sulphide and oxidised ores. Sulphide ores are usually compounds of copper, iron and sulphur.

The most plentiful and widely distributed sulphide ore is chalcopyrite*. The copper oxides $Cu_2O$ (cuprite*) and CuO (melaconite*) are respectively red and black in colour and of wide distribution. The patina* film that is formed on a copper object under corrosive conditions over a long period of time also often contains these compounds. (Thompson1958, Coghlan1975, Lechtman1991, Silva2008)

The electron configuration* of copper gives the metal its inherently good corrosion resistance. It also provides the good electrical and thermal conductivity of copper. Pure copper, in native as well as in as-cast state, is ductile even at room temperature due to the arrangement of the atoms in a face-centered cubic* (FCC, $\alpha$*) system. Some purposes require a hard material, like cutting edges. Pure copper can be work-hardened and these microstructures are characterised by slip* bands inside grains* (Fig. 8, left). Smaller grains at the outer surface compared to the centre of an object can also indicated hammering of the surface. (Thompson1958, Flinn1963, Coghlan1975, Russell2005)

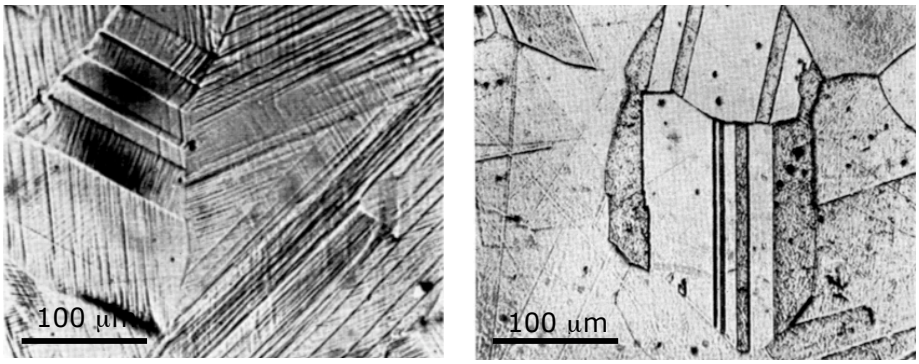


*Fig. 8: Left: slip bands in cold-worked copper. Right: twinned copper structure, characteristic for native copper or when cold-worked and annealed or hot-worked (Thompson1958).*

Native copper can have a twinned* structure like in Fig. 8, right. The metal mass started as minute solid particles in the parent rock and the individual grains grew into bigger ones under the repetitive hammering action of river gravel where it was embedded. This cold-worked state is characterised by deformed and elongated grains. Eventually, the pure metal will recrystallise in the course of thousands of years and thus become soft again. The result is a twinned structured as shown in Fig. 8, right. (Voce1951, Thompson1958, Silva2008)

When copper has been subjected to oxidising conditions, inclusions of copper oxide (mostly $Cu_2O$) can be found in the microstructure. If these oxides are present at the surface of the object, they are probably formed when the object was left in the environment at the end of its use-life. If inclusions occur in the bulk of the material, they have another origin. Cuprite co-occurs with the primary $\alpha$ phase in a eutectic reaction*, which occurs around 1066 °C for oxygen contents in the melt higher than 0.004 wt%. This is typical of copper molten under normal oxidising conditions. (Coghlan1975, Silva2008)

### *2.2.4 Arsenic Bronze*

Arsenic bronze was probably the first alloy of copper that was introduced. It is sometimes called arsenical copper to discern it from tin bronze, which is then considered as the usual type of bronze. Tin bronze alloyed with arsenic is occasionally also called arsenic bronze, but is not used as such in this report.

The addition of arsenic up to 0.5 wt% to copper is insignificant and often seen as a mere impurity from the ores used. Low-arsenic bronze is classified as copper containing 1-5 wt% arsenic and if more than 5 wt% arsenic is added, the term high-arsenic bronze is used in this report.

There are basically two ways of manufacturing an arsenic bronze:

(1) By the direct smelting of an ore that contains both copper (Cu) and arsenic (As). Examples of these types of ore are domeykite*, enargite* or tennantite*. The arsenic content that remains in the bronze in this way varies from about 1 to 10 wt%, but the product mostly is a low-arsenic bronze.
(2) The second route is mixing arsenic with copper. This can be done in various combinations, leading to high-arsenic alloys.
    (a) One can introduce arsenic ore (orpiment*, realgar*) to copper ore (cuprite, chalcopyrite) and smelt them simultaneously.
    (b) Metallic arsenic in solid state derived from the ore can be added to molten copper.
    (c) The addition of an arsenic-containing ore to already molten copper.

Arsenic can only be molten under high pressure, which was not attainable in the Bronze Age, so the possibility of adding any form of copper to molten arsenic is not realistic in this respect. Possibilities 2b and 2c are probably later developments. (Coghlan1975, Lechtman1991, Lechtman1996, Earl2000, Hauptmann2007)

Heating copper-arsenic alloys in air may result in the oxidative loss of the highly volatile arsenic from the surfaces of the solid and this can result in a fume of $As_2O_3$-particles. This white smoke is one of the ways in which the ancient smith could recognise a batch of copper with arsenic content. The white silvery colour of arsenic bronze was also an indication for the smith, together with the garlic smell of arsenic. Since these could be noticed without heating, man probably categorised arsenic bronze like this. (Thompson1958, Eaton1976, Gale1985)

In Fig. 9, the binary equilibrium diagram of copper-arsenic can be seen. In Fig. 10, a typical microstructure of a cold-hammered high-arsenic bronze is shown. The equilibrium solid solubility level of arsenic in copper at a temperature of 700 °C lies at about 8 wt% As (see Fig. 9). Under equilibrium conditions, lower concentrations of arsenic result in the alpha ($\alpha$) phase, higher concentrations also contribute the gamma ($\gamma$) phase to the microstructure of the bronze. When (cold) hammered, deformation* of the whole microstructure can be seen. Deformation lines (slip bands) (grey in Fig. 10) appear in the $\alpha$ phase (white), the $\gamma$ phase (dark grey) gets elongated, as well as the pores (black in Fig. 10). (Lechtman1996)

The presence of arsenic lowers, in comparison to pure copper, the melting point (see Fig. 9) and can alter the colour to a more silvery appearance compared to the red colour of pure copper (Gale1985, Ottaway2008). Solid solution strengthening* conferred by arsenic upon copper in alloys up to the solid solubility limit* is minimal (Lechtman1996). The strain hardening* behaviour in the Cu-As binary system is largely determined by the $\alpha$ solid solution, the $\gamma$ phase (if present, see Fig. 9) does not significantly contribute to the hardening. There is an almost constant ductility as a function of composition in the $\alpha$-phase. Up to the solid solubility limit, copper-arsenic alloys can be readily hot- and cold-worked, even at 87.5% reduction in thickness. Above 8 wt% As in Cu, the material becomes brittle as a result of the presence of the brittle $\gamma$ phase.

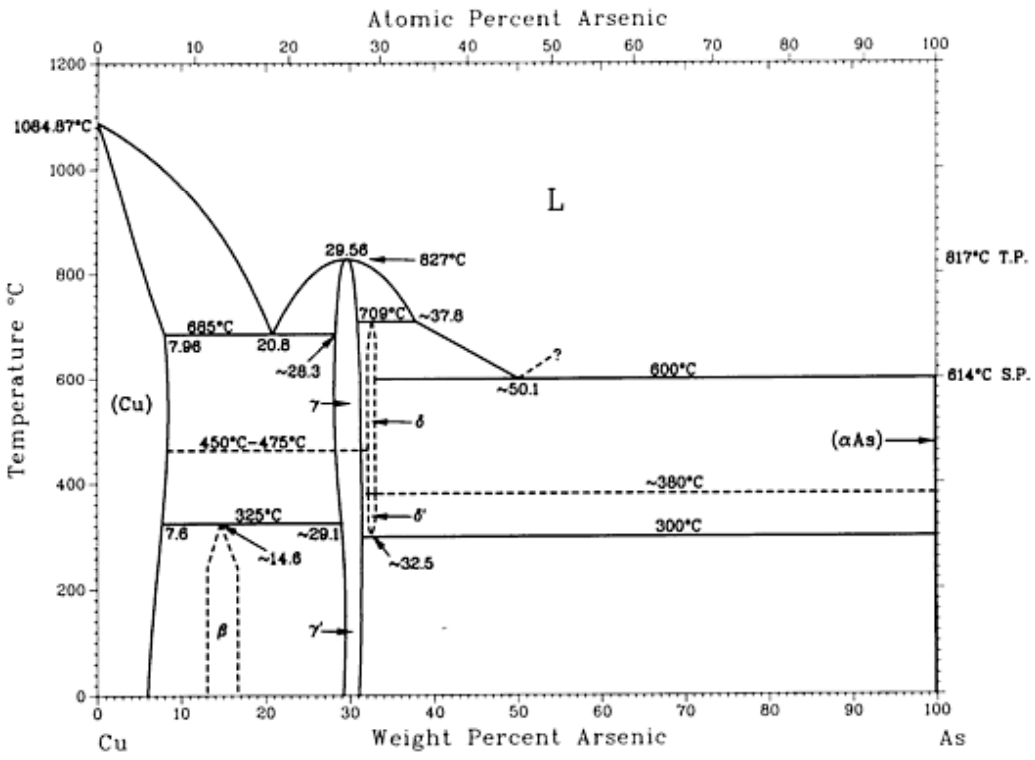


*Fig. 9: Equilibrium phase diagram of the binary alloy of copper with arsenic (ASM1992).*

Thus, although the addition of arsenic to copper confers only minimal hardness to a cast alloy, the presence of As atoms in the Cu crystal lattice* is responsible for the excellent work-hardening (cold and hot) properties of arsenic bronze (Lechtman1996, Ottaway2008).

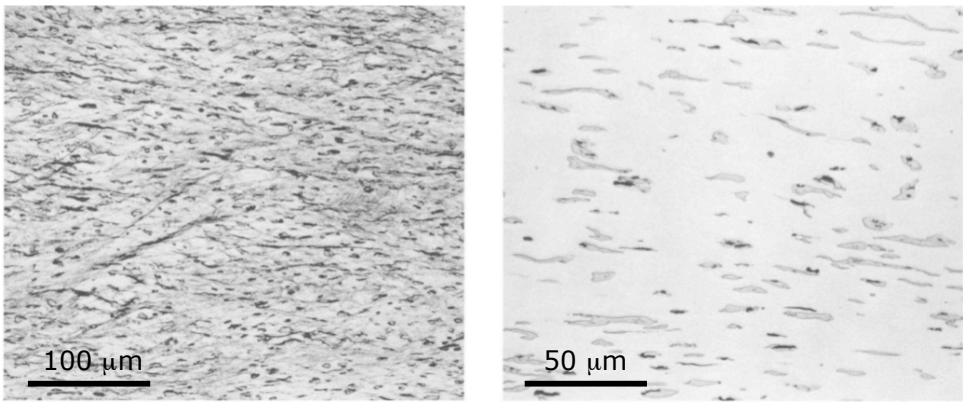


*Fig. 10: Typical microstructures of a cold-hammered high-arsenic bronze. White: α-phase; dark grey: γ-phase; black: compressed pores. (Lechtman1996)*

### *2.2.5 Tin Bronze*

There are three widely accepted possible explanations for the abandonment of arsenic bronze and the adoption of tin bronze, all based on physical grounds (Muhly1973, Lechtman1996).

(1) Tin bronze is a superior alloy; it is harder and stronger and overall exhibits better mechanical properties than arsenic bronze.
(2) Tin bronze is an intentional, or deliberate alloy, while arsenic bronze is not. There is a fundamental difference in the way these alloys are prepared. As a consequence, the composition of tin bronze can be controlled carefully; it is difficult to control the composition of arsenic bronze.
(3) Smelting ores containing arsenic produces arsenic trioxide fumes; the technology of arsenic bronze production created a health hazard, and production ceased when an effective substitute, tin bronze, became available.

Tin bronze can be made in the following four ways (Coghlan1975, Gale1985, Pare2000):

(1) One can smelt a naturally occurring copper-tin ore like stannite, but these ores are rare and mostly do not have the right ratio between copper and tin to produce tin bronze. The type of tin bronze produced in this way is low-tin bronze.
(2) By melting together a mixture of metallic copper and metallic tin (Sn).
(3) By intentional co-smelting of copper ore and cassiterite* ($SnO_2$, also called tinstone).
(4) The addition of the mineral* cassiterite to molten copper in a crucible*, under a charcoal cover will also yield tin bronze. This method is suitable to produce high-tin bronzes.

The addition of tin up to 5 wt% to copper is often seen as unworkable (in experimental archaeology), although these low-tin bronzes were used in the Bronze Age (Pare2000). High-tin bronzes are in this report defined as copper containing at least 10 wt% Sn in the binary alloy.

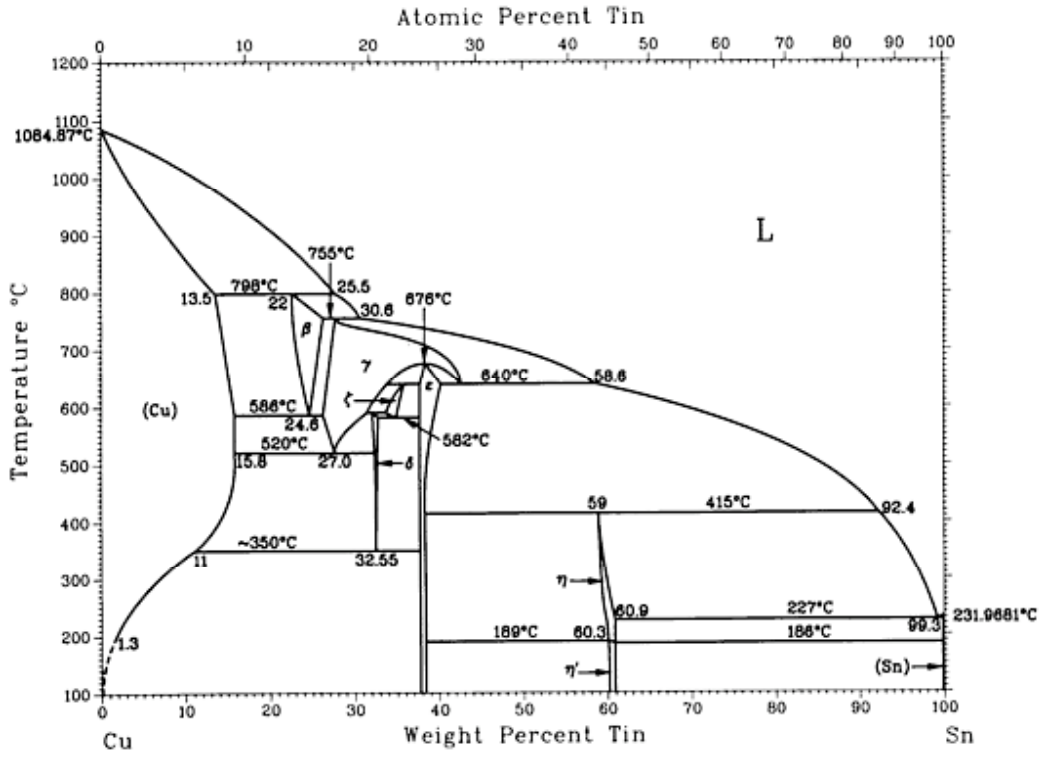


*Fig. 11: Equilibrium phase diagram of the binary alloy of copper with tin (ASM1992).*

The solid solubility level of tin in copper at a temperature of 700 °C lies at about 14 wt% Sn (see Fig. 11). Under equilibrium conditions, concentrations lower than this result in the formation of the alpha ($\alpha$) phase. Higher concentrations contribute other phases, like the brittle delta ($\delta$) and epsilon ($\varepsilon$) phases, to the microstructure of the bronze. Tin bronzes heated into the $\alpha+\beta$ field are ductile and undergo substantial elongation during hot working. When (cold) hammered, the dendritic microstructure is broken up into smaller pieces and deformation of the grains can be seen as well. (Lechtman1996, Lascalea2002, Gordon2006).

Very small amounts of tin (e.g. 0.5-1 wt% Sn) could be added to facilitate the processing of copper. Tin lowers the melting point, see Fig. 11, and increases the fluidity for casting. The colour of tin bronze is somewhat more goldish than the reddish colour of pure copper. Substantial hardening of cast tin bronzes can be achieved at levels of Sn near the solid solubility limit. Brittleness occurs at about 14 wt% tin due to the appearance of the brittle $\delta$ or $\varepsilon$ phase and at much lower elongation than arsenic bronze. This leads to the conclusion that 10 wt% tin-bronze tools were cold worked for many cycles and annealed to the $\alpha$-region to overcome the tendency of the material for brittleness. In Fig. 12, a typical dendritic microstructure of a cast tin bronze (7 wt% Sn) is shown. (Flinn1963, Eaton1976, Gale1985, Lechtman1996, Pare2000)

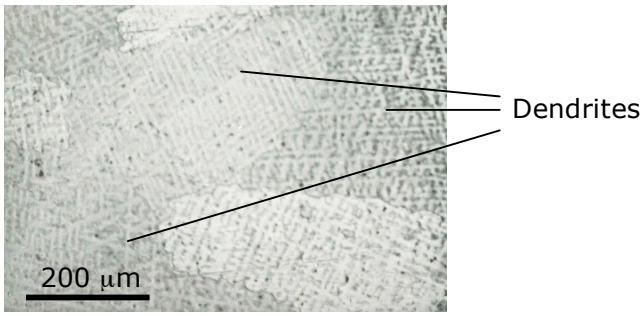


*Fig. 12: Typical microstructure of a cast tin bronze in as-cast condition. (Allen1970)*

There are several general statements that can be made about comparative mechanical properties of arsenic bronze and tin bronze. (Coghlan1975, Lechtman1996, Pare2000)

* Copper can be substantially hardened by the addition of tin and hardly through solid solution of arsenic.
* Both bronzes harden rapidly and at about the same rate as the atomic percentage of the alloying element increases.
* Tin bronze can be work hardened to higher strength than arsenic bronze.
* There is sufficient overlap in the mechanical behaviour of these two bronzes that they can be used interchangeably for specific functions within a rather broad alloy range (±2-7 wt% As or Sn).

It would be more appropriate to compare the efficacy of an alloying element by comparing relative effects for the equivalent number of atoms rather than by weight percentages, but that has not be done yet for archaeological artefacts.

The amount of arsenic in ore can hardly be estimated, while the amount of metallic tin to be added can be controlled more carefully. The volatility of arsenic also makes it difficult to produce objects with more than 5 wt% As. So arsenical bronze probably rarely reached the hardness of a typical 10 wt% tin bronze.

### *2.2.6 Other Bronzes*

In addition to arsenic and tin bronze, other copper alloys were in circulation in the Old World during the Bronze Age. Some of these were deliberate alloys, like leaded bronze, some of them were accidentally produced from ores that contained many other elements in addition to copper, like fahlerz*. This type of ore can contribute for example antimony, silver, nickel and bismuth in substantial amounts (up to 0.5 wt% per alloying element) to copper. It is thought that fahlerz was predominantly used during the Chalcolitic Age and the Early Bronze Age and lost its significance throughout the Bronze Age. (Biek1957, Thompson1958, Tylecote1977, Ottaway2008)

#### 2.2.6.1 Impurities

Impurities are elements (ranging from a few parts per million to several percents) originating from the ore and the smelting process. These elements, like silicon and iron, affect the mechanical and optical properties of the final object. In general, the effects of impurities are twofold: they are wanted in the melt since they facilitate the ease of manufacturing, but are unwanted in the final product since they can negatively influence the properties.
Iron, oxygen and sulphur are common impurities in bronze. Iron is added to remove oxides from the melt and to form a good, liquid slag. Sulphur and oxygen are almost always present in ores used to produce all types of bronze and especially sulphur is hard to remove. All these elements contribute to a higher brittleness of the end product. Silicon is either a remnant of the ores used or it is picked up from the mould during the manufacturing process. (Flinn1963, Coghlan1975, Tylecote1997, Maclean1998, Russell2005)

#### 2.2.6.2 Antimonal Copper

Antimonal copper was used primarily during the Late Bronze Age (in Central Europe) and seemed to be an intentional alloy (at least when the percentage of antimony is higher than 8 wt%).

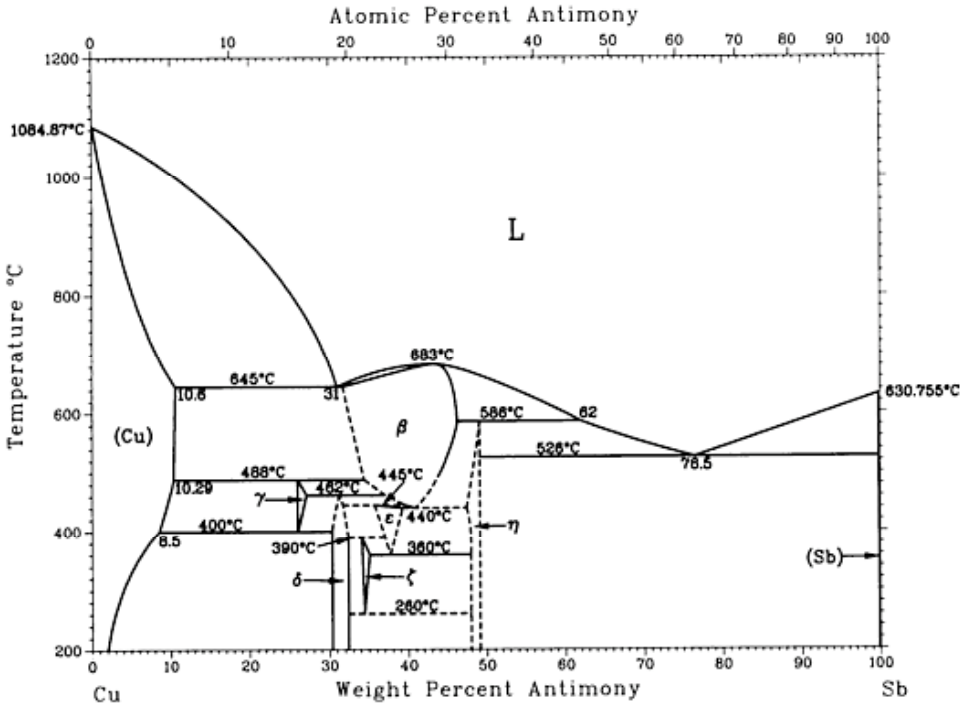


*Fig. 13: Equilibrium phase diagram of the binary alloy of copper with antimony (ASM1992).*

The phase diagram of copper-antimony can be found in Fig. 13. Elements like arsenic, lead and tin are often present up to percentage levels as well, which suggests the use of fahlerz. Castings of this type of antimony bronze were harder but slightly less brittle than arsenic bronzes, but their ductility was certainly not as good as that of tin bronze. In lead-antimony and tin-antimony bronze there is a considerable tendency for gravity segregation (see section 2.3.2.3) of the less dense primary antimony-rich crystals. Coring* is also seen in copper-antimony alloys. Working of the metal did not result in better mechanical properties. Hot-working* of copper-antimony alloys results in oxidative loss of antimony. Strange enough, weaponry made from these brittle alloys are found, which suggests that antimony was only used for its silvery attractive colour and tarnish-resistant function on martial items for display and/or status purposes. (Bailey1954, Thompson1958, Maclean1998, Junk2003)

### 2.2.6.3 Nickel Bronze

Many prehistoric bronzes contain nickel since it is sometimes associated with copper (and arsenic) in ore. A nickel content of less than 1 percent is considered as an inadvertent impurity, while in quantities larger than this, the effect of nickel alloying becomes noticeable. This element strengthens copper and bronze by solid solution and hardens it, making the alloy suitable for working. (Cheng1957, Flinn1963, Gale1985)

### 2.2.6.4 Lead Bronze

Lead bronze axes with a lead content of about 20-30 wt% have been found, for example in France and England, and are dated to the Bronze Age. The lead ended up in precipitates* in these artefacts by the addition of a lead-containing ore like galena*. However, it is rather unusual that such high percentages of lead were used for axes, since lead softens the bronze and decreases the wear resistance. This type of axe is sometimes seen as a specialised ingot form, used as currency.
The melting point of pure lead is very low (327 °C), lower than that of copper (1083 °C). When the lead bronze starts to cool down, the copper will already be solidified when the lead is still liquid, because the solid solubility of lead into copper is very low at these temperatures. For uniform cooling, this leads to segregation of lead to the grain boundaries and between dendrites arms.
This will subsequently weaken the material, see also section 2.3.2.3. When in addition to arsenic, lead is present in the ores used for producing bronze, unwanted effects can also occur. The removal of the lead during oxidation in the smelting process results in the virtual elimination of arsenic in the copper. (Coghlan1955, Thompson1958, Flinn1963, Tylecote1977, Northover1982, Gale1985, Earl2000, Lascalea2002, Craddock2009)

### 2.2.6.5 Ternary Bronzes

There are examples of ternary bronze* objects (like the Geistingen axes, see section 2.2.7) that contain two alloying elements in appreciable quantity (both in the percentages range), in addition to copper. Examples are arsenic-tin bronze and tin-lead bronze. These can be produced by smelting ores that contain all three elements, or by co-smelting different ores. In this way, properties of both alloying elements and their combination were used to alter the end characteristics of the bronze object. When the microstructure is to be explained in relation to composition of alloying elements and temperature, a ternary phase diagram has to be used. (Gale1985, Lechtman1996, Lascalea2002, Silva2008)

### 2.2.7 Geistingen Axes

As stated in section 2.1.3.4, the chemical compositions of several measured Geistingen axes vary strongly from axe to axe as can be seen in Table 1. The studied axes have unusual compositions compared to commonly found Late Bronze Age bronzes, with considerable amounts of the three elements arsenic, antimony and silver.

*Table 1: Compositions in wt% of some Geistingen axes, results of NRCA analyses (Postma 2005, Postma2009).*

| Find spot/ origin | Cat. No. | Cu (wt%) | Sn (wt%) | As (wt%) | Sb (wt%) | Ag (wt%) | In (ppm) |
|---|---|---|---|---|---|---|---|
| Maastricht | 1938/X4 | 94.30 | 0.063 | 0.667 | 1.63 | 0.544 | 5.1 ± 0.4 |
| Maastricht | 1938/X5 | 93.38 | 0.64 | 0.911 | 2.14 | 0.556 | 14.8 ± 0.5 |
| Geistingen hoard | BH 76 | 91.83 | 1.01 | 1.89 | 3.59 | 1.02 | 31 ± 2 |
| Kleve | NS 726 | 93.0 | 0.98 | 1.64 | 3.02 | 1.36 | 12 |
| Kleve | NS 727 | 86.2 | 6.54 | 2.32 | 2.66 | 2.10 | 15 |
| Nijmegen | 1931/2.74 | 85.0 | 7.1 | 3.4 | 3.2 | 1.36 | 19 |
| Vierlingsbeek | NS 750 | 80.93 | 12.72 | 0.06 | 0.01 | 0.04 | out of energy range |
| Ubbergen | AC 20 | 82.24 | 14.21 | 0.076 | 2.32 | 0.75 | 32 ± 3 |

These compositions have been determined through non-destructive neutron resonance capture analysis (NRCA) measurements and are representative for the bulk material of the axes. Local differences, among which surface effects, are not detected with this technique (see section 2.4.9).
The differences in composition suggest that the smiths had to work with metal of various compositions. Flaws in the supply of metal sources and bronze exchange might have led to this situation that is characteristic for the Late Bronze Age and Early Iron Age. (Postma2005, Lechtman1996, section 2.1.3.3).

## 2.3 Forming Bronze

Cold-forging* marks the first phase in the production of useful metal objects, hot-forging* was the next step. Casting* then developed and this was the dominant method used for millennia to shape metals. Details about these processes and strengthening mechanisms will be given in this section.

### 2.3.1 Forging

Forging* can be carried out upon the metal while it is at room temperature (cold-working*) or upon metal heated above its recrystallisation* temperature* (hot-working*). Both serve two purposes: shaping the material and increasing the strength and hardness of the metal. Shaping can only be achieved on sufficiently ductile materials since those can withstand the severe deformation without cracking. The way in which forming contributes to enhancing the strength of bronze through strain hardening will be discussed in section 2.3.3.3. Forging of cast objects occurs when the shape or hardness of the final artefact needs to be altered or when repairs on for example a cutting edge need to be performed.
Cold-forging uses a stone or bronze hammer (in prehistory) to force the cold material in shape on an anvil. When the cold-worked piece becomes too brittle through the forging action, annealing* the metal at an elevated temperature for a certain amount of time recrystallises the metal structure.

New grains will be formed, the dislocation density will be lowered and this leads to softening. This series of cold-working and annealing can be repeated several times until the desired shape is attained. The control of size and shape is higher for cold- than for hot-working bronze.
During hot-forging, the bronze is in a red-hot state (±700-900 °C) while it is being worked, allowing the material to recrystallise during deformation. This keeps the metal from strain hardening and thereby keeps the yield strength* and hardness low and ductility high. The resulting microstructure has fine spherically shaped grains. These grains increase the ultimate tensile strength*, ductility, and toughness of the material. The forging action can be repeated several times since the hot metal stays ductile. However, surface oxidation might occur, resulting in a poor surface finish and impurities in the bronze. (Coghlan1975, Callister2003, Ottaway2008)

When cold-forged, deformation of the whole microstructure can be seen. Deformation lines (slip bands) (for example in Fig. 8 and Fig. 10) appear and pores and some phases get elongated. When a dendritic microstructure is cold-worked, the dendrites are broken up into smaller pieces and deformation of the grains can be seen as well. Ductile phases undergo substantial elongation during hot working. (Lechtman1996, Lascalea2002, Gordon2006).

### *2.3.2 Casting*

Casting is the process of pouring molten metal into pre-shaped forms, called moulds. By casting, complex shapes can be obtained.
The degree of complexity attained differs per method. The most used casting methods in the Bronze Age and the types of moulds in prehistory will be described below.

#### 2.3.2.1 Methods

There are four important prehistoric casting methods (Coghlan1975, Callister2003, Kuijpers2008, Ottaway2008):

*(1) Open-mould casting*
There is little doubt that the earliest method used for casting copper and bronze was the simple open-mould method. A matrix of the shape of the object to be cast is cut into a block of material, mostly sandstone. The molten metal is poured into this cavity and sometimes the mould is covered by a capstone. In that case, the upper surface is less rough and irregular than in a truly open mould. The set-surface of a casting from an open mould is always flat. Therefore it will need modification in order to finish the object to obtain the required cross-section. Gases in the melt can escape from the metal through the open part of the mould, and will hardly leave any porosity behind inside the final product.

*(2) Bi-valve-mould casting*
In order to cast objects that do not have a flat surface, a more sophisticated and widely used method was developed, using closed (bi-valve) moulds. The moulds are made of clay or stone, see also section 2.3.2.2. For objects with a hollow portion, like socketed axes, an internal core in the mould is required, see Fig. 14. So-called metal chaplets* are used to provide additional support for the core during the casting operation if very thin walls are wanted. To allow free escape for air and other gases, venting openings and/or imperfect contact between the two halves need to be present. Inclining the mould during pouring allows gases to escape and ensures complete filling of the mould.

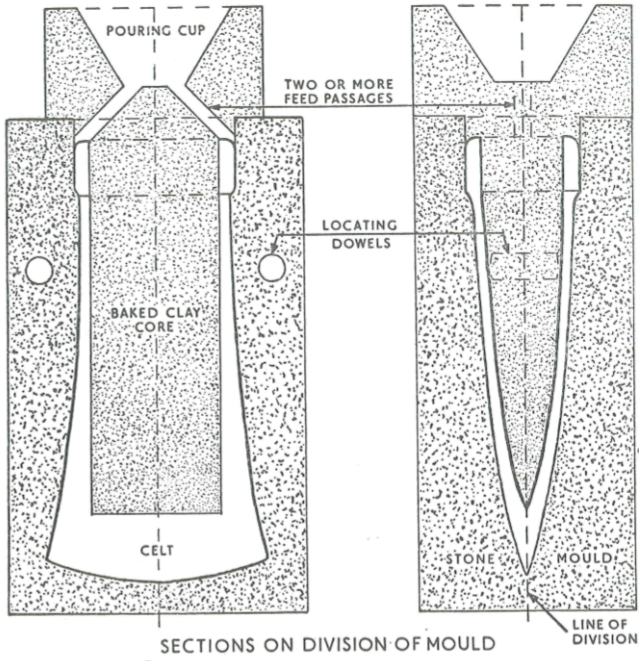


*Fig. 14: Bi-valve casting a socketed axe. Sections of a stone mould with a baked clay core. (Coghlan1975)*

*(3) Cire perdue (lost wax) investment* casting*

For solid *cire perdue* casting, a model in bees-wax is made of the object to be cast and this model is coated with a suitable investment (clay or a clay mixture) to form the mould. The ensemble is embedded in sand or earth and heated to remove the wax. When the mould has been baked, the metal is poured in and allowed to cool, after which the mould is broken away and the casting cleaned and finished.

Hollow *cire perdue* casting has also been used, where a core of clay (mixture) is used. This method has the advantages of a great economy of metal and the possibility to produce fine details. It allows for complex bronze forms to be cast, as the mould does not have to be opened to remove the model.

Although investment casting is an excellent system for casting complex objects in bronze, it calls for considerable skill. One of the difficulties is the free flow of metal to all parts of the work and avoidance of pockets in which gas could be trapped, resulting in porosity in the casting.

*(4) Sand-casting*

Another method, sand-casting, was probably used in prehistory but can hardly be proven since the sand mould leaves hardly remnants any after casting. However, there is some evidence for it in the case of the core material of socketed axes in the Late Bronze Age (Ottaway2008).

### 2.3.2.2 Moulds

The material from which the mould is made must be sufficiently refractory* to withstand the heat of the metal and fire and sufficiently strong to bear its weight. In general, moulds in the Bronze Age were made of clay, stone and occasionally metal (Ottaway2008). Clay moulds are dried after shaping and well baked to make them strong enough for use and to prevent gases from escaping during casting. They can be shaped easily with the help of a model (pattern*). Different conditions apply for stone as the moulding medium, because a pattern is of little help and the matrices have to be carved out of solid stone.

Bronze moulds first appear during the Middle Bronze Age. The metal mould can be considered as an instrument for mass production of well-finished, accurate artefacts and can be used up to an estimate of 50 times (Fontijn2002). There is no difficulty with fusion between the poured metal and the mould, even when the same alloys are used. This is possible because the rapid cooling of the casting is ensured by the considerably larger mass of the mould. Gas and ventilation problems give more trouble than in the case of clay and stone moulds, but by inclining the mould during pouring defective castings are largely avoided.
All types of moulds need to be pre-heated before use to avoid cracking or fracture due to thermal shock upon casting and to prevent the molten metal to solidify before the mould is completely filled. In that way, reasonably non-porous castings in bronze are obtained. (Coghlan1975, Kuijpers2008, Ottaway2008)

Moulds are underrepresented in the archaeological record when compared to the number of metal objects (in the Netherlands about 450 axes and 3 moulds). This would suggest that many moulds were made from materials such as clay and sand, which can disintegrate depending on the temperature at which it was fired prior to casting. More objects than moulds are also expected if re-usable moulds are used. Moreover, the type of axe that could be cast in the three moulds found in the Netherlands is hardly found there. (Ottaway2008, Kuijpers2009)

### 2.3.2.3 Microstructure and Segregation

In general, a cast microstructure of an alloy will show dendrites, see Fig. 12. The secondary arm spacing is a consequence of the cooling rate: the lower the cooling rate, the larger the spacing. The direction in which the dendrites grow is indicative for the direction of the heat flow. (Porter2001)

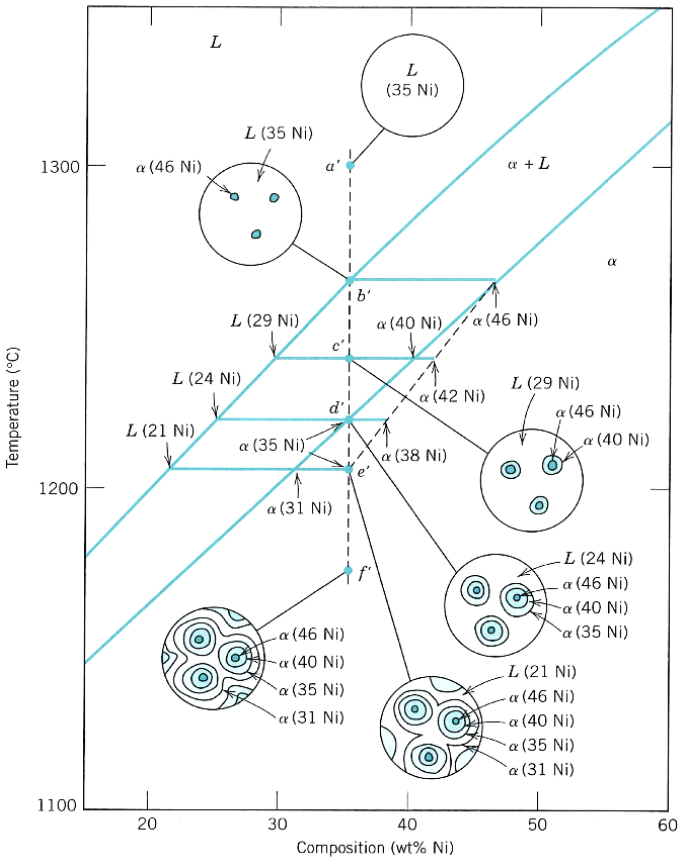


*Fig. 15: Schematic representation of the development of microstructure during the non-equilibrium solidification of a 35 wt% Ni-65 wt% Cu alloy (Callister2003)*

The microstructure of a stone-mould casting is distinctly coarser than that of a metal-mould casting as shown through experimental archaeology. However, this only applies to objects in original as-cast condition, without reheating and working in any way after casting. (Allen1970:35)
Frequently, cast metal is heterogeneous due to segregation, which means that concentration gradients are established throughout the metal on both micro- and macro-scale. Conditions of equilibrium solidification and the development of microstructures are effectuated for extremely low cooling rates and high diffusion rates. In practice, atom diffusion* is a time-dependent phenomenon and if there is not enough time at a certain temperature for the composition to readjust to the equilibrium state, microstructures with compositional gradients will develop. This leads to segregation and this phenomenon is schematically represented in Fig. 15. It is possible that two liquids with different compositions exist and that they cannot mix. In this situation, it is extremely difficult to avoid segregation in the liquid state. (Bailey1954, Eaton1976, Callister2003, Ingo2006, Craddock2009)

***Micro-heterogeneity*** (micro-segregation) is induced by coring. The centre of each grain, which is the first part to freeze, is rich in the element with the highest melting point, whereas the concentration of the low-melting element increases with position from this region to the grain boundary. This is termed a cored structure (see Fig. 16) and it will appear when a heated alloy cools in non-equilibrium conditions. If a casting with a cored structure is reheated, grain boundary regions will melt first, which introduces a thin liquid layer separating the grains. This results in a sudden loss in mechanical integrity.
Coring may be eliminated by a homogenisation heat treatment carried out at a temperature below the solidus point for the particular alloy composition. During this process, atomic diffusion produces compositionally homogeneous grains. However, it is unlikely that this was done in prehistory, since in general a homogenisation for several days at elevated temperatures is needed.

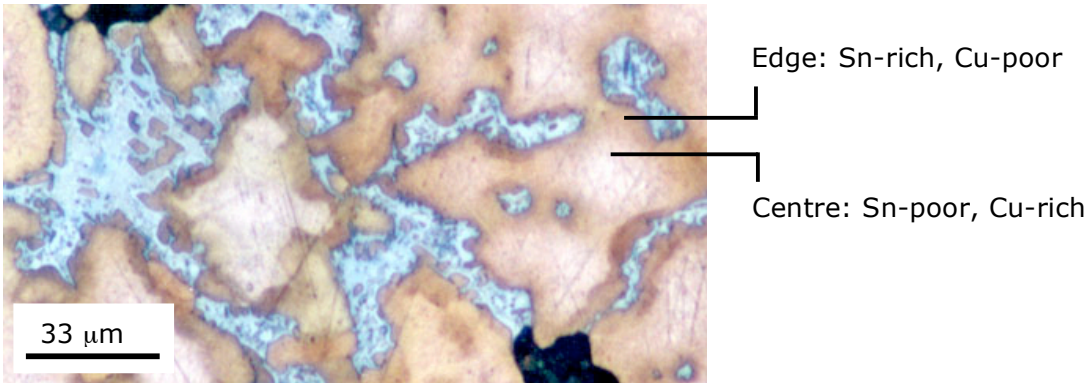


*Fig. 16: Cored structure of as-cast bronze, copper with 10 wt% tin (Cochrane2002).*

***Macro-heterogeneity*** (macro-segregation) shows pronounced concentration of impurities or constituents in certain parts of the casting. There are different types of macro-segregation:

* *Normal segregation*. The usual form of solidification is from the mould walls inwards. In alloys, the liquid solidifying in the centre towards the top and sides may become enriched in one metal or soluble impurity due to selective crystallisation. Similarly, there is a tendency for insoluble impurities and constituents forming at a later stage to be concentrated in the centre of the casting.

* *Inverse segregation (sweating)*. Here, a high concentration of lower-melting elements than copper (for example tin, arsenic, lead and phosphorous) is found at or near the outside of the casting. This can provide a complete outer skin of silver-coloured metal. This phenomenon was sometimes used as a colouring technique in the Bronze Age and could replace plating of metals.

  There are three main explanations for this phenomenon to occur:

  (1) The contraction of the solidified outer shell exerts pressure on the still molten metal inside and forces it through interdendritic channels to or towards the surface.

  (2) The evolving gas during solidification concentrates in the last part of the liquid and creates a pressure with the same effect as (1).

  (3) Molten metal from the centre of the casting is, due to the capillary effect, 'sucked' into the interstices of the dendrites growing inwards because of shrinkage.

  Generally, a high thermal gradient between outside and centre of the casting and a wide freezing range in the metal lead to inverse segregation.
* *Gravity segregation*. Differences in density between the constituents of solidifying metal gives rise to gravity segregation. Especially if the cooling is slow, formed crystals that are denser than the liquid can sink and less dense crystals can rise towards the top.

### *2.3.3 Strengthening Mechanisms*

All crystalline* materials contain dislocations that were introduced during solidification, plastic deformation* and as a consequence of thermal stresses* that result from rapid cooling. A dislocation is a linear defect in the crystal structure around which some of the atoms are misaligned. Plastic deformation corresponds to the motion of dislocations. Movement of dislocations leads to slip bands that can be seen in the microstructure. Strengthening a material implies that greater mechanical forces will be required to initiate plastic deformation, and thus the mobility of dislocations in the crystal needs to be reduced.
There are basically three strengthening mechanisms in single-phase metals and one in multiple-phase metals (alloys), all based on this principle (Callister2003).

#### 2.3.3.1 Grain Size Reduction

The strength of a metal increases with decreasing grain size, which is commonly known as the Hall-Petch relation. The fine-grained metal has a greater total grain boundary area to impede dislocation motion. When the misorientation* between adjacent grains is large, the hindering of dislocation movement is also effective. Grain size reduction improves not only strength, but also the toughness of many alloys. Grain size may be regulated by the rate of solidification from the liquid phase and also by plastic deformation followed by an appropriate heat treatment. During that treatment, the metal will be heated above its recrystallisation temperature and new, strain*-free grains will be formed. Their size depends on the time and temperature of the heat treatment. Larger grains will be the result of a longer time (at constant temperature) or a higher annealing temperature (at constant time).

#### 2.3.3.2 Solid Solution Strengthening

Solid solution strengthening is a technique to strengthen and harden metals through alloying with impurity atoms that go into either substitutional* or interstitial* solid solution. An example is arsenic in copper. These impurity atoms impose lattice strains on the surrounding host atoms. Lattice strain field interactions between dislocations and the impurity atoms are the result.

They increase the resistance to slip and dislocation movement is thereby restricted. This means that a higher applied stress is necessary to first initiate and then continue plastic deformation for solid-solution alloys. This method is thus enhancing strength and hardness.

#### 2.3.3.3 Strain Hardening (Work Hardening*)

This is the phenomenon whereby a ductile metal becomes harder and stronger as it is plastically deformed. The dislocation density in a metal increases with deformation or cold work, due to dislocation multiplication or the formation of new ones. Consequently, the average distance of separation between dislocations decreases. On the average, strain interactions between dislocations are repulsive and the net result is that the motion of a dislocation is hindered by the presence of other dislocations. Thus, the imposed stress necessary to deform a metal increases with increasing cold work. The effects of strain hardening can be removed by an annealing treatment. First, recovery* will take place, whereby some of the stored internal strain energy (that actually is the defect energy of the dislocations) is relieved by virtue of dislocation motion, as a result of enhanced atomic motion at the elevated temperature. When the temperature is increased further, above the alloy's recrystallisation temperature, new strain-free grains will be formed. As a result, the material will be softened.

#### 2.3.3.4 Precipitation Hardening* (Age Hardening*)

The strength and hardness of some metal alloys may be enhanced by the formation of a second phase. Extremely small uniformly dispersed second-phase particles (precipitates) form within the original phase matrix. Their formation can be achieved with a combination of two treatments below the melting temperature, to induce phase transformations. The first is a *solution heat treatment* in which all solute atoms are dissolved to form a supersaturated single-phase solution. For the second or *precipitation heat treatment*, this solution is subsequently annealed at a lower temperature for a certain amount of time to form small precipitates.
These particles inhibit the motion of dislocations and thereby enhance the strength and hardness of the precipitation-hardened alloy. Different alloys require different treatments with appropriate temperatures and durations. Through precipitation hardening, the hardness and strength of the bronze is increased, but at the expense of ductility. This hardening process is sometimes also called age hardening because the alloy strength develops with time.

### *2.3.4 Finishing*

After casting an object and exposing it to further shaping or hardening processes, the surface of the metal object is in most cases finished. Over periods of careful grinding and polishing with the use of sand, grit, water, fleeces and textiles, the desired surface is obtained. Further decoration through engraving of lines, the scribing of dots or impressing the surface to create shapes in relief (repoussée) with a variety of punches, scribes and chisels is evidenced throughout Europe. (Ottaway2008) These treatments can induce changes in microstructure between the surface and the bulk of the object.

## 2.4 Examining Bronze

Archaeometallurgical studies can be carried out using a variety of analytical techniques, both invasive and non-invasive.

This results in information about the (surface) composition of artefacts, the microstructure, mechanical properties, internal corrosion and on the metallurgical processes used in the manufacture. The techniques that can be used will be briefly described in the following sections.

### *2.4.1 Lead Isotope Analysis*

Lead Isotope Analysis (LIA) can provenance metal objects and link them to specific ores, thereby also giving a possibility for dating. The technique is based on the formation of four stable isotopes of lead. The concentration of $^{204}Pb$ corresponds to the original amount in the lead ore and is constant. The relative frequency of the other three lead isotopes is not constant throughout the world and the isotopes are unevenly dispersed in the earth's crust. The isotope abundance ratios depend also on the length of time during which they were able to form. By comparing all possible ratios of the lead isotopes, dating and provenancing of objects containing even trace amounts of lead (like in bronze) to ores is possible with a detection limit of about 30 ppm. A disadvantage is that bronze remelted from different ores and/or objects cannot be dated. (Gale1985, Hauptmann2007, Ottaway2008)

### *2.4.2 Hardness Measurements*

Local (micro-)hardness measurements support the qualitative microstructural information about the properties of the metal. The most used method is that of the Vickers hardness test, that indents a pyramid into the metal.
The resulting hardness number is determined by the load over the surface area of the indentation. The best results are obtained by using a flat, ground and polished specimen. The hardness measurements leave visible traces on the sample, which is a disadvantage. These traces mostly have the spherical or pyramid-shape of the indenter that can have a size varying between approximately 5 and 200 μm. (Allen1970, Coghlan1975, Lechtman1996, Lascalea2002)

### *2.4.3 Optical Microscopy*

Studying the microstructure of a metal artefact by metallographic analysis can determine whether or not an object has been cast, hammered or annealed. The microstructure can be made visible (after polishing and etching the sample) on micrometre scale with optical microscopy with a resolution of about 0.2 μm. However, the smallest details, like precipitates, in the microstructure are not discernable using an optical microscope. The influence of corrosion can also be studied using microscopy. Polarised light can show crystallinity and texture of phases. (Gale1985, Franceschi1997, Hauptmann2007, Ottaway2008, Silva2008)

### *2.4.4 Electron Microscopy*

Electron microscopy serves three goals: it creates an image of the microstructure of the metal on a scale smaller than one micrometre in a Scanning Electron Microscope (SEM), the quantitative elemental composition of phases can be determined locally (spot-analysis, Energy Dispersive x-ray Spectrometry (EDS)) as well as for larger areas with Electron Probe MicroAnalysis (EPMA or sometimes called WDS) and it gives qualitative information about the (local) crystallography (see section 2.4.7) with Electron BackScatter Diffraction (EBSD) as associated devices. These electron techniques are all based on the same principle. The conductive material is exposed to an electron beam, which interacts with atoms in the sample. The electrons that are consequently released from the sample through inelastic collisions with beam electrons are called secondary electrons*.

Secondary electron images show the topography of the surface and provide microstructural information. Back-scattered* electrons are primary electrons emitted as a result of elastic collisions with specimen electrons. The emission intensity and energy is related to the atomic type. Measuring this energy gives quantitative information about the concentration of a certain type of element, with a spatial resolution of about 0.5 μm and detection resolution 0.01% for EPMA, respectively about 5 nm and 0.1% for EDS.
To analyse a material with a scanning electron microscope requires the sample to be conductive. Therefore, non-conductive specimens need to be coated with for example carbon, silver or gold, which is in most cases unwanted. The measurements can be distorted and the sample is contaminated. (Randle2003, Franceschi1997, Lascalea2002, Alford2007, Silva2008)

### *2.4.5 Emission Spectroscopy*

In 1960, 1968 and 1974, the outcome of the Studien zu den Anfangen der Metallurgie (SAM) program resulted in more than 22,000 compositional analyses of copper and bronze objects. The method used was the Optical Emission Spectroscopy (OES) technique, using a spark source and photographic recording. The photons from the spark excite atoms and ions in the sample, which consequently emit characteristic electromagnetic radiation that is measured. In this way, the quantities of certain elements in a sample can be measured. However, this method has large uncertainties and the statistical interpretation of the data was heavily discussed.
During the 1980's, the highly accurate Inductive Coupled Plasma Atomic Absorption Spectroscopy (ICP-AAS) completely replaced OES. This method is a solution-based technique, which is a large disadvantage in the case of archaeological samples since the sample cannot be regained.
It is based on the absorption of light by atomised samples, which is different and characteristic for each element. It therefore gives quantitative information about the amounts of certain elements that are present in the bulk of the sample and trace elements can be detected as well, with a detection limit of about 1 ppm.
(Allen1970, Gale1985, Hauptmann2007, Pollard2007, Ottaway2008)

### *2.4.6 X-Ray Fluorescence*

X-Ray Fluorescence (XRF) is the emission of characteristic secondary x-rays from a material that has been excited by bombarding with high-energy x-rays or γ-rays. This technique is widely used for elemental and chemical analysis and it is able to quantitatively detect trace elements in ppm-levels. The average detection limit lies at about 10 ppm. It is therefore useful to characterise bronze and using the information about trace elements to deduce information about the production process. A disadvantage is that radiation from light elements can hardly be measured and this makes it difficult to quantify elements lighter than sodium. Results from small samples are difficult to interpret, because in that case, the primary radiation beam has larger dimensions than the sample. The resulting high background distorts the measurement. (Rouessac2000)

### *2.4.7 Diffraction Techniques*

The underlying principle of diffraction techniques is to deduce crystalline structures of solid materials by the diffraction of known incident radiation in a non-destructive way. The position and intensity of peaks in both diffraction patterns provide qualitative and quantitative information about the crystalline phases present, texture and stresses present in the sample. The type of incident radiation determines the technique.

When the incoming beam is an electron beam, one speaks of Electron BackScatter Diffraction (EBSD). In the case of x-rays, the technique is called X-Ray Diffraction (XRD). Electrons from the electron beam used have a smaller wavelength than the x-rays from the x-ray beam, which means that more reflections will arise due to constructive interference. Another advantage of using electrons is that the incident beam can be focused such that it irradiates a nanometre-scaled region, while x-rays can only be focused to micrometre-size. However, the diffracted electrons will have a lower angular resolution than their x-ray counterparts. This makes the determination of structures difficult and less reliable than determination with XRD. In both cases, the penetration depth of the sample is maximum 10 μm, which means these are techniques that are probing the surface of the specimen.
For EBSD, the sample needs to be extremely well polished, preferably with an ion beam. This is less crucial in the case of XRD. (Cullity1956, Alford2007)

### *2.4.8 Synchrotron and Radiation Techniques*

High-energy synchrotron x-rays can be used for diffraction and imaging to non-destructively study microstructures. Objects containing highly absorbent lead cannot be analysed with lower energy x-rays, but synchrotron radiation is able to provide reliable qualitative compositional results even with high percentages of lead. This type of radiation permits the use of small beams for diffraction studies as well as phase-enhanced quantitative imaging for higher contrast than traditional x-ray absorption methods. The major problem in conducting this type of measurements is the scarce availability of synchrotron radiation. (Young2006)
In order to determine whether an object is structurally homogeneous, γ-radiographs can be taken. The radiation will be more or less absorbed by different chemical elements (and air) and by sending highly energetic γ-radiation through an object, local differences in absorption can be seen quantitatively. The penetration depth of this type of radiation is in the order of millimetres, like that of synchrotron radiation. However, this is only a useful technique in rather simple and preferably solid objects. (Franceschi1997, Lascalea2002)

### *2.4.9 Neutron Techniques*

Neutron Activation Analysis (NAA) bombards neutrons on objects, thereby activating certain elements that consequently decay. The decay times and products are indicative for the elements present in the object and this makes NAA suitable to analyse compositions.
Another aspect of neutron capture is the occurrence of 'resonances' in the total and capture cross-sections as a function of neutron energy. Neutron Resonance Capture Analysis (NRCA) measures these characteristic resonances and is able to non-destructively and qualitatively identify components in the bulk of an object with a resolution of a few ppm. The activation of the object using this technique is lower than by using NAA. It can also measure certain elements (like thallium) that cannot be measured with NAA. Both techniques have the advantage of being non-invasive. The bulk composition can be measured, but gradients cannot be detected. Neutron sources are not widely available, which makes extensive use of these methods difficult. Another disadvantage is that elements like nickel, lead and iron can hardly be measured with these techniques. (Gale1985, Postma2001, Postma2005)

# 3 Experimental

This chapter will describe how and where samples are taken from the two available Geistingen axes and how there are prepared. The techniques used in this research will be described and specified.

## 3.1 Samples

There are two axes of the Geistingen type available: AC20 from Museum Het Valkhof in Nijmegen (The Netherlands) and BH76 from the Gallo-Romeins Museum in Tongeren (Belgium). Since both objects seem to be cast in a bi-valve mould with a remaining casting seam, the choice was made to take a sample from each half of the axe and one of the casting seam. All specimens are triangular in shape (see Fig. 21 and Fig. 23 in sections 4.1.1 and 4.1.2), so that a cross-section in the length-direction as well as in the width-direction is present.

### *3.1.1 The Nijmegen Axe*

A picture of axe AC20 from Nijmegen can be found in Fig. 17. The Geistingen axe is not intact since a part of the socket mouth is missing (see Fig. 3 for a reference of an intact Geistingen axe). The outside as well as the inside of the axe is covered with differently coloured corrosion products.


*Fig. 17: Picture of the axe from Nijmegen, AC20. Length: ± 12.5 cm.*

In total, four samples (see Fig. 18) are taken from the axe with a jeweller's saw. Some fragments have been scraped with a scalpel before removal to test for corrosion on basis of the colour. One of these samples (#2) is fully oxidised and fell apart during clamping for analysis, two others (#3 and #4) are partly corroded. Samples #1 and #2 come from one half of the axe, #3 comes from the other half. The sample from the casting seam is called #4.

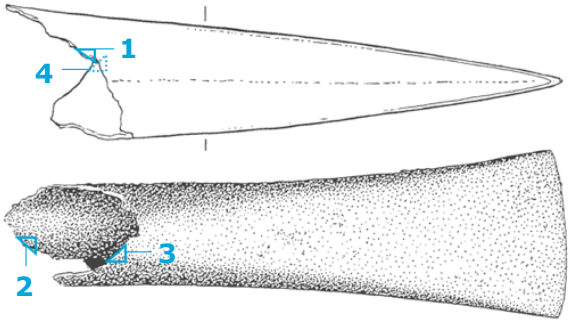


*Fig. 18: Sampling locations on axe AC20 from Nijmegen (Rijksuniversiteit Groningen).*

### 3.1.2 The Tongeren Axe

A picture of axe BH76 from Tongeren can be found in Fig. 19. This axe is damaged as well, the socket mouth is missing here as well. The colour of the axe is rather homogeneous and it looks like the whole object is covered with a dark brown patina.

*Fig. 19: Picture of the axe from Tongeren, BH76. Length: ± 12.5 cm.*

Three samples (see Fig. 20) are taken with a jeweller's saw. Sample #1 comes from one half of the axe, #2 originates from the other side and #3 is a sample from the casting seam.

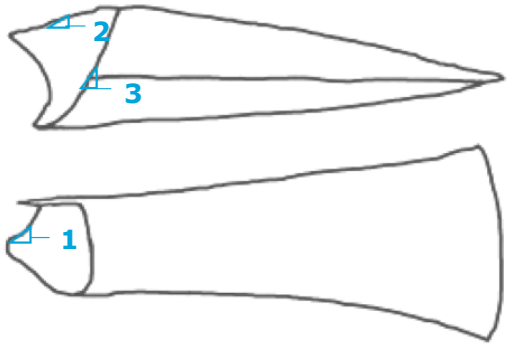


*Fig. 20: Sampling locations on axe BH76 from Tongeren.*

### 3.1.3 Preparation

Different grinding and/or polishing techniques are used to prepare the samples for each technique, while all samples remain unetched:

* X-ray fluorescence measurements are performed on untreated specimens.
* Both the long and the short side of all samples are ground for analysis with the electron microprobe with very fine SiC-**grinding paper** (4000) to remove most traces of sample taking. Due to the small size of the specimens, it was not possible to consequently turn it 90° to prevent scratches. A clear orientation is visible in the optical microscope as a result.
* The long side of sample AC20#1 and the short side of BH76#3 were chosen to be the most interesting for the whole axe, based on their corrosive state and the amount of surface area available for analysis. For electron microscopy and x-ray diffraction, these sides are therefore polished with a colloidal silica emulsion (**OP-S**) to provide a smoother surface. Hereafter, AC20#1 is polished with water, cleaned with methanol and wiped with a soft tissue. BH76 is only rinsed with methanol.
* In order to make these surfaces suitable for electron backscatter diffraction, a **cross-section ion beam polisher** (CSIP, Jeol SM09010 with an argon ion beam) is used for ±22 hours with a voltage of approximately 4 kV and a current of about 15 μA.

## 3.2 Instruments

Several analytical techniques have been used to examine the samples mentioned above. In this section, the technical specifications per method are given.

### *3.2.1 Optical Microscopy*

The samples are visually characterised with a stereomicroscope of Olympus, type SZX9. The magnification range of this microscope is from 63 to 570 times. A stereomicroscope produces a three-dimensional visualisation of the sample and is thus suitable for irregular samples like those in this research.
The samples are clamped in a steel holder to image the short and long sides.

### *3.2.2 Electron Microscopy*

Elemental measurements and the imaging of the microstructure are performed with Energy Dispersive Spectroscopy (EDS) as well as with Electron MicroProbe Analysis (EPMA or WDS). EDS-measurements are conducted in two different devices: the JEOL JSM 6500F and the FEI Nova 600 Nanolab Dual-Beam FIB. EPMA-measurements are conducted in a Jeol Superprobe JX A-8900R.
In all cases, back-scattered electrons are used to create an image of the microstructure and the energies of induced x-rays provide elemental information.
Different accelerating voltages were used, in general ranging from 10-20 kV.
The samples are clamped in a steel holder.

### *3.2.3 X-Ray Fluorescence*

A hand-held XRF-detector is used: Niton XL3t GOLDD with an Ag tube. The sample side to be measured was placed on a thin PP-foil that was stretched in a cup.

### *3.2.4 X-Ray Diffraction*

X-Ray Diffraction (XRD) patterns are recorded in a Bruker D8 Advance diffractometer equipped with a Vantec position sensitive detector. The sample was mounted on a Si {510} substrate and rotated during the measurement.

### *3.2.5 Thermodynamics*

In order to relate experimental results to thermodynamic characteristics, the database program Thermo-Calc is used. This software performs calculations on basis of thermodynamic data to generate for example phase diagrams. Different databases are available. In this research, Thermo-Calc for Windows, version 4, is used with the SOLDER database. This database comprises only ten assessed systems, including the elements silver, bismuth, copper, antimony, tin and lead. Other systems containing these elements are extrapolated. All calculations in this research are performed using atmospheric pressure.

# 4 Results

This chapter will describe the results of the analytical techniques used.

## 4.1 Optical Microscopy

All samples are characterised with a stereomicroscope (see section 3.2.1) and monitored after each preparation step. The most representative pictures of the samples from both axes will be shown here.

### *4.1.1 The Nijmegen Axe*

The outer as well as the inner surface of the axe is corroded, and thus corrosion products are visible on the samples as well. Different types of corrosion are visible as can be seen in Fig. 21. In all cross-sections, some oxidation (black patches) is seen (Fig. 22) and in AC20#4, dendrites are visible.

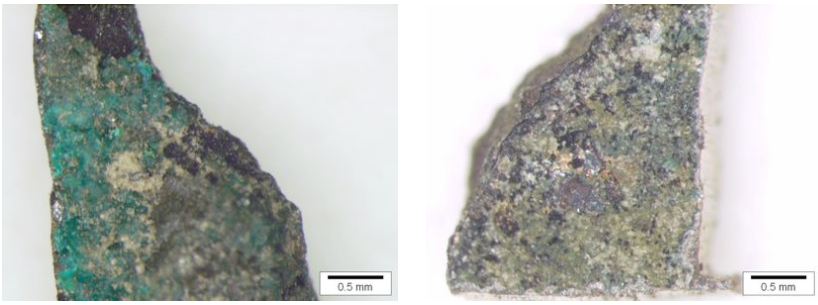


*Fig. 21: Different corrosion products on the inner (left) and outer (right) surface of sample AC20#1 from the Nijmegen axe; optical micrographs.*

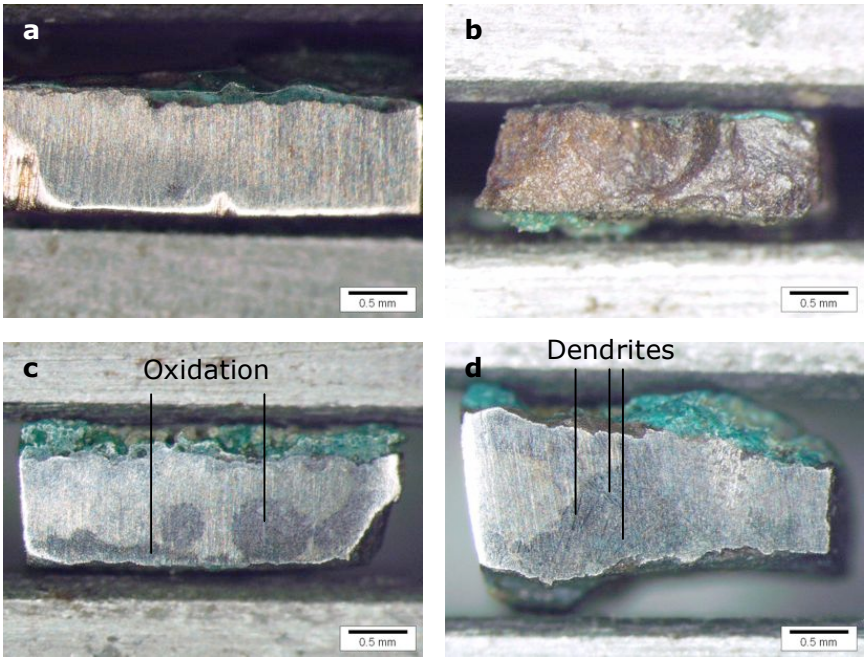


*Fig. 22: Ground (except b) cross-sections of AC20. a: long side AC20#1; b: long side AC20#2; c: long side AC20#3; d: short side AC20#4; optical micrographs.*

### *4.1.2 The Tongeren Axe*

A black patina covers the inner and outer side of the axe, shown in Fig. 23. Sample BH76#2 shows some corrosion in its cross-section (Fig. 24b), the cross-sections of the other samples show no oxidation that is visible with a stereomicroscope. The curvature of the axe walls can be seen in the short-side cross-sections in Fig. 24a and c.

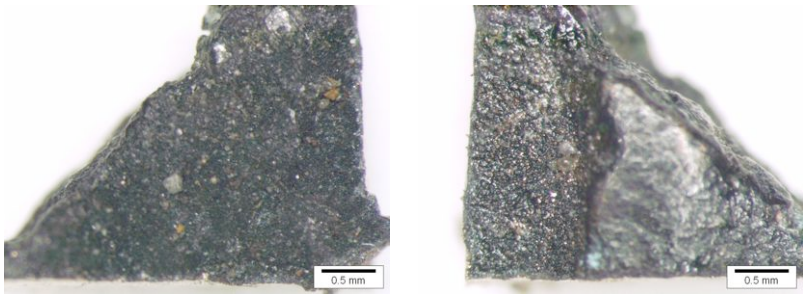


*Fig. 23: Morphology on the inner (left) and outer (right) surface of sample BH76#3 from the Tongeren axe. The casting seam is visible at the outer surface (right). Optical micrographs.*

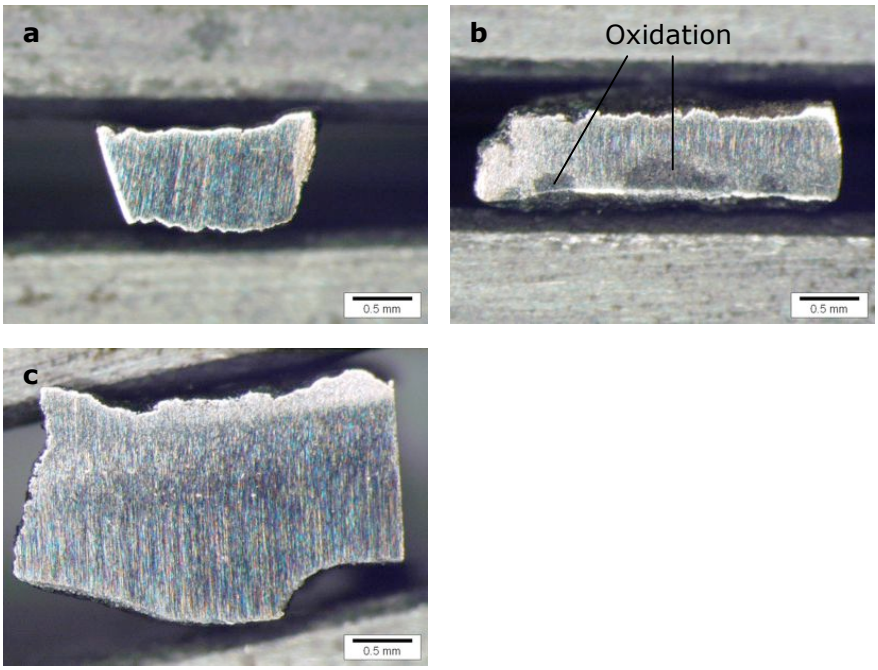


*Fig. 24: Ground cross-sections of BH76. a: short side BH76#1; b: long side BH76#2; c: short side BH76#3; optical micrographs.*

## 4.2 Electron Microscopy - Imaging

Electron micrographs are taken from the long and the short sides of four samples, two of each axe, see Fig. 25, Fig. 26 and Fig. 27.

### *4.2.1 The Nijmegen Axe*

An intact dendritic structure can be identified (grey phase, $\alpha$) on both the long and the short side of AC20#1, with an interdendritic phase (light grey, $\delta$).

On basis of images of the microstructure alone, it is not possible to identify the phase. For phase identification, the stoichiometry has to be known and this is measured with EPMA and XRD, see sections 4.4, 4.5 and 5.2.1 for the results and discussion. On basis of these results, the phases are from this moment on called $\alpha$, $\delta$ and $Cu_2S$. The dendrites have grown from the wall surfaces to the centre. The secondary dendrite arm spacing has an average value of 9 $\mu$m. Particles (black, called $Cu_2S$) in between the dendrites can be seen, with two different morphologies: spherical and star-shaped, see Fig. 25a and d. The average size of the spheres is about 10 $\mu$m, that of the star-shaped ones about 20 $\mu$m. At the short side, two larger spherical copper-sulphide inclusions are found, with a diameter of about 40 $\mu$m. Randomly spread other particles (white, called Ag/PbSb) of about 1 $\mu$m can be sporadically seen and about 0.2% porosity is present too, as well as some oxidation near the wall surfaces.

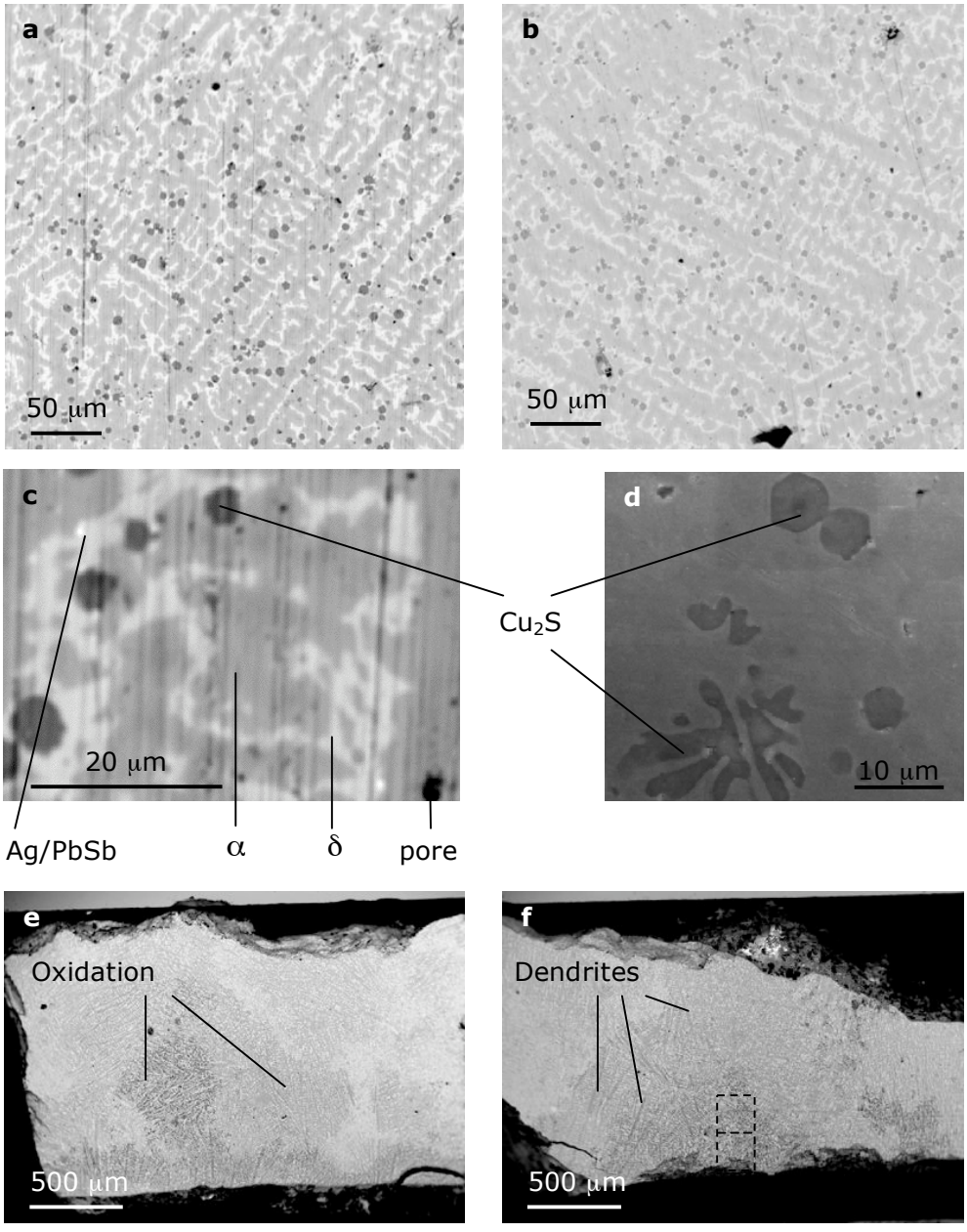


*Fig. 25: Microstructures of AC20. a: long side of AC20#1; b: short side of AC20#1; c and d: details of long side of AC20#1; e: long side of AC20#4; f: short side of AC20#4, magnifications of the indicated areas can be found in Fig. 26. Electron micrographs.*

Sample AC20#4, from the casting seam in the Nijmegen axe, is heavily oxidised and the corrosion products penetrate the axe wall mostly from the outer surface. The darkest parts in Fig. 25e and f represent the most corroded parts. A dendritic structure, which resembles the structure of the non-oxidised parts of the axe, is present, but it is difficult to distinguish the different phases. A closer look at this oxidised microstructure can be found in Fig. 26. At the surface of the axe (Fig. 26, right), the amount of corrosion is higher than closer to the middle of the walls (Fig. 26, left). It is difficult to say which phases are most prone to oxidation.

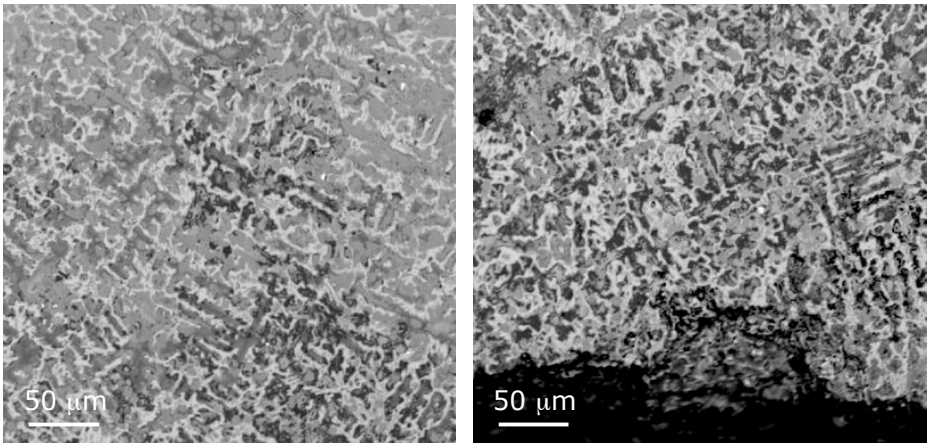


*Fig. 26: Details of the oxidised microstructure of the short side of AC20#1. Electron micrographs.*

The fraction of each phase in the microstructure of the axe from Nijmegen is determined using several electron micrographs of non-oxidised bronze at different scales and averaging the outcomes. The result can be found in Table 2.

*Table 2: Overview of the fractions of phases present in the Nijmegen axe, AC20.*

| | ***Phase*** | ***Fraction*** |
|---|---|---|
| **AC20** | Grey | 0.75 |
| | Light grey | 0.20 |
| | Black | 0.04 |

### *4.2.2 The Tongeren Axe*

In BH76#1, a clear dendritic structure is seen (grey phase, $\alpha$) on both the long and the short side. An interdendritic phase (light grey, $\eta$) is identified. The phase names are deduced in the same way as for the axe from Nijmegen. The dendrites seem to have grown from the wall surfaces to the centre. The secondary dendrite arm spacing has an average value of 14 μm. Particles (black, called $Cu_2S$) in between the dendrites can be seen (Fig. 27e), mainly with a rough star-shaped morphology. Their size ranges between a few micron and about 10 μm. Another type of particles (white, called PbSb) varying in size between about 1 and 5 μm can be seen as well. About 0.3% porosity is present.
The sample from the casting seam from the Tongeren axe, BH76#3, has a comparable microstructure throughout the sample, except for the slightly less structured ordering of phases compared to BH76#1. The same phases are present and in comparable fractions as well. This sample has about twice as much porosity as sample BH76#1, especially in the half of the sample that is close to the inner wall surface.

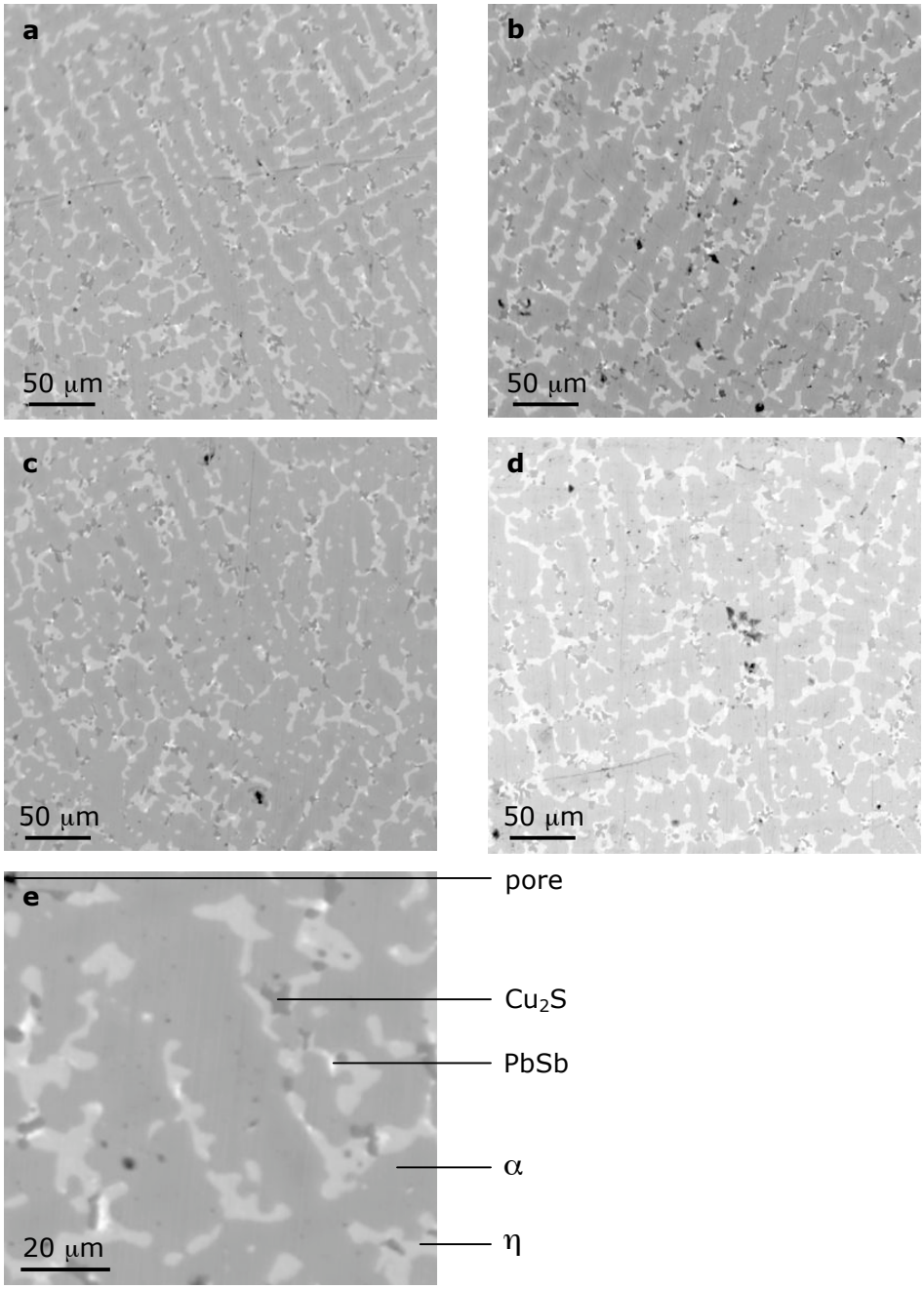


*Fig. 27: Microstructures of BH76. a: long side of BH76#1; b: short side of BH76#1; c: long side of BH76#3; d: short side of BH76#3; e: detail of short side of BH76#3. Electron micrographs.*

The fraction of each phase in the axe from Tongeren is determined in the same way as for the Nijmegen axe and the result can be found in Table 3.

*Table 3: Overview of the fractions of phases present in the Tongeren axe, BH76.*

| | ***Phase*** | ***Fraction*** |
|---|---|---|
| **BH76** | Grey | 0.791 |
| | Light grey | 0.174 |
| | Black | 0.031 |
| | White | 0.004 |

## 4.3 X-Ray Fluorescence

The long and short sides of three samples from the axe from Nijmegen (oxidised sample AC20#2 was unusable since it is completely corroded) and all three samples from the Tongeren axe are subjected to XRF-measurements to determine their average composition. Averaging the values of the six sides will create an average overall composition for the axe, assuming no significant differences between the samples appear. The results for both axes are summarised in Table 4.

*Table 4: Average composition in at% of the axes from Nijmegen (AC20) and Tongeren (BH76) measured with XRF (<DL means below detection limit).*

| | **Cu** | **Pb** | **Sn** | **Sb** | **Bi** | **Fe** | **Ni** | **Ti** | **Co** | **Zn** |
|---|---|---|---|---|---|---|---|---|---|---|
| AC20 | 84 | 0.21 | 11.3 | 1.7 | 0.01 | 0.74 | 1.32 | 0.34 | 0.34 | 0.24 |
| *error* | *5* | *0.01* | *0.8* | *0.1* | *0.01* | *0.05* | *0.09* | *0.07* | *0.02* | *0.05* |
| | | | | | | | | | | |
| BH76 | 89 | 0.7 | 0.6 | 4.4 | <DL | 0.36 | 3.44 | 0.3 | 0.8 | 0.16 |
| *error* | *6* | *0.1* | *0.1* | *0.3* | *<DL* | *0.02* | *0.02* | *2.0* | *0.2* | *0.04* |

## 4.4 Electron Microscopy - Compositional Analysis

Two samples are chosen to be the most interesting of the axes as a whole, on basis of their corrosive state and the amount of surface area available for analysis. The long side of AC20#1 from the Nijmegen axe has the largest non-oxidated surface area and the short side of sample BH76#3 from the Tongeren axe is a cross-section through the casting seam. The local chemical composition of both samples is measured with EPMA on the selected sides.

### *4.4.1 The Nijmegen Axe*

The average composition per phase in AC20#1 can be found in Table 5. There are no significant compositional differences between the spherical and star-shaped particles (the black phase). The composition of the white phase is not quantified, but about ten spot measurements show that half of the particles are composed of nearly pure silver, while the other half contains lead and antimony.

*Table 5: Average composition per phase in at% of the Nijmegen axe measured with EPMA.*

| | **Cu** | **Sn** | **Sb** | **As** | **Fe** | **Ni** | **S** | **O** |
|---|---|---|---|---|---|---|---|---|
| Grey | 88.7 | 6.78 | 0.69 | 0.50 | 0.19 | 2.7 | 0.39 | 0 |
| *error* | *0.6* | *0.08* | *0.02* | *0.03* | *0.02* | *0.2* | *0.02* | *0* |
| Light grey | 67.0 | 19.7 | 3.53 | 0.73 | 0.05 | 9.0 | 0.09 | 0 |
| *error* | *0.6* | *0.2* | *0.09* | *0.06* | *0.02* | *0.7* | *0.03* | *0* |
| Black | 73.0 | 2.48 | 0.50 | 0.17 | 2.41 | 0.31 | 19.1 | 1.85 |
| *error* | *0.5* | *0.03* | *0.01* | *0.01* | *0.02* | *0.01* | *0.3* | *0.01* |

The average composition of the long side of AC20#1 is calculated using the local composition measurements (without gradients) with EPMA (Table 5) and the phase fractions (Table 2). The result is shown in Table 6.

*Table 6: Average composition in at% of the Nijmegen axe (AC20) measured with EPMA.*

| | **Cu** | **Sn** | **Sb** | **As** | **Fe** | **Ni** | **S** | **O** |
|---|---|---|---|---|---|---|---|---|
| AC20 | 83.8 | 9.3 | 1.27 | 0.71 | 0.24 | 3.9 | 0.95 | 0.1 |
| *error* | *0.6* | *0.1* | *0.04* | *0.04* | *0.04* | *0.2* | *0.06* | *0.1* |

Line scans with a step size of 0.5 μm and a spot size of about 0.5 μm through the phases are made. Composition gradients near the edges of the phases are present as can be seen in Fig. 28.

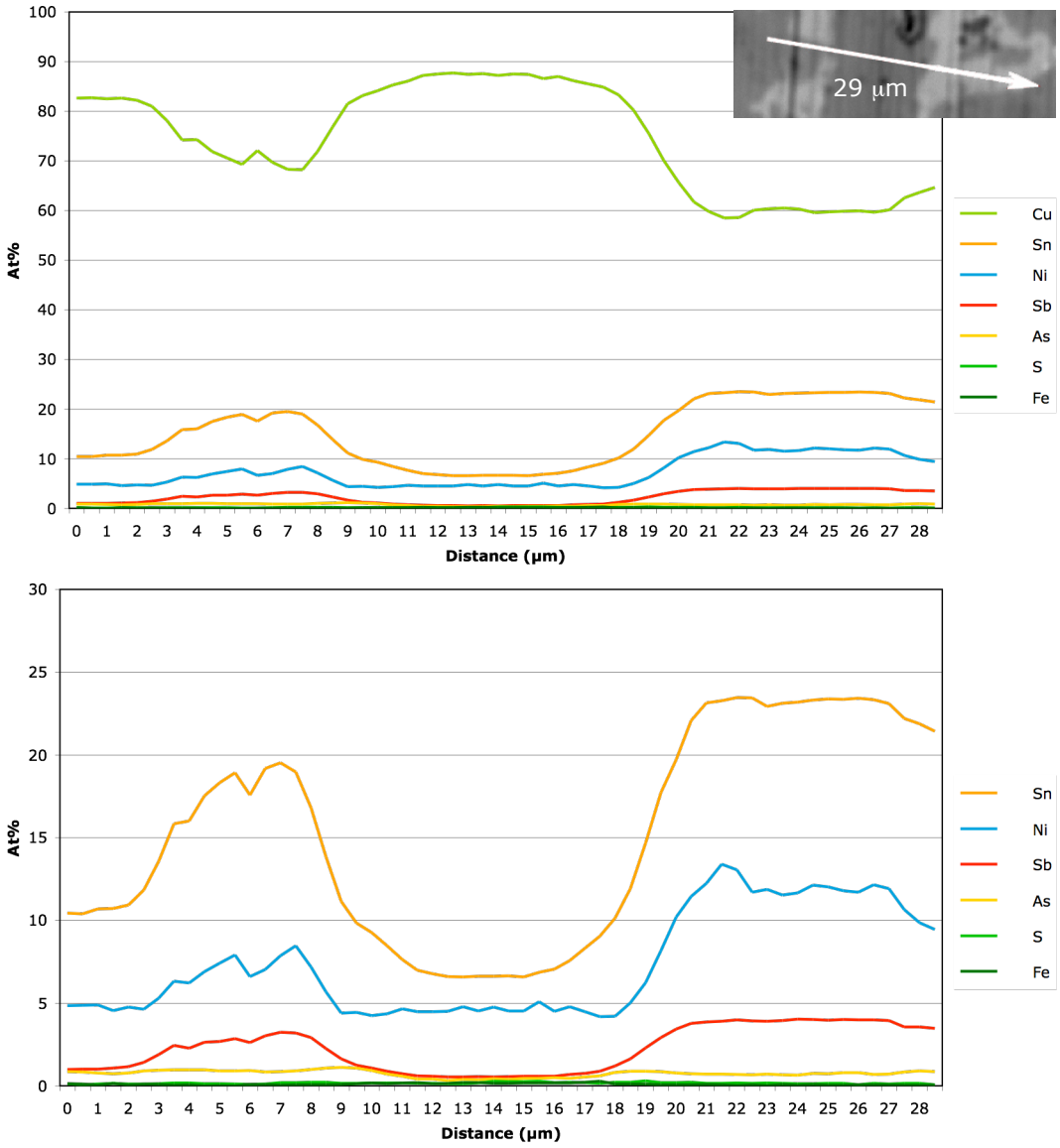


*Fig. 28: Line scan with EPMA through a representative part of the microstructure of the Nijmegen axe (long side AC20#1), showing the (gradients in) composition in at%.*

A qualitative mapping of the main elements measured in AC20 is made with EDS and the result can be seen in Fig. 29. Copper is omnipresent and tin, antimony and nickel are concentrated in the interdendritic phase. Sulphur is predominant in the spherical and star-shaped particles. This is in accordance with the results obtained with the line scan through the microstructure (Fig. 28).

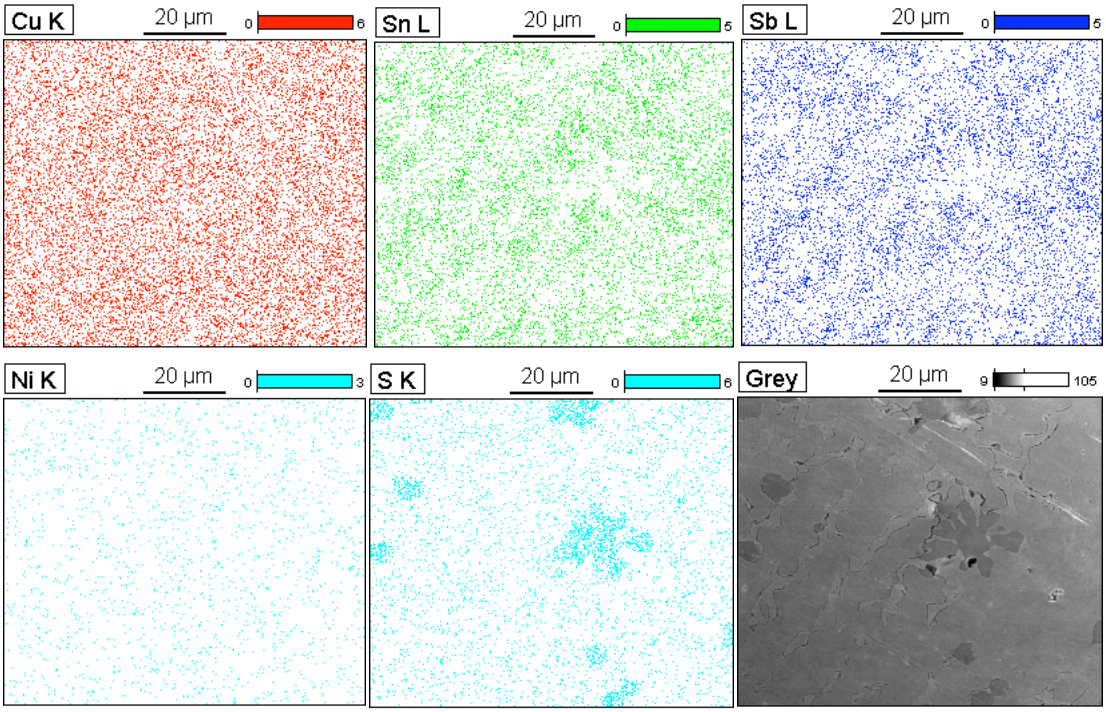


*Fig. 29: Elemental mapping of the microstructure of the long side of AC20#1 from the Nijmegen axe, made with EDS.*

### 4.4.2 The Tongeren Axe

The average composition per phase in BH76#3 can be found in Table 7. The chemical composition of the white phase is not quantified, only spot measurements are done. It is found that all white particles contain both lead and antimony. Since the short side of BH76#3 is a cross-section through the casting seam, the chemical composition on both sides of the seam is measured. It is found that there are no significant differences and that the composition is homogeneous over the width and height of the sample.

*Table 7: Average composition per phase in at% of the Tongeren axe measured with EPMA.*

| | **Cu** | **Pb** | **Sn** | **Sb** | **As** | **Fe** | **Ni** | **S** | **O** |
|---|---|---|---|---|---|---|---|---|---|
| Grey | 89.9 | 0.03 | 0.60 | 2.90 | 2.42 | 0.18 | 3.6 | 0.36 | 0 |
| *error* | *0.4* | *0.01* | *0.02* | *0.05* | *0.08* | *0.02* | *0.2* | *0.02* | *0* |
| Light grey | 50.6 | 0.42 | 1.46 | 18.6 | 6.0 | 0.67 | 22.1 | 0.23 | 0 |
| *error* | *0.3* | *0.05* | *0.04* | *0.1* | *0.1* | *0.05* | *0.7* | *0.02* | *0* |
| Black | 61.7 | 1.34 | 0.21 | 2.24 | 1.10 | 1.21 | 2.4 | 29.9 | 1.85 |
| *error* | *0.3* | *0.02* | *0.02* | *0.01* | *0.05* | *0.06* | *0.1* | *0.5* | *0.01* |

The total average composition of the short side of BH76#3 is calculated using the local composition measurements (without gradients) with EPMA (Table 7) and the phase fractions (Table 3). The result is shown in Table 8.

*Table 8: Average composition in at% of the Tongeren axe (BH76) measured with EPMA.*

| | Cu | Pb | Sn | Sb | As | Fe | Ni | S | O |
|---|---|---|---|---|---|---|---|---|---|
| BH76 | 81.8 | 0.14 | 0.73 | 5.61 | 2.98 | 0.30 | 7.7 | 1.26 | 0.00 |
| *error* | *0.4* | *0.03* | *0.03* | *0.07* | *0.08* | *0.04* | *0.2* | *0.09* | *0.00* |

Detailed line scans with a step size of 1 μm and a spot size of about 0.5 μm through the phases are made. Fig. 30 shows the presence of composition gradients.

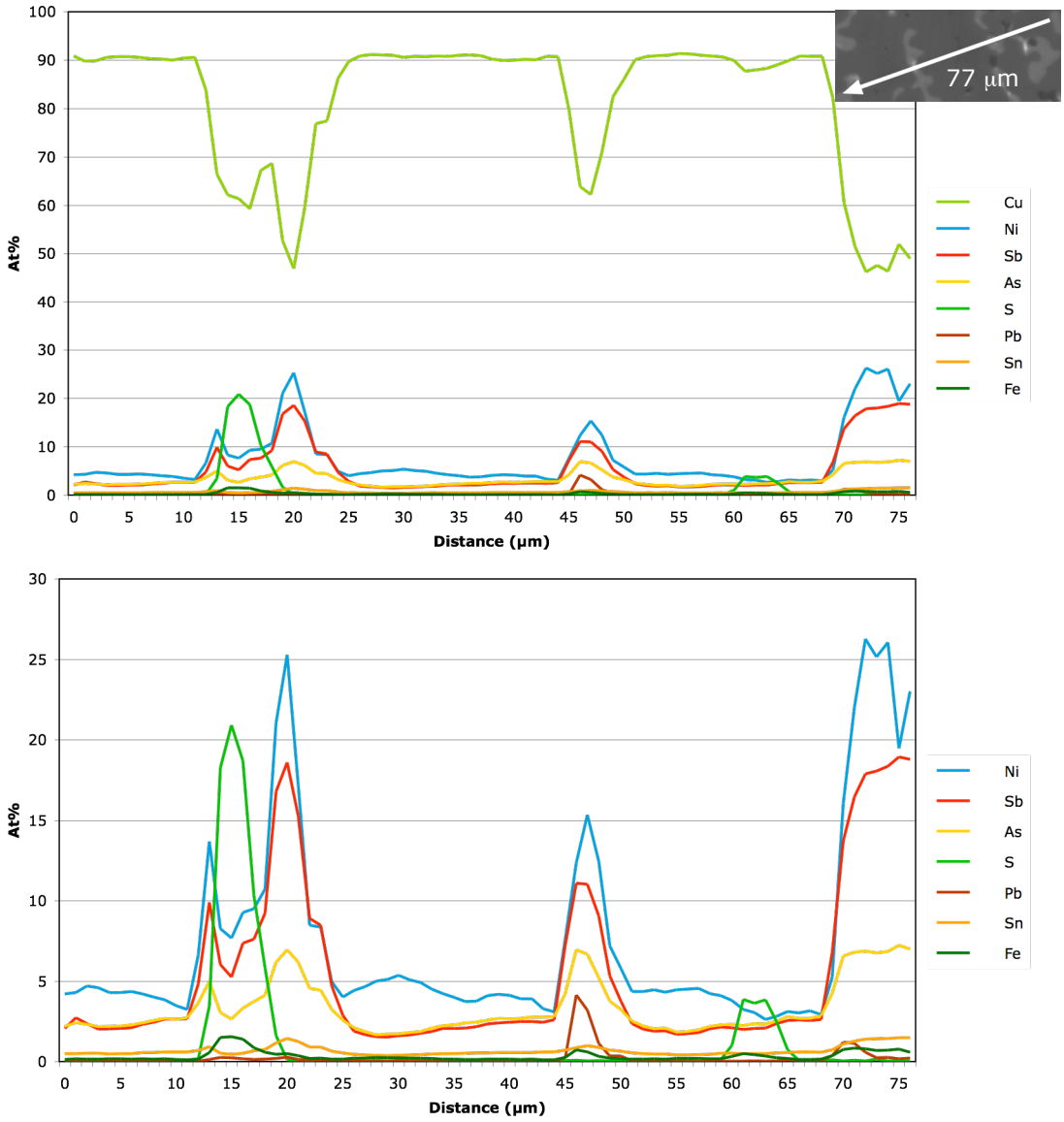


*Fig. 30: Line scan with EPMA through a representative part of the microstructure of the Tongeren axe (short side BH76#3), showing the (gradients in) composition in at%.*

A qualitative mapping of the main elements measured in BH76 is made with EDS and the result can be seen in Fig. 31. Copper can be seen throughout the microstructure. Tin, antimony and nickel are concentrated in the interdendritic phase. Sulphur is mostly present in the particles. This confirms the results obtained with the line scan through the microstructure as shown in Fig. 30.

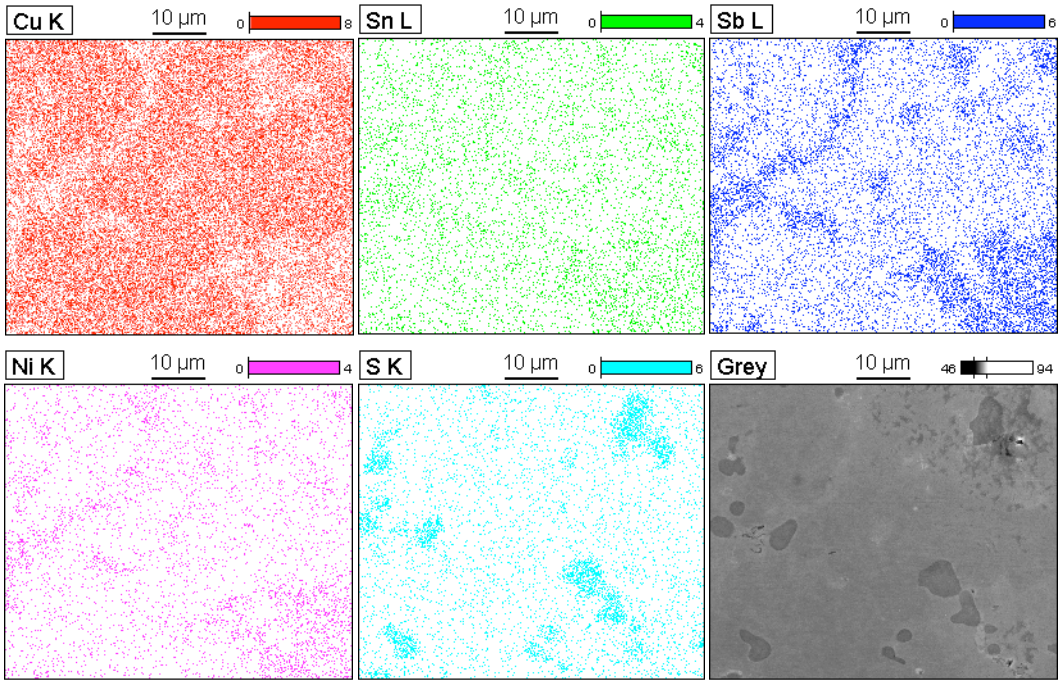


*Fig. 31: Elemental mapping of the microstructure of the short side of BH76#3 from the Tongeren axe, made with EDS.*

## 4.5 X-Ray Diffraction

The recorded diffraction patterns of the axes from Tongeren and Njmegen can be found in the appendix. The peaks of both axes show mainly instrumental broadening.

*Table 9: Peak positions and intensities for the phases found in the axe from Nijmegen (random intensity of one peak normalised to intensity of AC20, denoted with †).*

| Phase | 2θ (°) | Plane | I (random) | I (AC20) | Deviation (%) |
|---|---|---|---|---|---|
| α-CuSn | 49.69 | (111) | 101.4 | 12.8 | -692 |
| | 58.04 | (200) | 4.2 | 6.4 | +34 |
| | 86.62 | (220) | 3.8† | 3.8 | 0 |
| | 107.13 | (311) | 26.2 | 4.1 | -538 |
| | 114.31 | (222) | 7.5 | 1.2 | -524 |
| δ-CuSn | 40.36 | (444) | 1.0† | 1.0 | 0 |
| | 49.99 | (660) | 74.9 | 21.5 | -248 |
| | 55.68 | (664) | 1.2 | 1.2 | 0 |
| | 73.38 | (12,0,0) | 1.9 | 1.9 | 0 |
| | 94.08 | (12,6,6) | 7.0 | 3.6 | -94 |
| Cuprite | 42.56 | (111) | 4.7† | 4.7 | 0 |
| | 49.55 | (200) | 68.3 | 1.9 | -3497 |
| | 72.70 | (220) | 0.8 | 2 | +61 |

In the axe from Nijmegen (the long side of sample AC20#1), three phases can be identified: cuprite ($Cu_2O$), α-CuSn ($Cu_{0.932}Sn_{0.068}$) and δ-CuSn ($Cu_{41}Sn_{11}$). The axe from Tongeren (the short side of BH76#3) contains four identified phases: α-CuSb ($Cu_{0.95}Sb_{0.05}$), ε-CuSn ($Cu_3Sn$), η-CuSb ($Cu_2Sb$) and Pb, possibly with a few percent of Sb in solid solution.
The line positions are not significantly (<0.2%) shifted with respect to the theoretical values for all phases. The intensity ratios of the peaks are different from the ratios for a randomly oriented powder sample, see Table 9, Table 10 and the appendix. It is hardly possible to quantify the amount of each phase present with texture present and lacking calibration data.

*Table 10: Peak positions and intensities for the phases found in the axe from Tongeren (random intensity of one peak normalised to intensity of BH76, denoted with †).*

| Phase | 2θ (°) | Plane | I (random) | I (BH76) | Deviation (%) |
|---|---|---|---|---|---|
| α-CuSb | 50.14 | (111) | 30.6 | 10.8 | -184 |
| | 58.55 | (200) | 6.2 | 4.7 | -32 |
| | 87.49 | (220) | 2.0† | 2.0 | 0 |
| | 108.40 | (311) | 11.9 | 1.8 | -561 |
| | 115.79 | (222) | 2.1 | 0.5 | -321 |
| η-CuSb | 36.86 | (110) | 6.7 | 0.8 | -735 |
| | 40.81 | (111) | 1.1 | 0.1 | -977 |
| | 52.14 | (003) | 4.2 | 0.5 | -740 |
| | 53.14 | (200) | 1.4† | 1.4 | 0 |
| ε-CuSn | 44.37 | (020) | 1.0† | 1.0 | 0 |
| | 48.91 | (002) | 1.0 | 1.4 | +29 |
| | 50.93 | (221) | 5.0 | 4.9 | -2 |
| | 51.01 | (021) | 4.0 | 3.6 | -11 |
| | 68.08 | (212) | 0.7 | 0.7 | 0 |
| Pb | 36.48 | (111) | 3.3 | 1.6 | -106 |
| | 42.37 | (200) | 0.9† | 0.9 | 0 |
| | 61.49 | (220) | 0.9 | 0.8 | -13 |
| | 73.62 | (311) | 0.9 | 1.0 | +10 |

## 4.6 Thermodynamics

Pseudo-binary equilibrium phase diagrams are generated with Thermo-Calc in order to provide the information tailored to the composition of the axes.
As stated in section 3.2.5, Thermo-Calc has a limited amount of data for the calculation of phase diagrams. The data for the copper-tin diagram is acceptable and this diagram will form the basis of this section. A copper-tin alloy with 2 wt% antimony is considered, which resembles the composition of the Nijmegen axe. The assumption is made that the main alloying element is tin, and antimony is the second most important one.

Fig. 32, left, shows the binary equilibrium diagram of copper-tin and Fig. 32, right, shows the pseudo-binary diagram (or cross-section through the ternary diagram) of the copper-tin system with 2 wt% antimony. Details of the most relevant part of the diagrams are shown below.

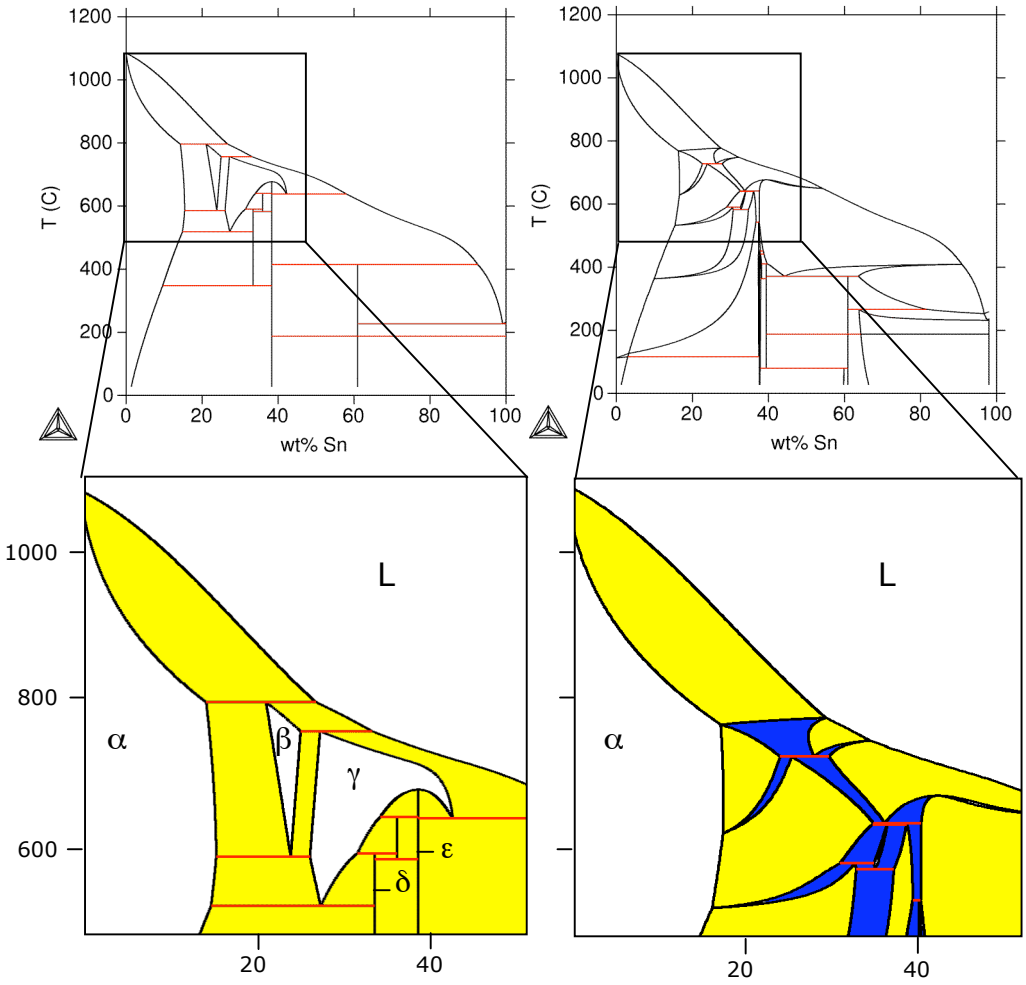


*Fig. 32: Equilibrium phase diagrams of the copper-tin system calculated with Thermo-Calc. Left: binary diagram of Cu-Sn; right: pseudo-binary diagram of Cu-Sn with 2 wt% Sb.*

The copper-tin binary equilibrium phase diagram from literature can be found in Fig. 11. Three-phase regions are absent in the latter diagram and the binary diagram shown in Fig. 32, only single- and two-phase regions are present. The pseudo-binary diagram at the right side of Fig. 32 shows how the Cu-Sn system changes with the addition of 2 wt% antimony, although the amount of data about this system is very limited. The solid solubility limit of tin in copper shifts to higher values. This means that an alloy containing for example 18 wt% Sn at 750 °C, the $\alpha$ phase is present instead of the $\beta$ phase it would consist of when no antimony is added. Three-phase regions appear (blue in Fig. 32), the shape of almost all two-phase regions changes (yellow in Fig. 32) and some single-phase regions, like $\beta$ and $\gamma$, disappear. This has consequences for the resulting microstructure upon cooling. The appearing three-phase regions should be taken into account when the cooling path through the diagram gives an idea about the resulting microstructure of the object. The same can be said about the size of the phase regions.

# 5 Discussion

In this chapter, the results treated in the previous chapter will be discussed. The chapter will be divided in subsections that do not correspond to the sections in previous chapters. In this way, the results of several analytical techniques can be combined and this will give a clearer overview per axe.

## 5.1 Composition

The composition of the axes from Nijmegen and Tongeren were previously measured with different techniques. The whole axes are measured with NRCA, which results in a composition of the bulk of the object, including the corroded surfaces. XRF provided the composition of the cross-sections of the axe walls. The local composition (of the microstructure) is measured with EPMA.

### *5.1.1 The Nijmegen Axe*

The axe from Nijmegen (AC20) can be characterised as a binary copper-tin bronze alloy. Its average composition, based on the combined results of NRCA, XRF and EPMA, can be found in Table 11. Tin is the major alloying element and nickel, antimony and arsenic are the minor alloying elements. Other elements present in amounts less than one atomic percent are lead, iron, silver, sulphur, titanium, cobalt and zinc.

*Table 11: Approximate average composition in at% of the Nijmegen axe.*

| | **Cu** | **Sn** | **Sb** | **As** | **Ni** |
|---|---|---|---|---|---|
| AC20 | 84 | 9 | 2 | 1.0 | 3 |
| *error* | 2 | 3 | 1 | 0.5 | 1 |

The results from NRCA are deviating from the ones obtained with XRF and EPMA. The main differences can be found in the number of elements and their percentages. NRCA only identifies five elements that are present (Cu, Sn, As, Sb and Ag). Lead, nickel and iron are, in addition to organic compounds like oxides and sulphides, hardly detectable with NRCA. XRF is able to measure these elements and they are identified in the Nijmegen axe. Titanium, cobalt and zinc are found in minor quantities (<1 at%) as well. These elements are often remnants of the ores used (Lindgren1933). Silver is an element that is only measured with NRCA and not with XRF and EPMA. The reason why it is not measured with XRF is that the detection limit of Ag is about 1-2 wt% due to the silver tube that is used to generate x-rays. Another disadvantage of the XRF technique is the way in which it deals with samples that are smaller than the spot size, which is the case in this research. It results in a relatively large background and a possible overlap in peaks from tin, antimony and titanium. The background correction is taken into account in the errors shown in Table 4. The amount of overlap is not quantified. Comparison of the composition with the one measured with EPMA shows that this overlap could be a reason for the differences in concentrations tin and antimony in the sample.
EPMA measures a selection of the elements found with the two other techniques, since only a limited amount of elements can be measured at a time due to the limited amount of detection crystals. Spot measurements performed in the electron microscope on parts of the microstructure indicated the main elements that are present.

On the basis of this observation, the choice was made to measure only a limited amount of elements with EPMA: copper, tin, nickel, antimony, arsenic, iron, sulphur and oxygen are chosen in order to get a representative measurement for the axe from Nijmegen. Spot measurements are done on the white particles found in the microstructure and some of them contain silver (see Fig. 25). Unfortunately, there is no quantification made, but it implies there is indeed silver present in the axe.
Another reason for the difference in concentrations between the different techniques is the scale on which the composition is measured and the number of samples. NRCA measures the whole object, including the patina. For XRF and EPMA, small triangular samples of about 2x1x1 $mm^3$ are taken from the axe. The penetration depth of the incoming beams can be responsible for the simultaneous measurement of two phases in the microstructure. However, since this depth is about 0.5-1 μm for EPMA and XRF and the sizes of the phases are larger, it will not cause a large deviation. The aim was to make the sampling locations as representative as possible, but there are limitations and these will be discussed in section 5.2. The long and short sides of three samples are measured with XRF and the results are averaged (the result is shown in Table 4). The average of the long sides of the axe is not deviating more than a few atomic percent from the average of its short sides and this is acceptable. In general, the samples from the axe walls and that of the casting seam show a comparable composition. However, the data of the oxidised sample show a different ratio between copper and tin, while the concentrations of other elements are comparable to the other, non-corroded, samples. Since the absolute numbers from this sample still deviate a few percent from the others, these results are taken into account in the calculation of the average composition of the Nijmegen axe. With EPMA, line scans are made and from these measurements, the composition per phase is deduced (Table 5). Oxygen is measured, but its concentration is zero because only non-oxidised parts of the microstructure are scanned. Pictures of the microstructure, made with the electron microscope, are analysed to deduce the fraction of each phase present. Six pictures with different scales are used and the results are close together, showing a maximum deviation of 7% of the average. The compositional data are combined with the phase fractions and this leads to the average composition of the axe measured with EPMA (Table 6). The composition is locally measured (on micrometre scale) but the data are extracted to macroscale, which induces an uncertainty that is difficult to show in numbers. It leads to the approximation found in Table 11, where the error is an estimation based on the previously mentioned uncertainty and the errors that are inherent to the measurement techniques.

### *5.1.2 The Tongeren Axe*

The axe from Tongeren (BH76) can be identified as a ternary copper-antimony-nickel bronze alloy. Its average composition, based on the combined results of NRCA, XRF and EPMA, can be found in Table 12. Antimony and nickel are present in about 5 at% and are considered as the major alloying elements. Tin and arsenic are the minor alloying elements. Other elements present in amounts less than one atomic percent are lead, iron, sulphur, titanium, cobalt and zinc.

*Table 12: Approximate average composition in at% of the Tongeren axe.*

| | **Cu** | **Sn** | **Sb** | **As** | **Ni** |
|---|---|---|---|---|---|
| BH76 | 86 | 1.0 | 5 | 2 | 5 |
| *error* | 4 | 0.3 | 1 | 1 | 2 |

The results from NRCA are deviating from the ones obtained with XRF and EPMA in the same way and for the same reasons as in the Nijmegen axe. Silver is an exception. This element is only measured with NRCA and not with XRF and EPMA. The detection limit for silver in XRF is too high to detect one percent Ag. Also for the Tongeren axe, the choice is made to let EPMA only measure a limited amount of elements and silver is not included. In the axe from Nijmegen, the white particles in the microstructure are the places where silver was found. In this axe from Tongeren, this type of particles is present as well (Fig. 27). About ten spot measurements show that there is no silver present in any of them. Unfortunately, no quantification is made. Based on these observations, it is concluded that silver is not present in the Tongeren axe.
The long and short sides of three samples are measured with XRF and the results are averaged (Table 4). The average of the long sides of the axe is not deviating more than a few atomic percent from the average of its short sides. In general, the samples from the axe walls and that of the casting seam show a comparable composition. The average composition of the Tongeren axe (Table 7) with EPMA is acquired in the same way as for the Nijmegen axe: the fractions of the phases are combined with the local composition measurements. Six pictures with different scales are used to determine the phase fractions and the results show a maximum deviation of 4% of the average. The results found with the different techniques lead to the approximation found in Table 12, where the error is an estimation based on the previously mentioned uncertainty and the errors that are inherent to the measurement techniques.

Overall, the same type of elements is found in the axes from Nijmegen and Tongeren, with silver as exception. This is partly due to the methods that are used to determine the chemical composition. However, the concentrations of elements present and the ratio between them are very different in the two axes.

## 5.2 Microstructure

The microstructures of two samples from axe AC20 from Nijmegen and two from the Tongeren axe (BH76) are obtained using an electron microscope (Fig. 25 and Fig. 27). The samples used to determine the microstructure of the Nijmegen axe originate from the upper part of the axe (i.e. the part closest to the original socket mouth), see Fig. 18. Sample AC20#1 comes from one half of the axe, AC20#4 is a part of one of the casting seams about 5 centimetres from the original socket mouth. Sample AC20#1 is chosen because it is hardly oxidised and should provide a representative image of the microstructure. The microstructure of sample AC20#4 is obtained to see whether there is any difference in the situation in the casting seam, and to take a closer look at the oxidation. Samples BH76#1 and BH76#3 are chosen for comparable reasons as respectively AC20#1 and AC20#4.
This means that conclusions about the microstructure are drawn using two samples per axe. In order to validate these conclusions, samples from the other half of the axe, the other casting seam and from different locations than the upper part should be examined as well.

### *5.2.1 The Nijmegen Axe*

A microstructure containing dendrites with a rounded outline can be seen in the Nijmegen axe. This type of structure is typical for a cast structure. The solidification direction of the dendrites from the wall to the centre of the axe wall strengthens this hypothesis. Also, mostly spherical pores are present, which is characteristic for a casting as well. The dendrites do not seem to be broken, which means that probably no subsequent working of the object took place.

The average chemical composition per phase is determined with EPMA measurements (see Table 5). The dendrites are mainly composed of about 88 at% copper, 7 at% tin and 3 at% nickel. It is argued in section 5.1.1 that the Nijmegen axe is essentially a binary copper-tin alloy. The composition of the dendrites given above gives no reason to discard this assumption, although the addition of nickel can give rise to the formation of different phases.
The database program Thermo-Calc (described in section 4.6) does not have specific data for the ternary Cu-Sn-Ni system. Therefore it is unfortunately not possible to deduce the influence of nickel on tin-bronze with Thermo-Calc. However, based on literature (Gupta2000) it is possible to extract this information. Nickel is soluble in copper for almost all nickel percentages and over a temperature range from about 350-1100 °C. This means that the addition of nickel to tin bronze will probably not induce three-phase regions, but nickel will dissolve in copper. The properties of the alloy do change, that is, it strengthens through this solid solution (section 2.2.6.3).
The binary equilibrium Cu-Sn phase diagram will be used to deduce the phases present in and between the dendrites. In principle, a pseudo-binary or ternary diagram of Cu-Sn-Ni should be used to deduce the phases present. But because of lack of data, the binary diagram of copper and tin is used instead. When a line is drawn in this diagram for 7 at% tin, the $\alpha$-phase is the resulting phase for the dendrites for about 350-800 °C. This means that the dendrites probably are composed of a solid solution of tin (and nickel) in copper. This is confirmed by the results of XRD, where the $\alpha$-phase is identified as $Cu_{0.932}Sn_{0.068}$, which means that about 7 at% tin is dissolved in copper. The ratio between copper and tin is indicative for the phases present, as can be deduced from the phase diagram. For a solid solution, a range of ratios is possible. In the case of a tin bronze, this ratio can vary up to 90 for the $\alpha$-phase, whereas a phase like $\delta$ has an almost fixed ratio of 41/11.

There seems to be one interdendritic structure, according to the details that can be resolved in an electron microscope. The average chemical composition of this phase is about 67 at% Cu, 20 at% Sn, 3 at% Sb and 9 at% Ni. When the alloy is still considered as a binary copper-tin alloy, the phase to be formed with this composition based on EPMA is not clear. The results from XRD are able to clarify the situation. The $\delta$-CuSn phase is identified ($Cu_{41}Sn_{11}$), in addition to the $\alpha$-phase just described. When the ratio between copper and tin is calculated from the EPMA results, this $\delta$-phase is not the outcome. A plausible hypothesis for this difference is that the interdendritic phase is actually a two-phase structure, containing the previously mentioned $\alpha$ and $\delta$. The numbers for the concentrations of copper and tin indicate that there is enough of both elements to form $\alpha$ as well as $\delta$, as long as Cu/Sn=41/11 in order to form $\delta$ and less than 90 to form $\alpha$. It is possible that the $\alpha$ phase found in the interdendritic space has a different composition than that of the dendrites. The $\alpha$-phase is able to contain a solid solution of nickel, as previously stated, but also of antimony. This element is soluble in copper up to about 6 at%, over a temperature range of about 350-1100 °C (ASM1992). This theory could thus explain the presence of antimony and nickel as well. One can wonder why then this structure is not seen in the electron micrographs, or in the x-ray diffractogram. A few explanations can be given. It is possible that the $\alpha$-phase with two different concentrations is indeed measured with XRD, but that the concentration differences are indiscernible because their lattice parameters are so similar. Also, since there is texture in the sample, the volume fractions of the phases cannot be quantified. It is thus not possible to distinguish different $\alpha$-phases with the current XRD measurement. The two-phase structure can be so finely dispersed that the resolution of the electron microscopes used is not high enough to show it. This is the case when the size of the separate phases is less than approximately 5 nm.

It is hard to depict the position of this phase in the binary phase diagram since the exact composition of α+δ and the relative phase amounts are unknown. However, an estimate can be made based on the fraction of interdendritic phase compared to the dendritic phase, and the average chemical composition. A graphical representation can be found in Fig. 33.
It should be kept in mind that by using this binary equilibrium diagram, a simplification of the situation is made. Furthermore, it is assumed that the dendritic α-phase contains 7 at% Sn and the average of the Nijmegen axe contains 9 at% Sn. Since 75% of the microstructure is composed of the dendritic phase, 0.75*7=5.25 at% of the total percentage of tin is concentrated in the dendrites. This means that the other 9-5.25=3.75 at% Sn should mainly be concentrated in the interdendritic region. This phase accounts for 20% of the microstructure, so 20% times the 'α+δ'-concentration should be 3.75%. This means the concentration tin in α+δ should be about 19 at%, which is confirmed with EPMA-measurements (Table 5). If this is true, the amount of α in the two-phase region is very small and the microstructure will predominantly show δ.

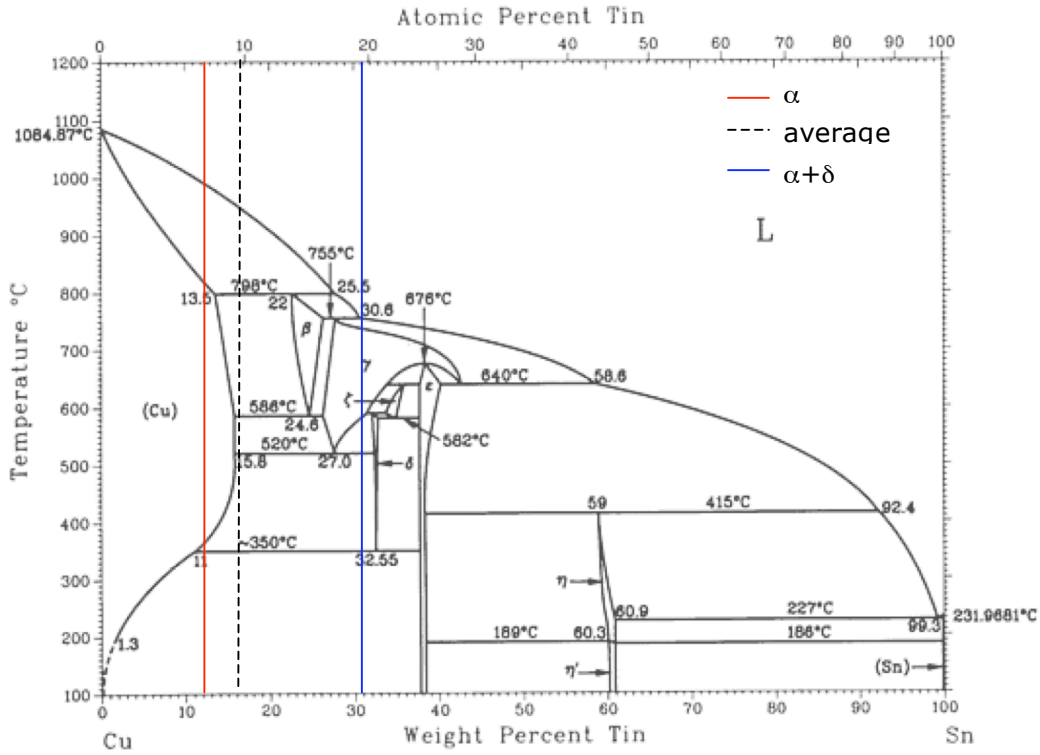


*Fig. 33: Binary equilibrium copper-tin phase diagram, used to designate the location of the phases present in the Nijmegen axe. (ASM1992)*

Spherical and star-shaped copper-sulphide particles are identified in the microstructure of the Nijmegen axe. The copper-sulphide particles (both star-shaped and rounded) are identified as $Cu_2S$ based on the EPMA measurements in this phase. However, a few other elements are found in this phase as well, like about 2 at% Fe, 2 at% Sn and 2 at% O. It is known that elements like these assemble in this type of inclusions (Muhly1973, Ronen1993, Lechtman1999, Segal2005). In all cases analysed, the sulphide inclusions are remnants of the ore. Since these are collections of different elements that do not appear elsewhere in the microstructure in significant amounts, it is assumed that these inclusions formed in the melt.

Experiments done in an archaeological setting show that this is indeed the case for an arsenic bronze smelted from the ore, in a crucible with a maximum temperature of about 1150 °C (Lechtman1999). The same morphologies with a volume fraction of about 5%, just like in this research, are formed: spherical and star-shaped (dendrite-like) $Cu_2S$. Unfortunately, no other data or information about the morphology and forming of these particles can be found in literature. While studying the $Cu_2S$-inclusions in the electron microscope, a hint of substructures within the spherical particles was visible, but it could not be mapped with sufficient accuracy. When looking at the equilibrium phase diagram of copper and sulphur, it is seen that $Cu_2S$ solidifies at a temperature of approximately 1130 °C. This could be a reason for the possible substructure: only a part of the copper-sulphide from the ore was able to melt and to contain the solute atoms like iron. With EPMA, very localised and limited line scans are made and it could well be possible that these substructure effects are averaged in this type of measurement. More research needs to be done on this research to extract conclusive information about the presence of these inclusions.

Smaller silver and lead-antimony particles are sporadically seen throughout the microstructure, but not observed with XRD. A reason for the absence of these lead- and silver-containing phases could be that the particles are too small to be detected and that the amount of this phase is too small to result in a discernable reflection. However, spot-measurements with EPMA confirm that silver and lead-antimony precipitates are present. Silver is often encountered in tin bronze since it could be a component in copper-containing ores and it is often encountered in lead containing ores like galena as well. (Muhly1973, Pigott1999, Lindgren1933). It is a noble metal and hard to remove from the melt by reduction or oxidation. The melting point of pure silver is 962 °C. The binary tin-bronze with 9 at% Sn starts to solidify at approximately 950 °C, as can be seen in Fig. 33. A plausible explanation is that the pure silver starts to solidify while the rest is still liquid. In that case, the particles will stay in the liquid, even when the dendrites start to solidify. It is dragged along with the melt until it ends up between the dendrites and the interdendritic phase. It indeed looks like that in Fig. 25. However, there is no clear distinction in morphology and location between these particles, which can be either pure silver or a lead-antimony alloy in the microstructure. But the same process of getting trapped between the dendrites and the interdendritic phase is possible for the lead particles. Lead has a very low solid solubility in copper for every temperature and will thus always form a precipitate. Antimony is able to dissolve in lead, without affecting the lattice parameter with more than a few percent. Both elements are often found in copper-containing ores (Lindgren1933) and this can be an explanation why antimony ends up in a lead particle.

One phase is not yet treated in this microstructure description. This phase is cuprite, or $Cu_2O$, which is measured with XRD in AC20#1. It is indeed present in the Nijmegen axe, but not in the centre of the axe walls. It is probably part of the patina, which is not imaged. Spot-measurements on corroded parts in AC20#4, which are not quantified, show the presence of oxygen in the sample. It is assumed that the dendritic microstructure of this latter sample (from the casting seam) is the same as for the non-oxidised parts. However, this is difficult to see since the different phases are hardly distinguishable. In this research, no efforts are made to find out what the type and origin of the corrosion is. It could be a coincidence that the sample from the casting seam looks more susceptible to oxidation. More research on this topic and on more samples from the Nijmegen axe in the future will result in more information about the similarity of the microstructures in the casting seam and the rest of the axe.

There is one other aspect of the composition of the Nijmegen axe that will be treated here, since the explanation of it probably lies in the formation of the microstructure. As can be seen in Fig. 28, concentration gradients appear in the EPMA line scan for all elements present in the bronze near the edges of the $\alpha$- and $\delta$-phases. Over a range of about 6 measuring points (which corresponds to 3 $\mu$m) a difference in composition of 10-20 at% can be seen for tin and copper. It is normal that there is a transitional region from one phase to the other, simply because the solubility of a given element is different in the different phases. It is also possible that such a gradient is a result of the way in which the line scan is made. If the spot size is larger than the step size, overlap between the different measurements can result in a gradient. The spot size is approximately 0.5 $\mu$m and the step size is 0.5 $\mu$m. This means that there is overlap of about 0.25 $\mu$m, so an overlap of maximum two points. The penetration depth of the electron beam is approximately 0.5 $\mu$m, but it is possible that it is the cause of overlap of phases. But this depth is much smaller than the size of the dendrites, so it can result in maximum several measuring points. The appearing gradients thus seem to be a consequence of diffusional processes. A faint change in grey tone over the width of the dendrite is visible in detailed microscopy images as well, where the centre of the dendrite has the darkest colour. This leads to the hypothesis that the diffusion in the interdendritic $\alpha+\delta$ is faster than in the $\alpha$-dendrites so that a concentration gradient establishes in this latter phase due to coring. However, the position of the line scan is not so precise that the exact position of the spot can be deduced. Some calculated values for the temperature-dependent diffusion coefficient can be found in Table 13. These values show that copper diffusion in the $\alpha$-phase is faster than in the $\delta$-phase. For tin, the diffusion in the $\alpha$-phase is faster than in the $\delta$-phase. Regarding the compositional gradients in Fig. 28, the behaviour of these two elements should be the same. This gives rise to the presumption that the calculated temperature-dependent diffusion constants might be incorrect. Since only diffusion constants are known for (in this case) copper and tin in pure copper, it was assumed that this coefficient does not significantly change when copper is alloyed. Obviously, this is a simplification of reality and the EPMA results show that this assumption is incorrect. However, since no reliable and realistic data are available, a better approximation to the concentration gradients cannot be made at this point. Unfortunately, this leads to the fact that no arguable hypothesis can be made about the amount of segregation on basis of diffusion models.

*Table 13: Temperature-dependent diffusion coefficients for copper and tin in $\alpha$ and $\delta$ (Landolt1990).*

| **Element** | **In phase** | **D ($m^2s^{-1}$)** | **T (°C)** |
|---|---|---|---|
| Cu | $\alpha$ | $6.8 \times 10^{-20}$ | 450 |
| Cu | $\delta$ | $2.1 \times 10^{-13}$ | 450 |
| Sn | $\alpha$ | $2.4 \times 10^{-18}$ | 450 |
| Sn | $\delta$ | $2.3 \times 10^{-22}$ | 450 |

Finally, the texture present in the microstructure of the Nijmegen axe will be discussed. There is no significant broadening of the peaks, only instrumental broadening. Also, the shift in line position is insignificant. This implicates there is no strain or stress present in the sample. In other words, these parts of the axe are probably not worked.
The intensity ratios of the peaks of the $\alpha$-phase are different from the theoretical randomly oriented powder sample. This indicates that certain crystallographic orientations are favoured while some are not: texture seems to be present.

Per measured phase, one of the peaks from the random oriented sample is scaled to the corresponding measured peak of the Nijmegen axe. The other measured peaks from that same phase mostly show a deviation from the theoretical values. The deviation from the theoretical values is calculated on basis of the peak intensity read from the pattern. It should be kept in mind that an uncertainty, which is difficult to quantify, appears here, especially if peaks from different phases overlap. It is also important to mention that a flat surface instead of a powder sample is used to record the pattern. When this surface contains large grains, or dendrites in this case, differences in peak ratios will appear. This does not automatically mean that this is texture, only that a large part of the measured surface has a certain orientation.
A large, positive deviation of the measured peak with respect to the random oriented sample means that the peak in the Nijmegen axe has a higher intensity than the theoretical value and that that orientation is favoured. This is the case for the $\alpha$-(220)-peak. The $\alpha$-(111)-, $\alpha$-(311)- and $\alpha$-(222)-planes have a negative deviation and are thus underrepresented in the sample. The dendrites thus have a certain orientation. This is expected when one looks at the microstructure and sees the direction in which they have grown: from the axe wall to the centre. In principle, the (111)- and (222)-planes represent the same set of planes and their deviations should be equal. This is not the case and it is not clear why. The observed texture can only give information on the production process if it is compared to known texture, for e.g. wrought or cast bronze. This comparison could unfortunately not be made in this research, also because there is no literature found on this specific bronze. Next to the scaled peak, two of the five $\delta$-phase peaks do not show a deviation from random orientations. This means that there hardly is any texture in this phase. The cuprite phase shows large deviations. This phase is predominantly found in the patina, which has not been analysed in this research. It is therefore not possible to conclude anything about the deviations found.

### *5.2.2 The Tongeren Axe*

The axe from Tongeren displays a dendritic microstructure where the dendrites have a rounded outline. As for the Nijmegen axe, this type of structure is typical for a cast structure, just like the solidification direction of the dendrites from the wall to the centre of the axe wall. The microstructure contains mostly spherical pores, which is also characteristic for a casting. The sample from the casting seam shows a slightly less ordered microstructure and more porosity than the samples from the axe wall. This structure is seen throughout the whole sample, with no significant changes near the outside or inside surface of the axe. However, the dendrites do not seem to be broken into pieces. Therefore it is still assumed that probably no subsequent hot or cold working of the object took place.

The average chemical composition per phase is deduced using EPMA measurements (see Table 7). The dendrites are mainly composed of about 90 at% copper, 3 at% antimony, 4 at% nickel and 2 at% arsenic. It is argued in section 5.1.2 that the Tongeren axe is essentially a ternary copper-antimony-nickel alloy. The composition of the dendrites given above gives no reason to discard this assumption. The database program Thermo-Calc (section 4.6) does not have any data for the ternary Cu-Sb-Ni system. Therefore it is unfortunately not possible to deduce the appropriate equilibrium pseudo-binary or ternary phase diagram with Thermo-Calc. However, based on very scarce literature (Sibata1941) about the ternary copper-antimony-nickel diagram it is possible to extract some information. Nickel forms a solid solution with Cu-Sb over the entire range of antimony and up to 6 wt% Sb in the $\alpha$-CuSb phase.

This means that there probably is a solid solution of copper, tin and antimony in the dendrites (where the conversion to wt% leads to about 3.5 wt% Ni, 5.5 wt% Sb and 2.3 wt% As) and this phase is called $\alpha$. Unfortunately, information about the temperature range for the phases is missing for the ternary diagram. Arsenic is also able to dissolve in pure copper up to 7 at% (see Fig. 9) and it is assumed this is also the case in the dendrite phase in the Tongeren axe. The recorded XRD pattern for this axe confirms that there is a solid solution of $\alpha$-CuSb that is identified as $Cu_{0.95}Sb_{0.05}$. The concentration of antimony in the sample is thus underestimated in this case.
However, it should be kept in mind that there might be a comparable $\alpha$-phase in the interdendritic region as well, with a slightly different composition. XRD is in that case hardly capable to distinguish these phases (as explained for the Nijmegen axe).

The average chemical composition of the interdendritic phase is about 50 at% Cu, 19 at% Sb, 22 at% Ni and 6 at% As. Also about 1 at% Sn is present in this phase. In principle, the alloy is still considered a ternary copper-antimony-nickel alloy. However, there are so many additional elements involved that the situation becomes very complex. XRD measurements are able to help out just a little. This technique identifies two phases, in addition to the previously mentioned $\alpha$, that match the composition of the elements in the interdendritic space. These are $\varepsilon$-CuSn ($Cu_3Sn$) and $\eta$-CuSb ($Cu_2Sb$). When the ratio between copper and tin is calculated from the EPMA results, this $\varepsilon$-phase is a possible outcome. However, there is only a small amount of tin found in the interdendritic phase, namely ± 1 at%. It would therefore be no surprise if also $\alpha$-copper-tin is present. In that case, the composition could be located in the two-phase region $\alpha+\varepsilon$. The peak positions and intensities correspond well to the theoretical values of the $\varepsilon$-phase. The reflections of a solid solution of copper and tin are not very different from those of a solid solution of copper and antimony. It is not unlikely that the peaks of these two phases overlap and thus both could be present. Therefore it is assumed the $\varepsilon$-CuSn phase is a part of the interdendritic region containing both $\alpha$- and $\varepsilon$-CuSn, even though there is no substructure found at the scale that is accessible with a scanning electron microscope. The same is true for the $\eta$-CuSb phase. For the sake of clarity, the interdendritic phase is still called '$\eta$', comparable to section 4.2.2. However, the presence of the high concentration of nickel still needs to be explained. XRD measurements did not identify any phase containing nickel, but this does not exclude its presence. One explanation is that the nickel forms a solid solution with copper and antimony, which is not detected by XRD. However, there is far too much nickel present to dissolve in the $\alpha$-CuSb phase (Sibata1941) and probably a different phase will form. No information about this process is found in literature, unfortunately, so no conclusions can be drawn about the presence and distribution of nickel. Arsenic is able to form a solid solution with copper and antimony, so it is assumed that this is also the case for the antimony present in the interdendritic phase. On the basis of the available information it is not possible to depict the position of this phase in a phase diagram since the exact phase structure of the interdendritic and the relative phase amounts are unknown. To check whether there is an $\alpha$-CuSb phase in the interdendritic region, the binary equilibrium diagram is used, which of course is a simplification of the real situation. However, an estimate can still be made based on the fraction of interdendritic phase compared to the dendritic phase, and the average chemical composition. A graphical representation can be found in Fig. 34. It is assumed that the dendritic $\alpha$-phase contains 3 at% Sb and the average of the Tongeren axe is 5 at% Sb. Since 79% of the microstructure is composed of the dendritic phase, 0.79*3=2.4 at% of the total percentage of antimony is concentrated in the dendrites. This means that the other 5-2.4=2.6 at% Sb should mainly be concentrated in the interdendritic region.

This phase accounts for 18% of the microstructure, so 18% times the 'η'-concentration should be 2.6 at%. This means the concentration antimony in the interdendritic region should be about 14 at%. That could be possible regarding the concentration of about 19 at% measured with EPMA. It is therefore plausible that there is also α-CuSb in the interdendritic region. However, the η-CuSb phase is identified with XRD, for which a higher percentage than 19 at% Sb should be present, see Fig. 34, or the material is cooled under non-equilibrium conditions. Again it should be mentioned that these calculations have been done for a simplified composition of the Tongeren axe and under equilibrium conditions.

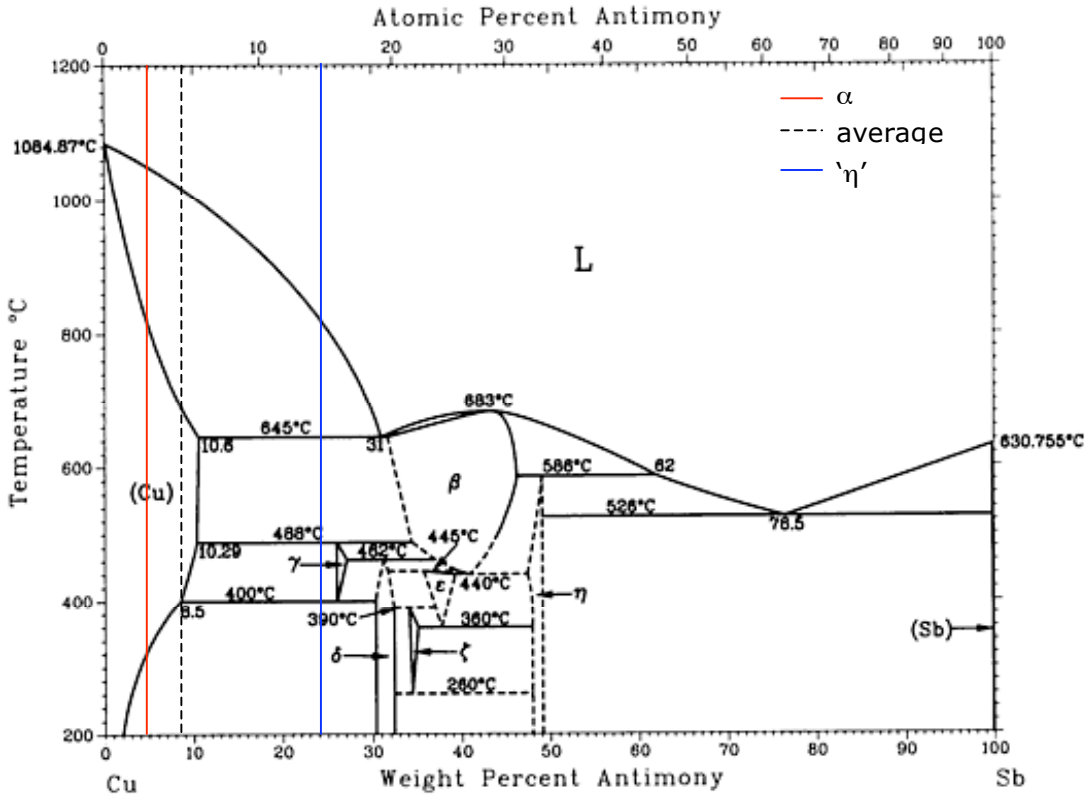


*Fig. 34: Binary equilibrium copper-antimony phase diagram, used to designate the location of the main phases present in the Tongeren axe. (ASM1992)*

Star-shaped copper-sulphide particles are identified in the microstructure of the Tongeren axe and are identified as $Cu_2S$ based on EPMA measurements. However, a few other elements are found in this phase as well, like about 1 at% Pb, 2 at% Sb, 1 at% As, 1 at% Fe, 2 at% Ni and 2 at% O. It is known that oxygen, lead and iron are remnants of the ore that can assemble in this type of inclusions (Muhly1973, Ronen1993, Lechtman1999, Segal2005). In a few EPMA measurements, the size of the spot is approximately the same as the size of the sulphide particles. It is then well possible that a part of the neighbouring phase is measured as well. This can explain the apparent presence of antimony, arsenic and nickel. As in the Nijmegen axe, it is assumed that these particles have formed in the melt and ended up between the dendrites and the interdendritic phase.

Small lead-antimony particles are seen throughout the microstructure, close to the sulphide particles. XRD identified indeed a lead-phase. Antimony is able to dissolve in lead up to a few atomic percent, without affecting the lattice parameter with more than a few percent.

In that case, it is hard to discriminate this PbSb-phase from pure lead with the XRD-measurement performed in this research. The same process of getting trapped between the dendrites and the interdendritic phase as the sulphide particles is assumed for the lead particles as argued for the Nijmegen axe.

Also in this axe, small concentration gradients appear in the EPMA linescan for all elements present in the bronze (see Fig. 30) near the edges of phases. Approximately 2-3 points (2-3 μm) are involved. This can probably be explained in the same way as for the axe from Nijmegen: the diffusion in the interdendritic phase is faster than in the α-dendrites. A concentration gradient establishes in this latter phase due to coring. However, the influence of the penetration depth of the incoming electron beam and the overlap between two steps should also be taken into account as part of the explanation.

Finally, the texture present in the microstructure of the Tongeren axe will be treated. As is the case in the Nijmegen axe, there is no significant broadening of the peaks, only instrumental broadening. The shift in line position is insignificant. Both characteristics lead to the conclusion that these parts of the axe are probably not worked.
The intensity of the peaks of the α-CuSb phase deviates from the theoretical randomly oriented powder sample. The peaks of α-(111), α-(200), α-(311) and α-(222) all have a negative deviation. The α-(220) is therefore probably the only plane that is favoured, even though this is the peak on which the theoretical values are normalised. The dendrites thus seem to have a certain orientation. When the microstructure of a cross-section of the axe wall is studied, it indeed shows that the dendrites have grown from the axe wall to the centre. The texture is in principle only useful for the analysis when it is compared to known texture for e.g. wrought or cast bronze. This comparison is not made in this research, also because there is no literature found on this specific bronze. Like in the Nijmegen axe, the (111)- and (222)- planes do not have the same deviation and it is not clear why. The same type of texture as for the α-phase is found for the η-phase: three of the four reflections have a negative deviation. The (200)-peak is the scaled peak for the η-phase. Since the other peaks are underrepresented in the sample, it is possible that the (200)-plane is the favoured crystallographic growth direction for $Cu_2Sb$. The ε-CuSn phase hardly shows any deviation from the theoretical values, which implicates this structure has an almost random orientation. In the lead-phase, the intensity of the (111)-plane is half as strong as the random value, but the (220)- and (311)-planes have an almost identical intensity as their theoretical value. It is therefore concluded there probably is no texture present in this phase.

## 5.3 Production

The results that are discussed in the previous sections will lead to an answer on the research question of this thesis: How are Geistingen axes made? That will be discussed in this section for both axes, mainly by comparing the two.

The axe from Nijmegen and the axe from Tongeren have approximately the same size, as far as can be deduced since they are both damaged. Their appearance is different, though, based on the colour and type of patina on the in- and outside. The Nijmegen axe is covered with a rough, greenish patina, while the surface of the Tongeren axe is predominantly smooth and dark brown. It is thought this is mainly due to the environments where these objects have been buried for about 3000 years, which are probably different for both axes. This could also account for the amount of oxidation inside the axe walls.

The Nijmegen axe is corroded through and through on some locations, while the Tongeren axe hardly contains oxidation products. However, more research should be done on this subject to be conclusive.

Casting seams are present on both axes, but the sample from the Tongeren axe has a more pronounced difference in thickness of the wall than the one from Nijmegen. It should be kept in mind that these samples only represent a small part of the casting seam, so it is possible that this is just a coincidence. Based on the porous dendritic microstructure with metallic and $Cu_2S$-inclusions, it is assumed that both axes are cast. Also, the hollow shape of the axes suggests a casting technique, probably using a bi-valve mould. Furthermore, the dendrites do not seem to be broken up and the pores are not elongated. The XRD-patterns do not show significant peak shifting. This indicates that no subsequent working of the axe has taken place on the sampling locations. However, it is still possible that the cutting edge of the axes is worked in order to sharpen it. Sampling the edge and analysing its sample in the same way as the samples in this research should verify this.

The microstructures of the axes are comparable: a dendritic matrix with rounded dendrites and an interdendritic phase. Porosity is found in both axes, but there is a higher fraction of pores present in the axe from Tongeren. Copper-sulphide particles are found in both axes, just like small lead-antimony particles. The Nijmegen axe contains spherical and star-shaped $Cu_2S$-particles, while the axe from Tongeren only contains star-shaped ones. Silver particles are found in the Nijmegen axe, but not in the Tongeren axe. The compositions of the phases are different from each other, which is partly due to the differing composition. The dendrites are both $\alpha$-phases: $\alpha$-CuSn in the Nijmegen axe and $\alpha$-CuSb in the Tongeren axe. The interdendritic phase could hardly be identified in the latter case, but it does contain $\eta$-CuSb and $\varepsilon$-CuSn. In the axe from Nijmegen, the interdendritic phase is identified as $\alpha+\delta$-CuSn. In both cases, nickel, tin and antimony concentrate in the interdendritic region. It is remarkable that two different copper-tin phases form in the different axes. Two complementing explanations can be given. One is the different amount of tin in the sample. With an average of 1 at% Sn in the axe from Tongeren, either $\alpha$ or $\alpha+\varepsilon$ can be formed, according to the equilibrium phase diagram. If the average amount of tin is higher, like 9 at% in the Nijmegen axe, there are more possibilities for phases to form. Which ones ultimately form in that case is mostly dependent on the cooling rate. The two-phase structure $\alpha+\varepsilon$ will form for both compositions when the melt is rapidly cooled from the liquid to typically 250 °C. If the melt is cooled to 450 °C, $\alpha$ will form in the case of 1 at% Sn, while $\alpha+\delta$ is formed for 9 at% Sn. It is therefore assumed that a different cooling rate is applied for both axes, even though the situation is too complex to be conclusive. A simple measure for the cooling rate is the secondary dendrite arm spacing. Their empirical relation can be expressed in an equation of the following form (Hwang1998):

$$\lambda = 101 \cdot R^{-0.42} \qquad \textit{Eq. 1}$$

where $\lambda$ is the secondary dendrite arm spacing in $\mu$m and $R$ the cooling rate in °$Cs^{-1}$. The constants in this equation are derived for a phosphor bronze containing approximately 7 % Sn. The calculated value for the secondary dendrite arm spacing in the Nijmegen axe is 9 $\mu$m and for the axe from Tongeren, $\lambda$=14 $\mu$m. This leads to cooling rates of respectively 316 °C/s and 110 °C/s. These are indeed different. The Nijmegen axe seems to be cooled faster than the Tongeren axe, which is an explanation for the difference in composition gradients found. A faster cooling will lead to a microstructure with more micro-segregation, since there is not enough time for diffusion to an equilibrium structure.

Coring will then appear within the dendrites and it is stated that that is indeed seen in the Nijmegen axe (see section 5.2.1). Consequently, the appearance of micro-segregation is less pronounced at a lower cooling rate, comparable to that of the Tongeren axe.
As argued in section 5.2, the copper-sulphide particles are the first to solidify. It is assumed that these particles are formed in the melt. This means that the temperature of the melt should at least be 1130 °C. If it is assumed that the Nijmegen axe is rapidly cooled to 450 °C (according to the existence of the δ-CuSn phase), this leads to a solidification time of approximately 2 seconds. It could be possible to achieve this with water cooling, although the estimation of the cooling rate is probably too high. The Tongeren axe is assumed to be rapidly cooled to 250 °C (because the ε-CuSn phase is present), which indicates a solidification time of approximately 8 seconds, a more realistic value.

Compositional measurements by XRF and EPMA show that the axes contain the same type of elements, but in different concentrations. It is argued that the axe from Nijmegen is a copper-tin bronze, while the Tongeren axe is a copper-antimony-nickel alloy. However, antimony and nickel are found in the first axe and tin in the latter one. They both contain sulphur, lead, and traces of iron, titanium, cobalt and zinc. One exception is silver. This element is found in the Nijmegen axe, but not in the Tongeren axe. However, it is not unlikely that it will be measured when the small particles are measured again and more systematically. This suggests that the same type of raw material is used for both axes, but in different quantities. To show that it is indeed possible to make two axes with different compositions using the same types of ore in different ratios, an example is given here. Suppose there are three ore-types available: fahlerz, cassiterite and cuprite. Their hypothetical composition in at% is given in Table 14. This table also shows that when these ores are mixed with a fahlerz:cassiterite:cuprite ratio of 3:1:3, the composition of the Nijmegen axe is obtained. Mixing the raw material with a ratio of 50:1:9 results in the composition of the Tongeren axe (see Table 14). In this example, a few assumptions are made. First of all, only the main elements in these types of ore are taken into account. This automatically leads to the composition of the main components in the two Geistingen axes. However, as stated before, more elements are present in both axes: sulphur, lead, and traces of iron, titanium, cobalt and zinc. Silver is also found in the axe from Nijmegen. It is assumed that all these elements are present in the ores, mainly in the fahlerz (Lindgren1933, Arlt1998, Gainov2008). Cassiterite and cuprite are both oxidised ores. In the microstructures of both axes, there is hardly any oxygen found, but the patinas have not been analysed. XRD shows the presence of cuprite in the Nijmegen axe and it is stated that this phase is mainly present in the patina. When these ores are indeed used, oxygen is expected somewhere in the axe. If it is in minor quantities, the extraction of tin and copper from the ores is well established. It should be kept in mind that fahlerz, cassiterite and cuprite are examples of ores that could have been used.
Experimental archaeology (Lechtman1996) confirmed that a similar microstructure like the ones of these Geistingen axe is formed when ores are used. This co-smelting experiment was carried out using a temperature of about 1150 °C and the molten material was allowed to cool to ambient temperature without the aid of a cooling agent. However, little is known about what the microstructure would look like if bronze objects would be recycled, so molten and re-cast. More information needs to be known in order to conclude on this topic. However, the shape of the different phases and the different components suggest that Geistingen axes are produced by smelting.

*Table 14: Hypothetical composition in at% of three types of ore and the resulting axe compositions in at% after mixing these ores with two different ratios.*

| | **Cu** | **Sn** | **Sb** | **As** | **Ni** |
|---|---|---|---|---|---|
| Fahlerz | 45 | 0 | 3 | 1 | 3.5 |
| Cassiterite | 0 | 35 | 0 | 0 | 0 |
| Cuprite | 67 | 0 | 0 | 0 | 0 |

| | | | | | |
|---|---|---|---|---|---|
| Nijmegen (3:1:3) | 84 | 9 | 2 | 1 | 3 |
| Tongeren (50:1:9) | 86 | 1 | 5 | 2 | 5 |

## 5.4 Recommendations

To be more conclusive about some subjects, further research needs to be done. Several recommendations will be given in this section.

The compositional and microstructural measurements are analysed on a limited number of samples. The obtained data becomes more complete and thus more reliable when more samples are measured. Samples from different locations than the upper half of the axe are desirable as well. This is also the case for the determination of the microstructure. The conclusions about the microstructure are drawn using two samples per axe. In order to validate these conclusions, samples from the other half of the axe, the other casting seam and from different locations than the upper part should be examined as well. A sample from the cutting edge can clarify if working took place there. It could also serve as a reference for the other samples, of which now is stated that no working has taken place.

The composition of the silver/lead-antimony particles in both axes needs to be quantified in order to derive more information about the production process from them. Also, the presence of silver in the Tongeren axe can then be excluded.

XRF measurements are performed on the scale of the samples. For clarity and comparison, the same measurements should be done on micrometre scale and on the bulk of the axes. Micro-XRF measurements will complement the data obtained in this research, just as XRF on the whole axe will. A disadvantage of the latter analysis is that mainly the surface of the axe will be measured, which will make the comparison harder.

There is still uncertainty about the type of phases present in both axes. The first method to be tried is chemical etching of the samples with ferric chloride. This etchant evidences the grain structure and is able to show possible substructures in the interdendritic space. More information about coring or severe segregation can be revealed in this way as well.
EBSD can be more conclusive on the type of phases present in the different parts of the microstructure and about substructures. The recorded patterns will be indexed to known phases, so any knowledge about the phases present beforehand is necessary. EBSD cannot be performed on an etched specimen.
Special texture measurements for long times with XRD on the strong reflection peaks will give more and more detailed information about the phases and texture present.

With the correct reference measurements, the fraction of the phase can be identified as well. Combined with the current information, this will give more insight in the cooling trajectory of the axes.
Longer measuring times with XRD might also prove whether the phase identified as pure lead in the Tongeren axe is in fact a solid solution of antimony in lead.
Another way to identify the phases present or possible substructures in the microstructure is using Transmission Electron Microscopy (TEM). This technique is able to see microstructures on nanoscale when a very thin cross-sectional sample is used.
It is not clear from this research whether the found $Cu_2S$-inclusions contain substructures or not, and why two types of morphologies are found. The first problem can be clarified when TEM is used. A more structural approach with EPMA and/or an electron microscope with a large spatial resolution will also help, if the microstructure and its composition are locally mapped. More literature research and eventually experiments can help answering the questions about morphology.

More literature research to find reliable diffusional data for the bronze systems in this research could provide more information about the kinetics and the amount of segregation in the two axes.

Lead isotope analysis on samples from the Geistingen axes from Tongeren and Nijmegen might provide additional information on the types of ores used and possibly about their provenance.

A more systematic characterisation of the present corrosion products and the patina is recommended. EPMA can identify the type of oxidation in the microstructure as well as determine which phase is most prone to corrode. Also the patina can be analysed using electron microscopy. Electrochemical measurements can provide more information about this latter subject as well.

# 6 Conclusions

Two bronze Geistingen axes, one from Nijmegen and one from Tongeren, are examined and analysed in order to answer the question 'How are they produced?'.

The first conclusion that can be drawn is that the Nijmegen axe is characterised as a binary copper-tin bronze, while the Tongeren axe is regarded as a ternary copper-antimony-nickel alloy. Both axes possess a porous dendritic microstructure with an interdendritic phase, which is typical for a cast material. In between these phases, $Cu_2S$- and lead-antimony particles are present. The axe from Nijmegen also contains silver particles in addition to the previously mentioned ones. It is assumed that these particles all originate from the raw material, namely the ores used, and that they are formed in the melt.
This leads to the following conclusion: both Geistingen axes are produced by smelting and casting. It is thought that the same types of ore are used to produce these specific axes since the same type of elements appear in the final object. However, the ratio of these elements is different for both axes, so the ore ratio should be different as well.

The melt of both axes has been at least at a temperature of 1150 °C, based on the presence of $Cu_2S$-particles. Probably, both objects are water-cooled after pouring the liquid in the bi-valve mould, according to the secondary dendrite arm spacing. The Tongeren axe has a lower cooling rate than the Nijmegen axe. This means that probably a more efficient way of cooling has been applied in the latter case.
The dendrites do not seem to be broken up and the pores are not elongated. The diffraction patterns do not show significant peak shifting. This all indicates that no subsequent working of the axes has taken place on the sampling locations. However, it is still possible that the cutting edge of the axes is worked in order to sharpen it.

**In conclusion, the two Geistingen axes are produced by co-smelting the same types of ore in different ratios. The bronze is consequently cast into a bi-valve mould. This is then water-cooled to let the object solidify. No subsequent hot- or cold-working has taken place.**

# Glossary

**α-Cu.** Copper with an *FCC* crystal structure.

**Age Hardening.** See *precipitation hardening*.

**Alloy.** A mixture of two ('binary alloy') or more metals in order to alter the end product to have the right combination of characteristics for a specific application.

**Annealing.** A generic term used to denote a heat treatment wherein the *microstructure* and, consequently, the properties of a material are altered. It frequently refers to a heat treatment whereby a previously *cold-worked* metal is softened by allowing it to *recrystallise*.

**As-cast.** The state of a metal when *melted* and poured from a *crucible*, without any treatment after *casting*. Similarly *as-forged*.

**Back-scatter electron.** An electron that is scattered from a surface by primary incident particles of sufficient energy.

**Binary equilibrium phase diagram.** A graphical representation of the relationship between temperature and composition of a binary *alloy* under equilibrium conditions.

**Brittleness.** Ability to undergo hardly any *plastic deformation* before fracture (i.e. low ductility).

**Bronze Age.** In Europe, this is the period between roughly 2200 and 800 BC.

**Bronze.** A binary *alloy* of copper and another metallic element, like tin or arsenic. When a third alloying element is present, it is called a *ternary bronze*.

**Cassiterite.** Tin oxide *mineral*, $Sn_2O$, mostly dark-coloured. Also called *tinstone*.

**Casting.** The process of pouring molten metal into pre-shaped forms, called *moulds*.

**Chalcopyrite.** Yellow copper iron sulphide *mineral*, $CuFeS_2$.

**Chaplet.** A metal form used to provide additional support for the core of the *mould* during *casting*.

**Cold-forging.** See *cold-working*.

**Cold-working.** The *plastic deformation* of a metal at a temperature below that at which it *recrystallises*. Also called *cold-forging*.

**Coring.** Micro-segregation process whereby the centre of a *grain* is rich in the high-melting element and the grain boundary is rich in the low-melting element.

**Crucible.** A heat-resistant container in which materials can be heated to very high temperatures.

**Crystalline.** The state of a solid material characterised by a periodic and repeating three-dimensional array of atoms, ions, or molecules.

**Cuprite.** Red copper oxide *mineral*, $Cu_2O$.

**Deformation.** See *elastic deformation* and *plastic deformation*.

**Deposit.** An *ore* deposit is a portion of the earth's crust from which some industrial raw material can be extracted at a profit.

**Deposition.** The act of putting objects in the ground. In this context: deliberately placing of *bronze* artefacts in the soil.

**Diffusion.** Mass transport by atomic motion.

**Dislocation.** A linear *crystalline* defect around which there is atomic misalignment.

**Domeykite.** Greyish copper arsenide *mineral*, $Cu_3As$.

**Ductility.** A measure of a material's ability to undergo appreciable *plastic deformation* before fracture.

**Elastic deformation.** *Deformation* that is non-permanent and totally *recovered* upon release of an applied *stress*.

**Electron configuration.** The manner in which possible electron states for an atom are filled with electrons.

**Enargite.** Blackish copper arsenic sulfosalt *mineral*, $Cu_3AsS_4$.

**Eutectic reaction.** A reaction wherein, upon cooling, a liquid *phase* transforms isothermally and reversibly into two intimately mixed solid phases.

**Eutectic.** An *alloy* of two or more components having the lowest *melting* point.

**Face-centered cubic (FCC).** A *crystal* structure, where atoms are located at all corner and face-centered positions in the cubic unit cell.

**Fahlerz.** Grey copper *ore* of the tetrahedrite ($Cu_{12}Sb_4S_{13}$) or *tennantite* (CuAsS) series, with small quantities of other metals like silver. Also called fahlore.

**Forgeability.** Capability of a metal for undergoing *forging* actions.

**Forging.** Mechanical forming of a metal by hammering, either *cold* or *hot*.

**Furnace.** An enclosed chamber or structure in which heat is produced.

**Galena.** The natural *mineral* form of lead sulphide, PbS.

**Grain.** An individual *crystal* in a *polycrystalline* metal or ceramic.

**Hardness.** The measure of a material's resistance to *deformation* by surface indentation or by abrasion.

**Hearth.** A fireplace or part of a *furnace* on which the fire rests.

**Hoard.** Place where multiple (valuable) objects are deliberately *deposited* in the ground.

**Hot-forging.** See *hot-working*.

**Hot-working.** Any metal-forming operation that is performed above a metal's *recrystallisation temperature*. Also called *hot-forging*.

**Interstitial solid solution.** A *solid solution* where relatively small atoms occupy interstitial positions between the solvent or host atoms.

**Investment.** Ceramic *mould* used in cire perdue *casting*.

**Kiln.** A *furnace* or *oven* for drying, burning, or baking (ceramic) materials. Also used for smelting *ore* to extract metal.

**Lattice.** The regular geometrical arrangement of points in crystal space.

**Malleability.** Capability of a metal for undergoing *deformation* in all directions by forging or pressing. Synonymous with *ductility*.

**Melaconite.** See *tenorite*.

**Melting.** Changing a metal from the solid to the liquid state.

**Metallurgy.** The study of metals and their properties in the bulk and at the atomic level.

**Microstructure.** The structural features of an *alloy* (e.g. *grain* and *phase* structure) that are subject to observation under a microscope.

**Mineral.** A naturally occurring *crystalline* solid.

**Misorientation.** The orientation difference between two coordinate systems in electron backscatter diffraction.

**Mould.** Pre-shaped formed used to *cast* objects in.

**Native copper**. Pure copper, found in chemically uncombined state as a natural *mineral*.

**Old World.** Europe and the Near East in prehistory.

**Ore.** A type of rock that contains (an aggregate of) *minerals* such as metals.

**Orpiment.** Yellowish arsenic sulphide *mineral*, $As_2S_3$.

**Oven.** An enclosed compartment for heating, baking or drying food or other materials.

**Patina.** A coating on metal (like bronze) of various chemical compounds such as oxides or carbonates formed on the surface during exposure to the elements.

**Pattern.** A model used to shape a *mould* for *casting*.

**Phase.** A homogeneous portion of a system that has uniform physical and chemical characteristics.

**Phase equilibrium.** State of a system where the *phase* characteristics remain constant over indefinite time periods.

**Plastic deformation.** *Deformation* that is permanent or non-*recoverable* after release of the applied load. It corresponds to the motion of a large number of *dislocations*.

**Polycrystalline.** A *crystalline* material composed of more than one crystal or *grain*.

**Precipitate.** The solid that is formed in a solution during a chemical reaction.

**Precipitation hardening.** Hardening and strengthening of a metal *alloy* by extremely small and uniformly dispersed particles that *precipitate* from a supersaturated *solid solution*. Also called *age hardening*.

**Realgar.** Orange arsenic sulphide *mineral*, AsS.

**Recovery.** The relief of some of the internal

*strain* energy of a *cold-worked* metal, usually by heat treatment.

**Recrystallisation.** The formation of a new set of *strain*-free *grains* within a previously *cold-worked* material; normally an *annealing* heat treatment is necessary.

**Recrystallisation temperature.** The minimum temperature at which complete *recrystallisation* will occur within approximately one hour for a particular *alloy*.

**Refractory.** A material that retains its strength at high temperatures.

**Secondary electron.** An electron that is emitted from a surface by primary incident particles of sufficient energy.

**Slip.** *Plastic deformation* as the result of *dislocation* motion; also, the shear displacement of two adjacent planes of atoms.

**Smelting.** The process by which a metallic *ore* is converted to metal through the agency of heat and chemical energy.

**Socketed axe.** A type of axe in which the body of the tool is hollow so that it can receive a shaped projection at the end of the haft in order to secure the haft to the metal axe head.

**Solid solution.** A homogeneous *crystalline phase* that contains two or more chemical species. Both *substitutional* and *interstitial solid solutions* are possible.

**Solid solution strengthening.** Hardening and strengthening of metals that result from *alloying* in which a *solid solution* is formed. Also called *solid solution hardening*.

**Solubility limit.** The maximum concentration of solute that may be added without forming a new *phase*.

**Strain (engineering).** The change in gauge length of a specimen (in the direction of an applied *stress*) divided by its original gauge length.

**Strain hardening.** The increase in hardness and strength of a ductile metal as it is *plastically deformed* below its *recrystallisation temperature*. Also called *work hardening*.

**Stress (engineering).** The instantaneous load applied to a specimen divided by its cross-sectional area before any *deformation*.

**Substitutional solid solution**. A *solid solution* where solute atoms replace or substitute for the host atoms.

**Tennantite.** Grey copper arsenic sulfosalt *mineral*, $Cu_{12}As_4S_{13}$.

**Tenorite.** Black copper oxide *mineral*, CuO. Also called *melaconite*.

**Tensile strength.** The maximum engineering *stress*, in tension, that may be sustained without fracture. Also called *ultimate tensile strength*.

**Ternary bronze.** A ternary *alloy* of copper and two other metallic elements.

**Twin boundary.** A special type of *grain* boundary across which there is mirror *lattice* symmetry.

**Ultimate tensile strength.** See *tensile strength*.

**Votive.** Dedicated or given in fulfilment of a vow or pledge.

**Work hardening.** See *strain hardening*.

**Yield strength.** The *stress* required to produce a very slight (yet specified) amount of plastic *strain*.

List of Abbreviations:

EBSD: Electron BackScatter Diffraction
EDS: Energy Dispersive x-ray Spectrometry
EPMA: Electron Probe MicroAnalysis
NRCA: Neutron Resonance Capture Analysis
OM: Optical Microscopy
SEM: Scanning Electron Microscope
XRF: X-Ray Fluorescence

# Bibliography


Akker, H.E.A. van den & Mudde, R.F. (2003[2]) *Fysische Transportverschijnselen I*, Delft University Press, Delft

Alford, T.L., Feldman, L.C., Mayer, J.W. (2007) *Fundamentals of Nanoscale Film Analysis*, Springer, New York

Allen, I., Britton, D. & Coghlan, H. (1970) *Metallurgical Reports on British and Irish Bronze Age Implements and Weapons in the Pitt Rivers Museum*, Oxford University Press, Oxford

Arlt, T. & Diamond, L.W. (1998) 'Composition of Tetrahedrite-Tennantite and "Schwazite" in the Schwaz Silver Mines, North Tyrol, Austria', *Mineralogical Magazine* **62**(6), 801-820

ASM (1992), *ASM Handbooks*, Vol. 3, ASM International, United States of America

Bailey, A.R. (1954), *A Text-Book of Metallurgy*, Macmillan and Co. Ltd., London

Biek, L. (1957) 'The Examination of Some Copper Ores: A Report of the Ancient Mining and Metallurgy Committee', *Man* **57**, 72-76

Bradley, R. (1988) 'Hoarding, Recycling and the Consumption of Prehistoric Metalwork: Technological Change in Western Europe', *World Archaeology* **20**(2), 249-260

Van den Broeke, P. (2005) 'Graven voor de Goden' in *Nederland in de Prehistorie*, L.L. Kooijmans, Uitgeverij Bert Bakker, Amsterdam, 659-679

Butler, J.J. (1973) 'Einheimische Bronzebeilproduktion im Niederrhein-Maasgebiet', *Palaeohistoria* **15**, 319-343

Butler, J.J. & Steegstra, H. (2001/2002) 'Bronze Age Metal and Amber in the Netherlands (III.2) Catalogue of the Socketed Axes, Part A', *Palaeohistoria* **43-44**, 263-319

Butler, J.J. & Fokkens, H. (2005) 'Van Steen naar Brons' in *Nederland in de Prehistorie*, L.L. Kooijmans, Uitgeverij Bert Bakker, Amsterdam, 371-400

Callister, W.D. (2003[6]) *Materials Science and Engineering: an Introduction*, John Wiley & Sons, Inc., New York

Cheng, C.F. & Schwitter, C.M. (1957) 'Nickel in Ancient Bronzes', *American Journal of Archaeology* **61**(4), 351-365

Childe, V.G. (1930) *The Bronze Age*, Biblo & Tannen Publishers, New York

Cochrane, R.F. (2002) DoITPoMS Micrograph Library #525, University of Leeds

Coghlan, H. H. (1955) 'Reports of the Ancient Mining and Metallurgy Committee: Analyses of Three Continental Axes and of Specimens of Irish Ores.', *Man* **55**, 6-8

Coghlan, H.H. (1975) *Notes on the Prehistoric Metallurgy of Copper and Bronze in the Old World (Occasional Paper on Technology IV)*, Oxford University Press, Oxford

Craddock, P. (2009) *Scientific Investigation of Copies, Fakes and Forgeries*, Butterworth Heinemann, Oxford

Cullity, B.D. (1956) *Elements of X-Ray Diffraction*, Addison-Wesley Publishing Company Inc., Reading

Earl, B. & Adriaens, A. (2000) 'Initial Experiments on Arsenical Bronze Production', *Journal of the Minerals and Metals Society* **52**(3), 14-16

Eaton, E.R. & McKerrell, H. (1976) 'Near Eastern Alloying and Some Textual Evidence for the Early Use of Arsenical Copper', *World Archaeology* **8**(2), 169-191

Flinn, R.A. (1963) *Copper, Brass and Bronze Castings*, Non-Ferrous Founders' Society, Inc., Park Ridge

Fontijn, D.R. (2002) *Sacrificial Landscapes. Cultural Biographies of Persons, Objects and 'Natural' Places in the Bronze Age of the Southern Netherlands, c. 2300-600 BC.* (Analecta Praehisorica Leidensia 43/44) Peeters, Leiden/Leuven

Fontijn, D.R. & Fokkens, H. (2007) 'The Emergence of Early Iron Age 'Chieftains' Graves' in the Southern Netherlands: Reconsidering Transformations in Burial and Depositional Practices' in *The Earlier Iron Age in Britain and the Near Continent*, Haselgrove, C. & Pope, R., Oxbow Books, Oxford, 354-373

Franceschi, E., DelLucchese, A., Palazzi, D., Rossi, G. (1997) 'Aspects of metallurgical activity in Liguria (Italy) in the Middle and Late Bronze Age', *Journal of Thermal Analysis* **49**(3), 1593-1600

Gainov, R.R., Dooglav, A.V., Pen'kov, I.N., Mukhamedshin, I.R., Savinkov, A.V., Mozgova, N.N. (2008), 'Copper Valence, Structural Separation and Lattice Dynamics in Tennantite (Fahlore): NMR, NQR and SQUID Studies', *Physics and Chemistry of Minerals* **35**, 37-48.

Gale, N.H., Stos-Gale, Z.A., Gilmore, G.R. (1985), 'Alloy Types and Copper Sources of Anatolian Copper Alloy Artifacts', *Anatolian Studies* **35**, 143-173

Gordon, R. & Knopf, R. (2006) 'Metallurgy of Bronze Used in Tools From Machu Picchu Peru', *Archaeometry* **48**(1), 57-76

Gupta, K.P. (2000) 'An Expanded Cu-Ni-Sn System (Copper-Nickel-Tin)', *Journal of Phase Equilibria* **21**(5), 479-484

Hauptmann, A., Begemann, F., Schmitt-Strecker, S. (1999) 'Copper Objects from Arad: Their Composition and Provenance', *Bulletin of the American Schools of Oriental Research* **314**(314), 1-17

Huth, C. (2003) 'Poor Belgium, Rich Belgium. Some Reflections on the Nature of Metalwork Deposits in the Late Bronze Age and Early Iron Age' in *Bronze Age and Iron Age Communities in North-Western Europe*, Bourgeois, J., Bourgeois, I., Cherretté, B., Koninklijke Vlaamse Academie van België voor Wetenschappen en Kunsten, Brussel, 39-60

Hwang, J.D., Li, B.J., Hwang, W.S., Hu, C.T. (1998) 'Comparison of Phosphor Bronze Metal Sheet Produced by Twin Roll Casting and Horizontal Continuous Casting', *Journal of Materials Engineering and Performance* **7**(4), 495-503

Ingo, G.M., Plescia P., Angelini, E., Riccucci, C., De Caro, T. (2006) 'Bronze Roman Mirrors: the Secret of Brightness', *Applied Physics A: Materials Science & Processing* **83**(4), 611-615

Junk, M. (2003) *Material Properties of Copper Alloys Containing Arsenic, Antimony, and Bismuth - The Material of Early Bronze Age Ingot Torques*, Technischen Universität Bergakademie Freiberg, Freiberg

Kristiansen, K. & Larsson, T.B. (2005) *The Rise of Bronze Age Society - Travels, Transmissions and Transformations*, Cambridge University Press, Cambridge

Kuijpers, M.H.G. (2008) 'Bronze Age Metalworking in the Netherlands (c. 2000-800 BC): a Research into the Preservation of Metallurgy Related Artefacts and the Social Position of the Smith', Master's thesis, Faculty of Archaeology, Leiden University

Kuijpers, M.H.G. (2009) Personal Communication

Landolt-Börnstein (1990) 'Diffusion in Solid Metals and Alloys' in *Numerical Data and Functional Relationships in Science and Technology - Group III: Crystal and Solid State Physics*, Mehrer, H., Springer-Verlag, New York, Volume 26

Lascalea, G.E., Pifferetti, A., Fernandez de Rapp, M.E., Walsoe de Reca, N.E., Northover, J.P. (2002) 'The Material Characterization of a Santamarian Ceremonial Axe', *Archaeometry* **44**(1), 83-94

Lechtman, H. (1991) 'The Production of Copper-Arsenic Alloys in the Central Andes: Highland Ores and Coastal Smelters?', *Journal of Field Archaeology* **18**(1), 43-76

Lechtman, H. (1996) 'Arsenic Bronze: Dirty Copper or Chosen Alloy? A View from the Americas', *Journal of Field Archaeology* **23**(4), 477-514

Lechtman, H. & Klein, S. (1999) 'The Production of Copper–Arsenic Alloys (Arsenic Bronze) by Cosmelting: Modern Experiment, Ancient Practice', *Journal of Archaeological Science* **26**, 497-526

Lindgren, W. (1933[4]) *Mineral Deposits*, McGraw-Hill Book Company, Inc., New York
Maclean, P. (1998) 'Forgotten Realms, Forgotten Alloys: Exotic Metallurgy in Bronze Age Europe', Early Materials' Forum, London
Massalski, T. (1990), *Binary Alloy Phase Diagrams*, ASM International, Materials Park, Ohio
Muhly, J.D. (1973) *Copper and Tin: the Distribution of Mineral Resources and the Nature of the Metals Trade in the Bronze Age*, Archon, Connecticut
Northover, J.P. (1982) 'The Exploration and Long Distance Movement of Bronze in Bronze Age and Early Iron Age Europe', *Institute of Archaeology Bulletin* **19**, 45-72
O'Brien, W. (1996) *Bronze Age Copper Mining in Britain and Ireland*, Shire Archaeology
Ottaway, B.S. & Roberts, B. (2008) 'The Emergence of Metalworking' in *Prehistoric Europe: Theory and Practice*, Jones, A., Wiley-Blackwell, 193-225, Chichester
Pare, C.F.E. (2000) 'Bronze and the Bronze Age' in *Metals Make the World Go Round: The Supply and Circulation of Metals in Bronze Age Europe - Proceedings of a conference held at the University of Birmingham in June 1997*, Pare, C.F.E., Oxbow Books, Oxford, 1-39
Pigott, V.C. (1999) *The Archaeometallurgy of the Asian Old World*, University of Pennsylvania Museum, Philadelphia
Pollard, M., Batt, C., Stern, B., Young, S. (2007) *Analytical Chemistry in Archaeology*, Cambridge University Press, Cambridge
Porter, D.A. & Easterling, K.A. (2001) *Phase Transformations in Metals and Alloys*, Nelson Thornes Ltd., Cheltenham
Postma, H. (2001) 'Neutron-resonance Capture Analysis of Materials', *Journal of Radioanalytical and Nuclear Chemistry* **248**(1), 115-120
Postma, H., Fontijn, D.R., Schillebeeckx, P., Perego, R.C., Butler, J.J. (2005) 'Neutron Resonance Capture Analysis of Geistingen Axes', *Lunula: Archaeologia Protohistorica* **XIII**, 41-46
Postma, H. (2009) Personal Communication
Randle, V. (2003[2]) *Microtexture Determination and its Applications*, Maney, Leeds
Ronen, Y. & Rozenak, P. (1993) 'The Development of the Screw - An Early Metallurgy', *Journal of Materials Science* **28**, 5576-5579
Rouessac, F. & Rouessac, A. (2000) *Chemical Analysis - Modern Instrumentation Methods and Techniques*, John Wiley & Sons, Inc., New York
Russell, A.M. & Lee, K.L. (2005) *Structure-Property Relations in Nonferrous Metals*, John Wiley & Sons, Inc., New York
Segal, I. & Rosen, S.A. (2005) 'Copper Among the Nomads: Early Bronze Age Copper Objects from the Camel Site, Central Negev, Israel', *Institute for Archaeo-Metallurgical Studies* **25**, 3-8
Silva, R.J.C., Figueiredo, E., Araujo, M.F., Pereira, F., Fernandes, F.M.B. (2008) 'Microstructure Interpretation of Copper and Bronze Archaeological Artefacts from Portugal', *Advanced Materials Forum IV* **587-588**, 365-369
Tatsch, J.H. (1975) *Copper Deposits*, Tatsch Associates Massachusetts, Sudbury
Thompson, F.C. (1958) 'The Early Metallurgy of Copper and Bronze', *Man* **58**, 1-7
Tylecote, R.F., Ghaznavi, H.A., Boydell, P.J. (1977) 'Partitioning of Trace Elements Between the Ores, Fluxes, Slags and Metal During the Smelting of Copper', *Journal of Archaeological Science* **4**(4), 305-333
Voce, E. & Childe, V.G. (1951) 'Ancient Mining and Metallurgy Committee: Report on Examination of Miscellaneous Copper and Bronze Artifacts.', *Man* **51**, 139-141
Young, M., Casadio, F., Schnepp, S., Almer, J., Haeffner, D., Dunand, D. (2006) 'Synchrotron X-Ray Diffraction and Imaging of Ancient Chinese Bronzes', *Applied Physics A-Materials Science & Processing* **83**(2), 163-168

# Appendix

**X-ray diffraction pattern of the Nijmegen axe (long side of AC20#1)**

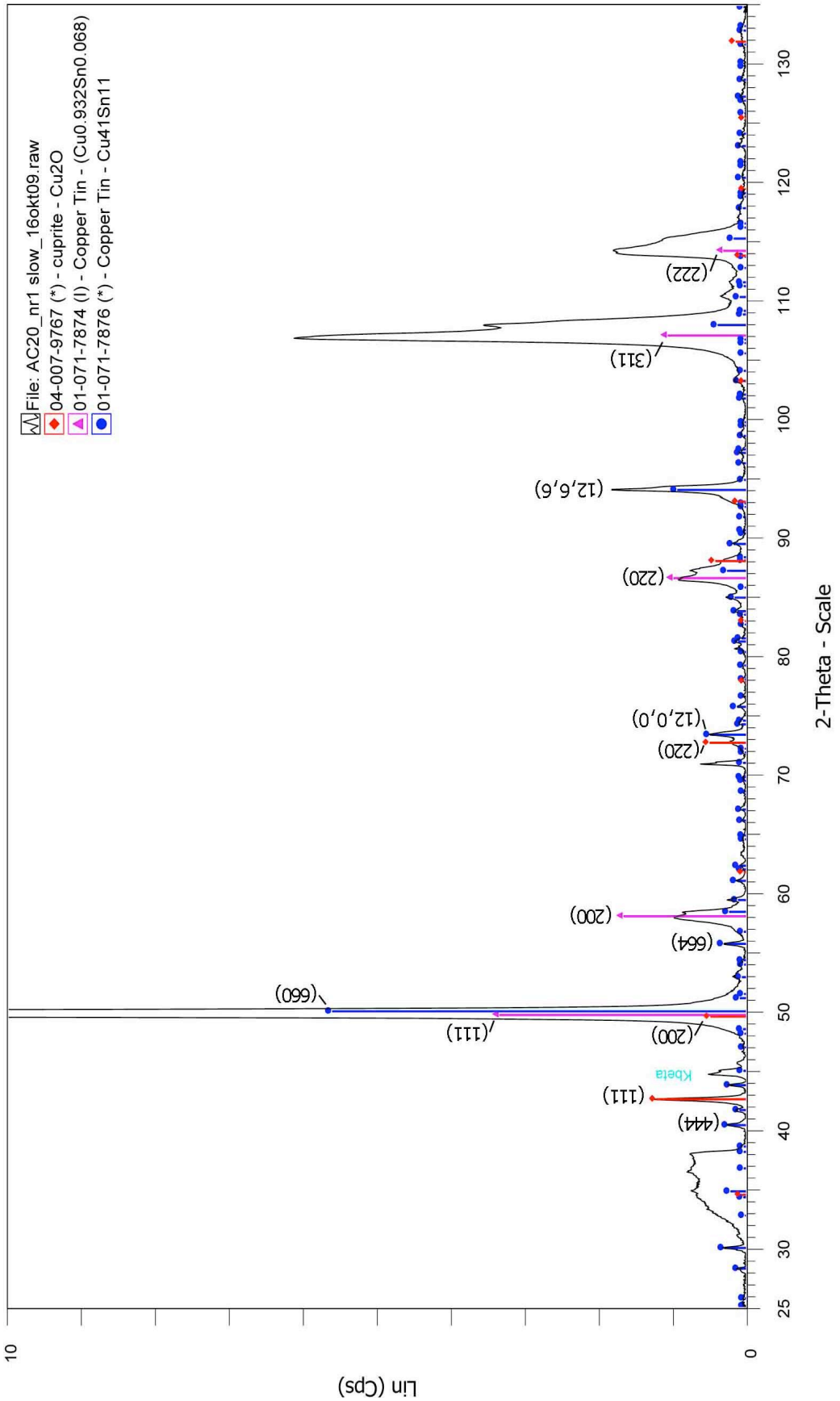

**X-ray diffraction pattern of the Tongeren axe (short side of BH76#3)**